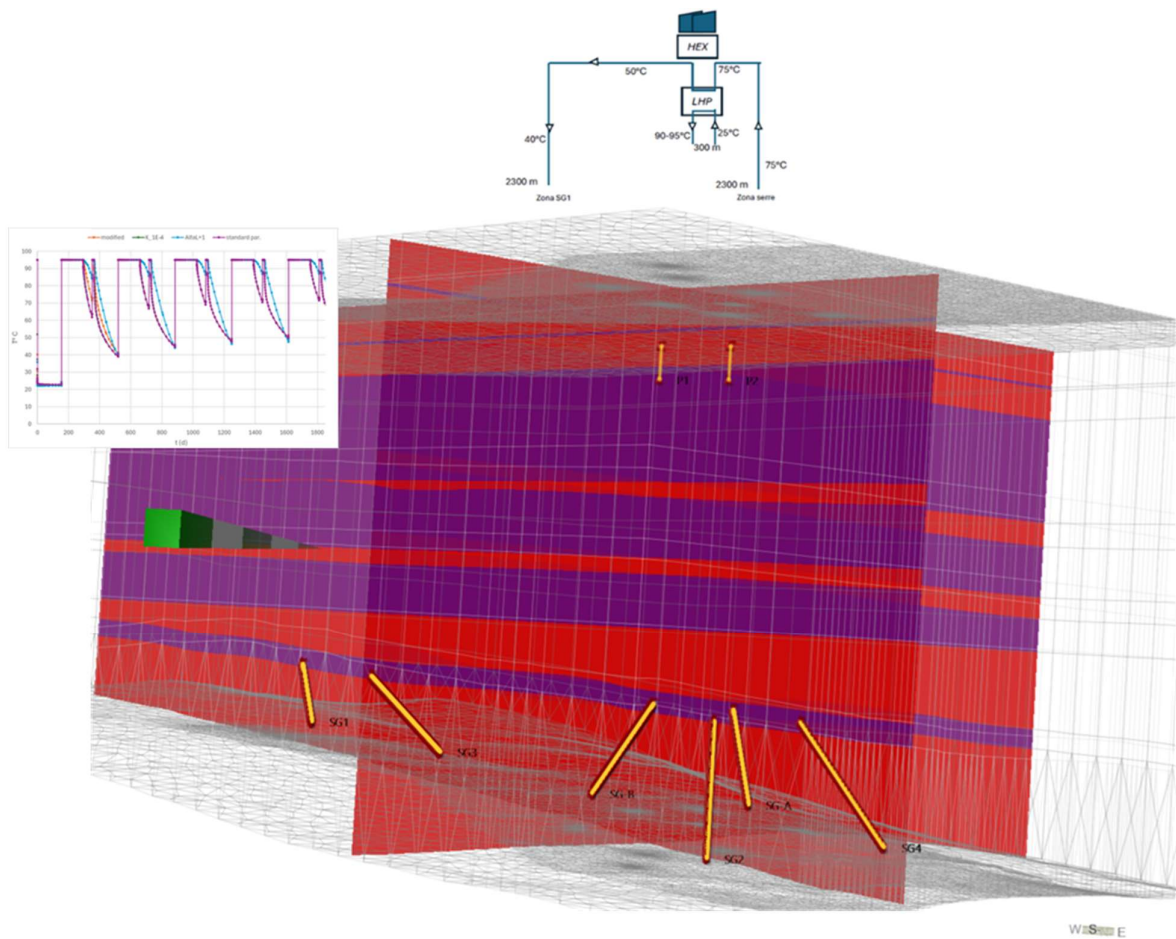


Flow and heat transport modeling for deep reservoir exploitation and ATES in the site of Ostellato (Ferrara)

Phase A - Solutions screening

Report



This report has been prepared under the DHI Business Management System certified by Bureau Veritas to comply with ISO 9001 (Quality Management)

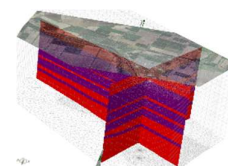


Flow and heat transport modeling for deep reservoir exploitation and ATEs in the site of Ostellato (Ferrara)

Phase A - Solutions screening

Report

Client FRI-EL GEOPower S.r.l.
Client Representative: Ph.D. Andrea Marchetti, ing. Matthias Scheuber



Comprehensive deep geological model

Project manager	Marco Bersano Begey
Quality supervisor	Andrea Crosta
Author	Marco Bersano Begey
Project code - document	22805081-01-00102
Approval date	28/02/2025
Revision	Final 2.0
Classification	Limited

SUMMARY

1	Introduction	1
2	Computational code used.....	3
3	Geological and stratigraphical frame for the model setup	5
4	Implementation of the static geothermal model.....	6
5	Geothermal dynamic model (plant operation).....	9
5.1	Scenario 1	11
5.1.1	Model setup.....	11
5.1.2	Simulation results	14
5.1.3	Key insights on Scenario 1 ATES performance.....	15
5.1.4	Preliminary estimation of exchanged power and process efficiency	20
5.1.5	Sensitivity analysis and model uncertainty	22
5.2	Scenario 2	25
5.2.1	Model setup.....	25
5.2.2	Simulation results: heat storage section (reservoir A1-a).....	29
5.2.3	Key insights on Scenario 2-a ATES performance	34
5.2.4	Key insights on Scenario 2-b ATES performance	40
5.2.5	Key insights on Scenario 2-c ATES performance.....	46
5.2.6	Simulation results: heat production section (reservoir A3-a).....	47
5.2.7	Sensitivity analysis and model uncertainty	50
6	Thermal interference evaluation: assessing and minimizing ATES heat transfer to shallow aquifers.....	53
6.1	Model setup.....	54
6.2	Simulation results	55
6.2.1	Scenario 2-b.....	55
6.2.2	Scenario 2-c, 2c-1	55
6.3	Key insight.....	56
7	Summary of simulation results	61
7.1	ATES Sections (storage wells)	61
7.2	Production (geothermal well doublets)	63
8	Conclusions.....	64

1 Introduction

This report presents the methodology and findings of a numerical modeling study aimed at simulating geothermal exchange systems for deep reservoir utilization and ATEs energy storage in the Ostellato (FE) area.

The project includes the following key aspects:

- the construction of extraction-reinjection wells in the aquifer composed of post-Pliocene silicoclastic deposits, reaching a maximum depth of approximately 2300 m and temperatures up to 75°C;
- the heat exchange with thermovector fluid, followed by heating to approximately 95°C using high-temperature heat pumps, whose electricity consumption is supplied by a zero-emission solar park, for the district heating of a hydroponic greenhouse system;
- an ATEs (Aquifer Thermal Energy Storage) plant for hot water storage during the seasonal period with a positive energy balance—when the heat production potential exceeds the district heating demand— and subsequent reuse.

The project development scenarios cover the sector including the "Pozzo San Giovanni" and "greenhouse" areas, approximately 2.6 km apart, as shown in Figure 1.

The current phase of the project is specifically aimed at qualifying for the EU Innovation Fund 2024 call, meeting the required criteria of innovation, technological maturity, scalability, technical-economic efficiency, and implementation timeline in reference to EU climate objectives.



Figure 1 Locations for the Extraction and Reinjection Wells

The model setup refers to baseline elements and data provided by FRI-EL GEO, derived from both ongoing geological modeling activities and evaluations concerning seasonal energy demand and operational constraints. In particular, the following data was employed:

- a) Structural and thermal model of the extraction and reinjection targets in digital format (LEAPFROG geological modeling software environment and exported vector geometries—3D point maps, 3D shapefiles, etc.);

- b) Hydrogeological and thermophysical parameters of the target reservoirs (ref. Table 2)
- c) Technical constraints (e.g., reinjection temperatures and discharge, maximum pressures, minimum efficiency target).

The hydrogeological and petrophysical parameters sensitive for the modelling results are provided in three main probabilistic intervals: P90 – P50 – P10. Where probability percentiles cannot be reliably derived, the current phase relies on average, conservative, and optimistic scenarios based on the best available forecasts, provided by FRI-EL GEO.

The modeling activity is structured through the following interconnected and sequential phases:

- implementation and calibration of the static geothermal model (pre-operational, steady-state);
- simulation of operational plant scenarios;
- preliminary uncertainty analysis and sensitivity testing;
- comparative analysis of the results for the different modelled scenarios.

At this stage of the project (Phase A – 'Solutions Screening'), simulations provide key operational data for each scenario, including injection and extraction pressures, thermal cycles, heat rate and period budgets, ATES recovery efficiency, and energy balance (produced vs. invested, where significant). This data supports FRI-EL GEO in the preliminary selection of the most efficient design scenario for the district heating system.

Specifically, the following scenarios currently under study by FRI-EL GEO are being evaluated (Figure 2 and Figure 3, detailed description at par. 5.1, 5.2):

- Scenario 1: Extraction and thermal storage reinjection in the "Serre" area, winter reinjection (cold water) in the "Pozzo San Giovanni" area, within the same reservoir at the base of the multi-aquifer complex (~2300 m from ground level).
- Scenario 2: Extraction in the "greenhouses" area and coldwater reinjection in "Pozzo San Giovanni", in the same deep reservoir at the base of the multi-aquifer complex (~2300 m from ground level), similarly to Scenario 1. Additionally, an independent doublet system in a shallower aquifer in the "greenhouses" is dedicated to thermal storage. For this scenario, two different operation patterns are evaluated (Scenario 2-a, 2-b).

Each scenario is simulated based on the operating regime provided by FRI-EL, including the temporal evolution (e.g., weekly, monthly) of extracted and reinjected flow rates and temperatures for the geothermal doublets, as well as the flow rates and temperatures of the reinjected storage water.

SCENARIO 1

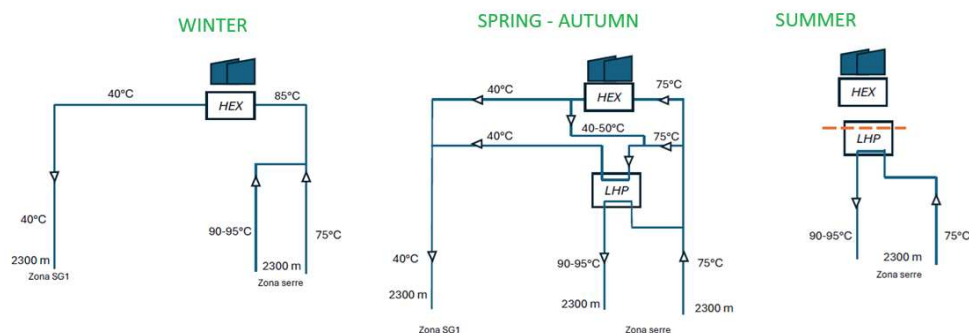


Figure 2 Scenario 1: Project and Seasonal Utilization Scheme (HEX – Heat Exchanger, LHP – Liquid Heat Pump).

SCENARIO 2

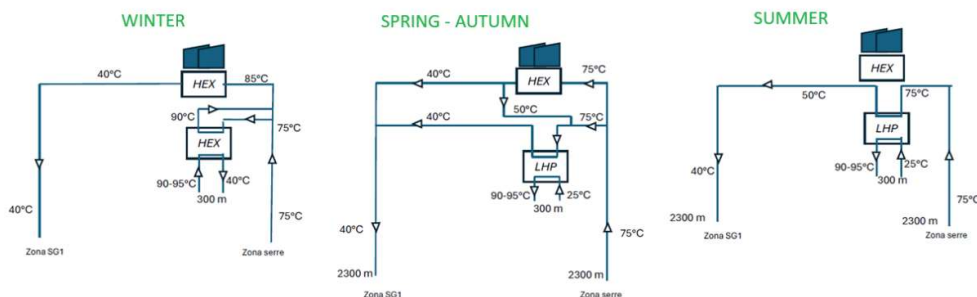


Figure 3 Scenario 2: Project and Seasonal Utilization Scheme.

2 Computational code used

The simulations have been carried out primarily using the FEFLOW FMH3 (DHI-WASY) computational code, in its current version 10.0 (2025).

FEFLOW (Finite Element Subsurface FLOW System) is a software designed for simulating groundwater flow, mass transport, and heat transport in porous and fractured media. The program uses the finite element method to solve equations for groundwater flow under saturated and unsaturated conditions, as well as for mass and heat transport, incorporating fluid density effects and multi-component reaction kinetics.

The code was originally developed (1979-1990) at the Institute of Mechanics of the German Academy of Sciences (Berlin), later by WASY, and has been continuously updated since 2007 by the DHI international team, leading to its current version 10.0 (2025).

For the specific application of medium-temperature geothermal system simulations, particularly for Liquid Dominated Geothermal Plants, FEFLOW is considered the international standard and an optimal technical tool, as it integrates essential functionalities dedicated to this type of application. Specifically, it provides:

- Finite element mesh discretization of the simulation domain, with partially or fully unstructured grids, allowing high-detail modeling of complex structures and large-scale heterogeneities in

deep geothermal reservoirs, such as faults, thrust surfaces, folds, and directional wells for geothermal fluid extraction and reinjection, regardless of trajectory or orientation.

- Integrated inverse geological modeling.
- The ability to insert and modify structures with remeshing of the original grid (mesh repair functions). This feature enables rapid implementation of different geological models and well trajectories, making it a critical tool for statistical approaches in deep geothermal resource assessment, as it allows testing a high number of probable configurations and reservoir setups.
- Solution for mass and heat transport in multi-component fluid mixtures.
- Variable-density flow modeling, with density dependence on temperature and mass concentration (density-dependent convective flow simulation).
- Variable-viscosity fluid flow modeling, with viscosity dependence on temperature and mass concentration.
- Stable convergence and fast equation solving, including:
 - Parallelized computation,
 - Linear and parallel solvers,
 - GPU parallelization,
 - Cloud-based high-performance computing (DHI cloud option).
- Integrated hydrogeochemical modeling of chemical equilibria and precipitation, via the piChem plugin (coupling with USGS-PHREEQC).
- Integrated geomechanical modeling, using the piHMC plugin (coupled hydro-mechanical processes), which models the stress field, enabling the simulation of:
 - Effective load variations as a function of hydrostatic pressure and its variations under operational conditions (extraction and reinjection).
 - Ground surface and subsurface deformations (for subsidence assessment).
 - Reduction of permeability and porosity due to compaction and fluid expulsion.
- Integrated simulation of flow, mass and heat transport within extraction and reinjection wells (thermohaline simulations).
- Customizable heat exchanger simulation, through the embedded BHE (Borehole Heat Exchanger) module.
- Plant heat exchange simulation, via a dedicated boundary condition, enabling:
 - Temperature differential (ΔT) assignment between extraction and reinjection systems.
 - Assignment of exchanged thermal power (P) at the plant level.
 - Open programming capabilities, allowing efficient automation of modeling workflows.
 - Brine extraction and lithium recovery simulation, using the Mike Mine Lithium module.
 - Advanced sensitivity analysis and model optimization functionalities, which enable:
 - Evaluation of key parameter effects on geothermal system behavior.

Optimization of geothermal production design and operational strategies.

This comprehensive set of functionalities makes FEFLOW one of the most advanced and widely recognized software tools for geothermal system simulation and optimization.

In newest releases, a new Equation of State (EOS) feature has been integrated to enhance geothermal energy calculations. This addition allows for more accurate modeling of fluid properties under varying geothermal conditions. Key aspects of this feature include:

- Nonlinear Fluid Density and Viscosity Calculations: Fluid density can now be expressed as a nonlinear function of concentration, temperature, and pressure. Both fluid density and viscosity are computed directly at local finite element nodes, improving calculation accuracy. This implementation supports temperature ranges from 0 to 300°C, concentrations from 0 to 300 g/l, and fluid pressures up to 100 MPa (1000 bar).
- Temperature Relative to Boiling: A new auxiliary parameter, Temperature relative to boiling, has been introduced. This parameter calculates the difference between the local temperature and the pressure-dependent boiling point, helping identify regions where phase changes might occur.
- Equation of State Configuration: A dedicated Equation of State page in the Problem Settings dialog provides options to control fluid density and viscosity. Users can define how these properties depend on concentration, temperature, and pressure, allowing for tailored simulations of geothermal systems.

This comprehensive set of functionalities makes FEFLOW one of the most advanced and widely recognized software tools for geothermal system simulation and optimization.

3 Geological and stratigraphical frame for the model setup

The subsurface of the Ostellato area (Ferrara), down to a depth of approximately 2300 m, consists of a complex multi-aquifer system characterized by a succession of deltaic and turbiditic deposits, interbedded with aquitards that regulate fluid flow and compartmentalization.

From a stratigraphic perspective, the sequence is composed, from bottom to top, of:

- delta plain and delta front deposits (Plio-Pleistocene), representing sedimentary environments influenced by fluvial and coastal dynamics.
- turbiditic sequences (Upper Pliocene to Lower Pleistocene), indicating episodic deep-water sedimentation, typically associated with rapid depositional events linked to sea-level fluctuations and tectonic activity.

These deposits belong to the northern Apennine foredeep basin, where sedimentation was controlled by the interplay of Po Plain subsidence and sediment supply from the Apennine chain.

From a hydrogeological standpoint, the alternation of permeable aquifer layers and lower-permeability aquitards defines a multi-layered system with distinct hydraulic units. The deeper confined aquifers, hosted within sandy and silty formations, are largely separated by clayey aquitards, which help preserve thermal energy and limit fluid migration between layers.

For a detailed geological, hydrogeological, and geothermal characterization, full reference should be made to the technical reports and studies prepared by specialized consultants.

The following table provides a brief overview of the stratigraphic sequence and the reference aquifer levels for contextual purposes only. A specific coding system is assigned to the aquifer units (e.g., A1-a), which will be referenced in the description of the numerical model and the

corresponding scenarios. The table also highlights the “target reservoirs” designated for geothermal production and seasonal storage.

Specifically:

- Aquifer Unit A3-a: target reservoir for production doublets Scenarios 1-2, ATES Scenario 1
- Aquifer Unit A1-a: target reservoir for ATES Scenario 2

Table 1 Hydrostratigraphic model (see geological report for details) – light blue: aquifers

Volumes	Surfaces - Depth	Depositional Environment
Aquifer Unit A0-a (shallow aquifers)	Ground level - 185 m	Delta Plain – Delta Front – Shallow aquifers with predominantly brackish water – Possible presence of shallow wells.
Aquitard Unit A0-b	185 m - 200 m	
Aquifer Unit A1-a <i>target reservoir (ATES Scenario 2)</i>	200 m - 360 m	Delta Front (predominantly sandy facies – delta front sandy sheets)
Aquitard Unit A1-b	360 m - Base of Sequence Q3 (~895 m)	Prodelta (predominantly fine silty-clayey facies with possible sandy intervals)
Aquifer Unit A2-a	Base of Sequence Q3 (~895 m - 1170 m)	Medium-proximal turbidites with predominant multi-meter sandy sheets compared to fine silty-clayey facies
Aquitard Unit A2-b	1170 m - 1330 m	Distal turbidites – Epibathyal with predominantly fine facies
Aquifer Unit A2-c	Base of Sequence (Q2-b 1330 m - 1450 m)	Medium-proximal turbidites with predominant multi-meter sandy sheets compared to fine silty-clayey facies
Aquitard Unit A2-d	~1450 m - ~1570 m	Epibathyal
Aquifer Unit A2-e	1570 m - Base of Sequence Q2-a (~1770 m)	Medium-proximal turbidites with predominant multi-meter sandy sheets (quartz sand) compared to fine silty-clayey facies
Aquitard Unit A2-f	Base of Sequence Q2-a (~1770 m) - Base of Sequence P7 (1865 m)	Epibathyal
Aquifer Unit A3-a <i>target reservoir (production doublets Scenarios 1-2, ATES Scenario 1)</i>	Base of Sequence P7 (1865 m) - Base of Sequence PL3-b (~2240 m)	Medium-proximal turbidites with predominant multi-meter sandy sheets compared to fine silty-clayey facies

4 Implementation of the static geothermal model

The static model was implemented at full scale to reproduce the overall initial thermal state, from the ground surface down to the base of the deep reservoir (A3-a, ~2240 m).

The static model was implemented with reference to the sector and volume under investigation in the geological-geothermal study. The stratigraphic framework was derived from the geological model developed in LEAPFROG GEO, using the import tools within the FEFLOW environment.

Figure 4 shows the stratigraphic schematization extracted from the model, represented through cross-sections across the project areas.

The purpose of the model is to verify, under equilibrium conditions, the consistency of the vertical thermal profile with the geothermal flux and the thermophysical parameters of the subsurface materials.

Consequently, the model is purely conductive, run in steady-state mode, and implemented with the following boundary conditions

- model bottom: Heat flow, 50 mW/m² (after calibration);
- model top: average air/ground temperature, Fixed temperature BC, 14°C.

An additional temperature boundary condition (Temperature BC, 28.1°C) was applied at the base of the A1-a aquifer unit (approximately 360 m depth) to achieve a more detailed temperature distribution in the shallow complex, which is involved in some of the geothermal exploitation scenarios under investigation.

Material property inputs, derived from the hydrogeological and geothermal study, are limited to the basic set relevant to pure conductive heat transport, as no heat advection or convection is accounted for in the static model:

- thermal conductivity of solid: 2.4 J/m/s/K (shallow aquifer A1-a), 2.3 (deep aquifer A3-a and aquitards);
- thermal conductivity of fluid: shallow aquifer A1-a (ref. T=25°C, freshwater / 2.7 g/l), 0.606 J/m/s/K, lower aquitards and aquifers, including A3-a (ref. T=69°C, saltwater 40 g/l), 0.63 J/m/s/K; note that the values are similar, due to the compensating effects of temperature increase and salinity-induced reduction.
- porosity: 0.25 [adim.], constant

Note that FEFLOW calculates the equivalent parameters as a weighted average, taking into account porosity and thermophysical properties.

The results, obtained by calibrating the geothermal flux to the specified final value, are highlighted in the isothermal line representation in Figure 5.

In the upper image, the geological layers corresponding to the shallow complex A1-a and the deep reservoir A3-a are shown.

In Figure 6, the summary thermal data calculated by the model for the shallow aquifer A1-a and the deep reservoir A3-a are presented.

The A1-a aquifer (calculated mean T=24.9°C) is modeled with a constant thickness, resulting in a vertically uniform temperature distribution, driven by the thermal gradient.

As for the A3-a reservoir (calculated mean T=68.6°C) the percentile distribution of temperature is irregular, due to the layer's shape, progressively narrowing in N-E direction, resembling a wedge, which determines a non-uniform distribution of temperatures within the aquifer.

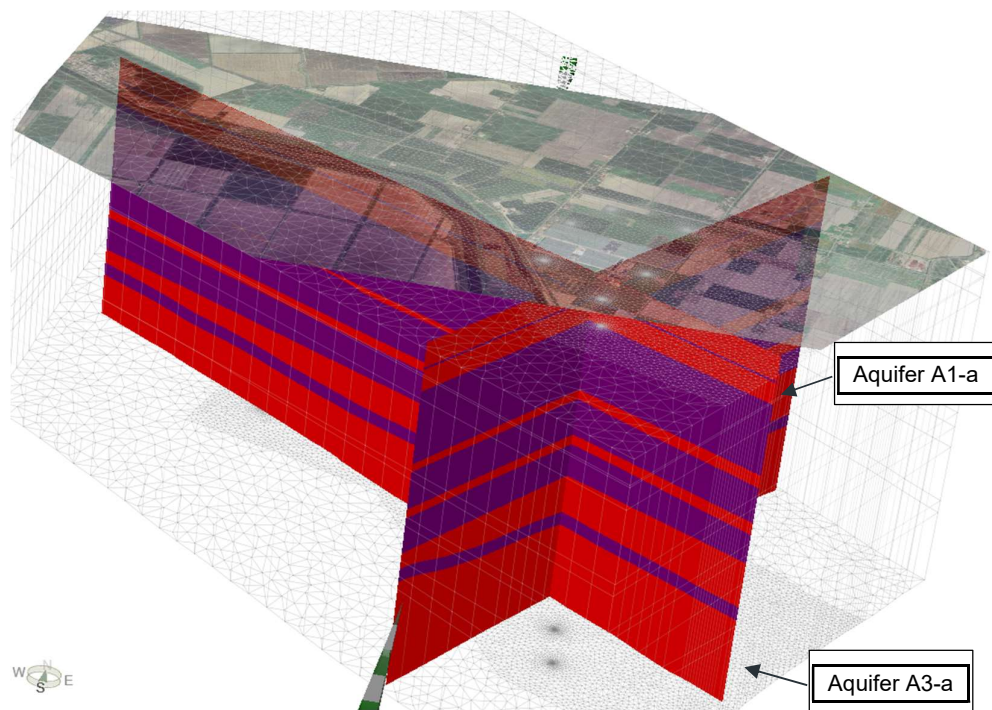


Figure 4 Stratigraphic scheme: aquifers/reservoirs in red, aquitards/aquicludes in purple.

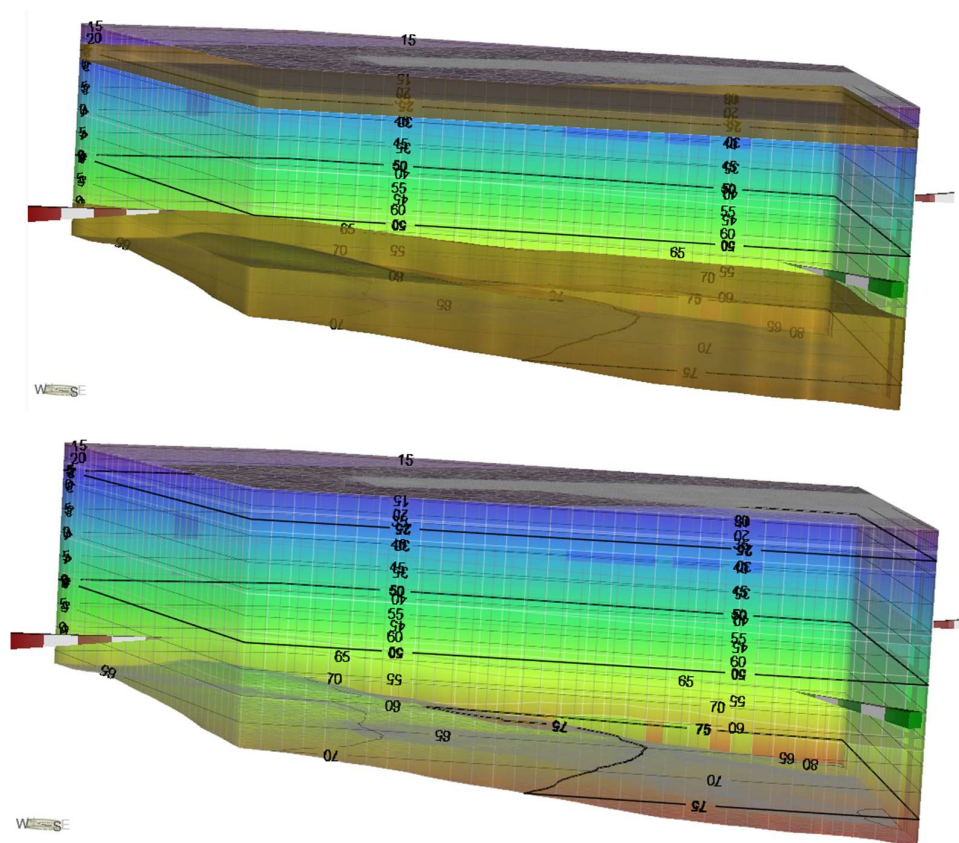


Figure 5 Temperature values resulting from the simulation of the static thermal model - The upper target reservoir (A1-a) and the lower target reservoir (A3-a) are highlighted. See also previous Figure 4

Shallow aquifer A1-a

Min	21.8056 [°C]	Max	28.05 [°C]	Skewness	-1.12883e-10 []
Mean	24.9278 [°C]	Std dev	1.95966 [°C]	Kurtosis	1.7832 []

Deep reservoir A3-a

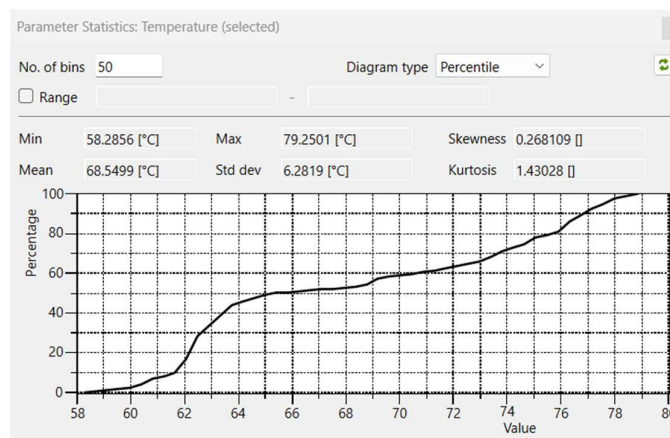


Figure 6 – Temperature distributions, aquifer A1-a, reservoir A-3a.

5 Geothermal dynamic model (plant operation)

The dynamic models are based on Scenarios 1 and 2, previously introduced (Figure 3), along with their respective variations. These scenarios include two geothermal doublets for production and reinjection, as well as an ATEs doublet for seasonal thermal energy storage.

The transient simulation of advective-convective flow requires a high-resolution computational grid. To achieve the necessary level of detail, the dynamic models were developed by isolating the individual aquifer levels (A1-a and A3-a) and constructing high-resolution stand-alone models for each.

The initial input parameters for the dynamic models, referring to the two reservoirs (A1-a, A3-a), are listed in Table 2 (based on FRI-EL geological study). For some parameters, values were varied during the sensitivity analysis.

The dynamic simulations replicate the operational conditions of the system, enabling the generation of the following outputs for each scenario:

- graphical representations of temperature distributions, including hot and cold thermal plumes;
- time-dependent plots of key parameters, including:

Hydraulic heads along the well axis and other selected locations.

Heat rate budget representing the instantaneous thermal power exchange within the geothermal system, expressed in megawatts (MW).

Water temperature at extraction, injection, storage wells, and other selected locations.

Heat period budget (MWh), showing the cumulative thermal energy injected and extracted from the reservoir over time, expressed in megawatt-hours (MWh).

Thermal recovery efficiency charts for the ATEs system, illustrating its thermal performance over time.

The thermal recovery efficiency chart is derived from the Heat Period Budget by calculating the ratio of cumulative heat extracted to cumulative heat injected over time:

$$\eta_{thermal} = \frac{Q_{out} (MWh)}{Q_{in} (MWh)} * 100$$

This chart provides a direct measure of how effectively the system recovers stored heat.

A high efficiency indicates good thermal retention in the reservoir, while a declining efficiency trend may suggest increasing thermal losses, heat dispersion, or inefficient well placement.

This assessment is crucial for optimizing ATEs system performance, refining operational strategies, and identifying potential design improvements.

By integrating these performance metrics, it is possible to identify trends, optimize system performance, and compare the effectiveness of various geothermal configurations, ensuring a data-driven selection of the best operational strategy.

Table 2 **Dynamic modeling parameters**

(*) multiple temperature scenarios

				A1-a	A3-a
A	Hydrogeological and geothermal parameters	symbol	units		
	Horizontal or equivalent hydraulic conductivity	Ke	m/s	2.6E-5	8.2E-7
	Vertical hydraulic conductivity (estimated as kh/kv)	Kv	m/s	4.3E-6	1.4E-7
	Drain fillable porosity	ne	[-]	0.30	0.21
	Specific Storage (compressibility)	Ss	1/m	2e-5	1e-5
	Hydraulic gradient (indicative piezometry, Unit A1-a)	i	[-]	3e-5	0
	Temperature profile (H vs. T)	T	m, °C	0.045	0.0247
	Local heat baseflow	HF	mW/m2	50	
	Thermal longitudinal dispersivity	αT	m	10	10
	Thermal transverse dispersivity	αL	m	1	1
B	Aquifer thermophysical parameters				
	Thermal conductivity of the solid matrix	λ (s)	J/m/s/K	2.4	2.3
	Volumetric heat capacity of the solid matrix	Cv (s)	J/m3/K	2.2E+6	2.2E+6
	Thermal conductivity of the fluid	λ (f)	J/m/s/K	0.61	0.63
	Volumetric heat capacity of the fluid	Cv (f)	J/m3/K	4.1E+6	4.0E+6
	Fluid density	w-ρ	kg/m3	999.2	1009.8
C	System operating parameters				
	"Hot" water injection temperature (ATES)	T max (out)	°C	60÷95 (*)	95
	Minimum fluid temperature, "cold" water reinjection	T min (out)	°C	40	35

5.1 Scenario 1

5.1.1 Model setup

Scenario 1 involves the deep reservoir A3-a, featuring two geothermal doublets (production wells SG2, SG4 and reinjection wells SG1, SG3) along with two ATES storage wells (SG-A, SG-B).

The production and ATES wells are drilled from the same drilling station located in the "Serre" area, while the reinjection wells are drilled from the existing platform in the "San Giovanni" area.

All wells are inclined at 36°. The length of the wells in the model domain (well filter development in target reservoir A3-a) is:

- *production wells*: SG2 = 720 m, SG4 = 766 m
- *reinjection wells*: SG1 = 562 m, SG3 = 508 m
- *ATES wells*: SG-A = 632 m, SG-B = 628 m

The wellhead locations, their projections, and their three-dimensional positions within the stratigraphic model are shown in the following Figure 7 and Figure 8.

For the simulation, a detailed model of the A3-1 reservoir was extracted.

Preliminary simulations indicated that the dynamic footprint of the system extends beyond the originally reconstructed volume of the geological-geothermal model.

For this reason, the model domain was expanded beyond its initial volume, with the sole purpose of applying boundary conditions outside the system's area of influence on the piezometric field. This adjustment was based on a wider buffer zone around the extraction and reinjection wells to ensure accurate hydraulic boundary representation.

The area and volume of validity for the model results are, in any case, referred to the geological-stratigraphic investigation volume and the refined computational grid (see Figure 9, yellow volume).

The ultimate model grid, deconstructed, consists of 13.7E+6 tetrahedral elements, with a minimum diameter of 1 m around the wells. The model was initially run in steady state to redefine, on the new computational grid, the same thermal state already simulated under static conditions ($t=0$ condition for dynamic simulations). Subsequently, the model was run in transient state (flow/heat transport) under the conditions corresponding to the operational design rule.

The "Operational Design Rule for Scenario 1" is illustrated in Figure 11. The diagram specifically represents the flow rates of individual production, storage, and reinjection wells (note: positive values indicate extraction, while negative values indicate reinjection). Additionally, the reinjection temperature is specified: 95°C for storage wells and 35°C for reinjection wells.

The figure shows the typical annual trend. All simulations were conducted assuming a 30-year operational period, with the annual cycle repeated successively throughout the entire timeframe.



Figure 7 Scenario 1 - Wellheads and projection of oriented wells: production (SG2, SG4). ATES storage (SG-A, SG-B), reinjection (SG-1, SG-3)

3333

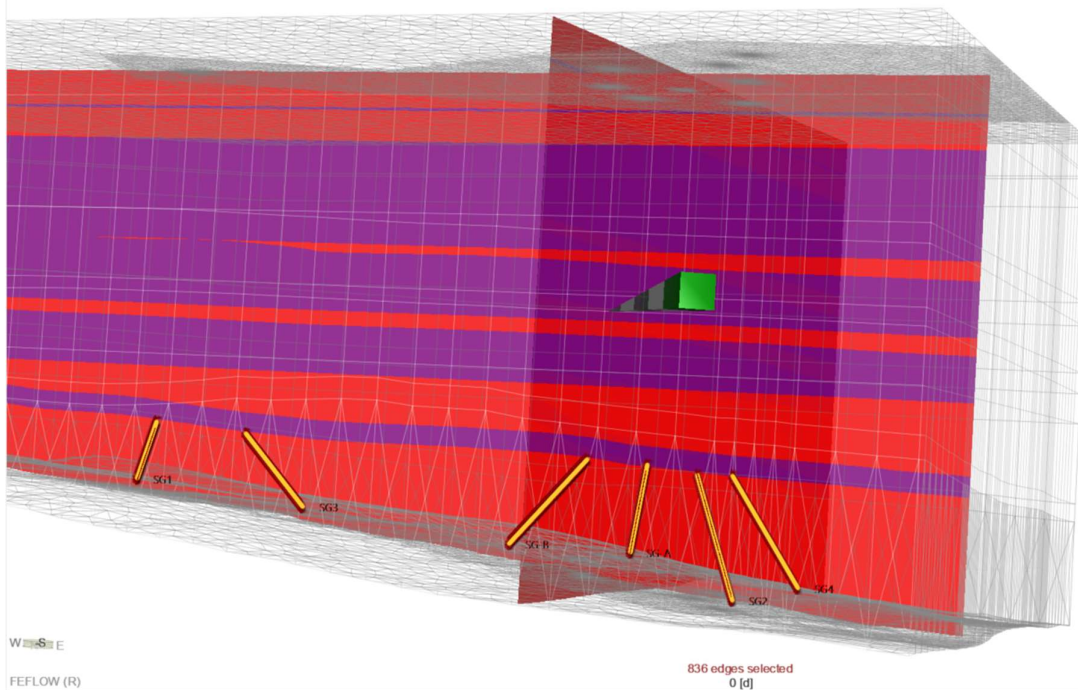


Figure 8 Scenario 1 - Stratigraphic model including production, storage, and reinjection wells (deep 3333reservoir A3-a)

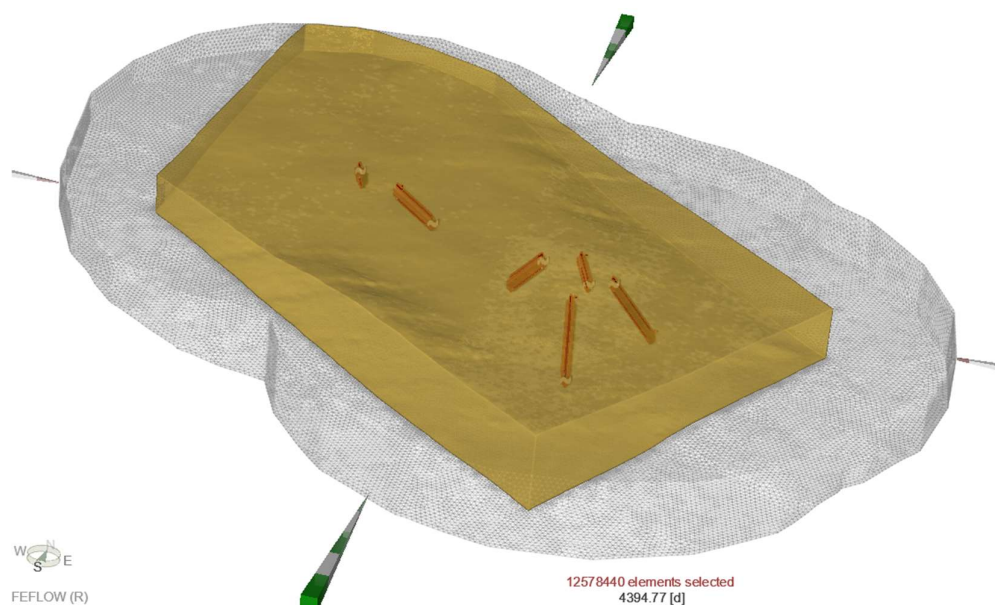


Figure 9 Scenario 1 - Extract from the lower target reservoir model A3-a – Calculation grid.

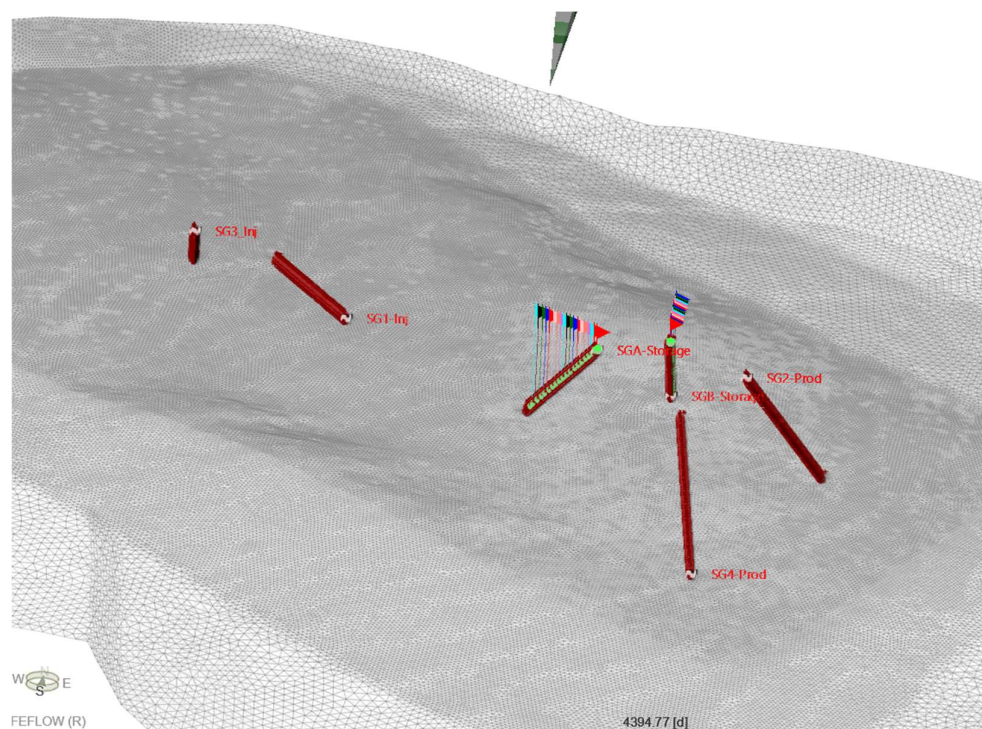


Figure 10 Scenario 1 - Extract from the lower target reservoir model A3-a – Calculation grid, detail.

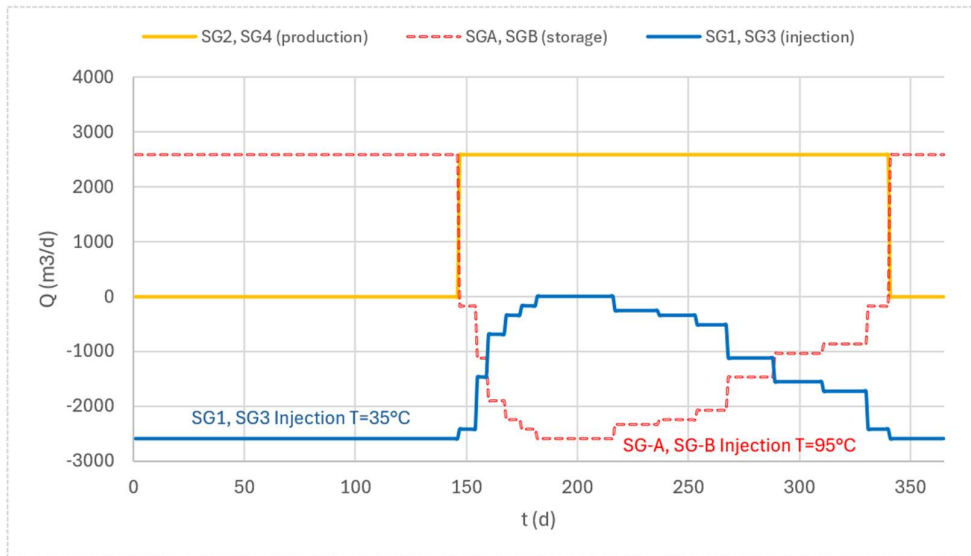


Figure 11 Scenario 1 - Annual pumping schemes (Production, Storage, Injection), and prescribed temperatures at recharge sections - cyclic. Note: positive values = extraction, negative values = reinjection.

5.1.2 Simulation results

The simulation results are presented in the "time-dependent plots of key parameters" (Figure 13÷Figure 19), as previously described and consistently generated for all analyzed scenarios.

- *Hydraulic heads* along the well axis (m) – ref. Figure 13.

Due to moderate to moderately low permeability (50th percentile), the maximum dynamic heads range from +142 m to -110 m, with a static value around 0 m a.s.l..

The difference between positive and negative heads is linked to an increase in the dynamic effect observed during the first two years of extraction and reinjection operations, followed by an asymptotic stabilization of water levels.

- *Heat rate budget* (MW) – ref. Figure 14.

The chart shows the periodic pattern over time (~365-day cycles), indicating the seasonal operation. Peaks (~ +6 MW) correspond to periods of heat injection (storage phase), troughs (~ -6 MW) correspond to periods of heat extraction (recovery phase).

The first cycle exhibits a more pronounced transient response, likely due to initial thermal imbalance and reservoir adaptation. In subsequent cycles, the heat rate budget stabilizes, indicating that the system reaches a predictable quasi-steady-state operation.

The stable pattern suggests no significant thermal breakthrough or short-circuiting occurring within the modeled time frame. No cumulative thermal drift (gradual loss of stored energy due to diffusion) or potential thermal degradation of the aquifer over cycles is observed.

The long-term stability of the heat rate budget suggests that the system is thermally sustainable under current operational conditions.

- *Water temperature* at ATEs storage wells – ref. Figure 15.

The early years show a steeper decline in post-extraction temperatures, indicating that the system was still stabilizing in its initial cycles.

After a few cycles, the temperature decline during extraction becomes less severe, suggesting thermal equilibration of the storage volume.

Over time, the base temperature (post-extraction phase) shows a gradual increase, stabilizing near 75°C. This trend indicates thermal retention in the aquifer, which may be attributed to:

- Heat accumulation in the surrounding formations.
- Incomplete thermal recovery (some heat is not extracted each year).
- *Heat period budget (MWh)* - Figure 17, Figure 18, and *Thermal recovery efficiency charts* for the ATES system (Figure 19)

The heat period budget increases progressively over time, with a clear seasonal cyclic pattern over the simulation period (~30 years). Each cycle corresponds to a full storage and extraction event (injection in summer, extraction in winter).

A positive long-term trend suggests that heat is accumulating in the system, meaning that a portion of the stored energy is not being recovered each year.

The thermal recovery efficiency starts at ~35-40% in the first cycles and gradually increases over time. After 30 years, efficiency reaches above 60%, showing that the system is progressively stabilizing. However, the efficiency does not exceed 65%, which suggests some persistent heat losses in the system.

This issue is likely to be related to the excessive length of the ATES wells increasing the lateral surface of the heat plume other than the strong angle of orientation.

The long inclined wells create an elongated heat plume along their trajectory. Note (Figure 12) that the plume appears stretched along the well length, which means that not all injected heat remains in the optimal thermal recovery zone.

Moreover, since the permeability is much higher in the horizontal direction (6-7 times K_v), strongly inclined wells spread heat laterally, leading to wider heat dispersion instead of a compact thermal zone.

This increased lateral surface area increases conductive and convective heat losses to the surrounding formation, and reduces heat concentration near the production well, making recovery less efficient. Heat loss for buoyancy could also be typical of oriented ATES wells, increasing heat dissipation and more uneven temperature gradients.

5.1.3 Key insights on Scenario 1 ATES performance

Based on the analysis of thermal, hydraulic, and heat recovery trends, the ATES system exhibits stable seasonal operation with gradual improvements in efficiency over time. However, the long term thermal efficiency is suboptimal (~60-65%), with a portion of the injected heat being lost.

✓ Positive Aspects

- ✓ **Stable Seasonal Heat Storage & Extraction:** The heat rate budget and dynamic heads confirm that the system follows a well-defined annual thermal cycle, with no operational anomalies.
- ✓ **Progressive Efficiency Improvement:** The thermal recovery efficiency increases over time, suggesting that some heat is retained within the storage zone, benefitting subsequent extraction cycles.

✓ Hydraulic Stability Without Reservoir Depletion: the dynamic head chart (~+140 m to -110 m) shows strong pressure variations, but no long-term decline in hydraulic performance. The system is operating within safe limits without excessive drawdown or formation damage.

✓ No Early Thermal Breakthrough: The temperature plots do not show abrupt declines, indicating good thermal containment within the aquifer.

⚠ Key issues & Limitations

⚠ Excessive Heat Accumulation Over Time (Incomplete Recovery). The Heat Period Budget chart shows progressive heat accumulation, meaning that not all injected heat is extracted. This suggests that some heat is being permanently lost due to lateral dispersion into less recoverable zones.

⚠ Efficiency Plateaus Around 60-65%: The recovery efficiency is improving but remains below optimal values (>70-80%). This suggests that some heat losses persist, likely due to thermal diffusion and aquifer dispersion effects.

Relevant reasons for inefficiencies:

⚠ Excessive well length / storage surface. If the total heat stored is large, a long well may be beneficial. However, if storage is not proportionate to well length, the large exchange surface increases heat loss rather than improving recovery. In this case, the long well appears to increase lateral heat dispersion instead of contributing to efficient stratified storage.

Design key questions: *does the long well contribute to higher recovery, or does it mostly increase heat loss? Is the well length proportionate to the total amount of heat stored?*

⚠ Anisotropic Permeability ($K_h \approx 6-7 K_v$) + inclined well promotes lateral heat spread (increased thermal dispersivity. A steep well (closer to vertical) helps confine heat in a more compact, stratified manner, while an inclined well (like the design 36° setup) allows heat to spread more laterally, increasing loss potential.

Design key question: *Would a different well orientation reduce heat dispersion while maintaining sufficient storage?*

⚠ operations in bidirectional ATEs systems cycles involve sudden reversals in flow direction, with maximum overall pressure variations reaching several hundred meters (see also uncertainty analysis, par. 5.1.5.1). Potential geotechnical issues and long-term effects due to these pressure buildup/fall in the fine-sandy and silty-sandy reservoir deposits should be carefully evaluated through geotechnical and well performance modelling.

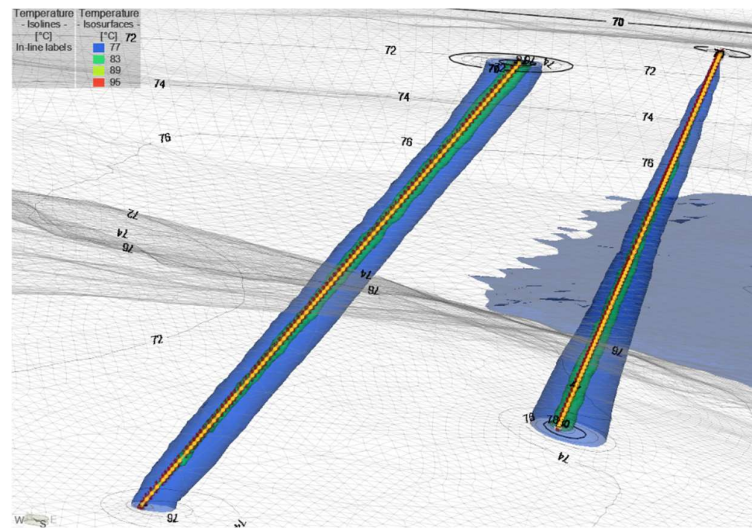


Figure 12 Scenario 1 – Isosurfaces of the thermal plume at ATES wells.

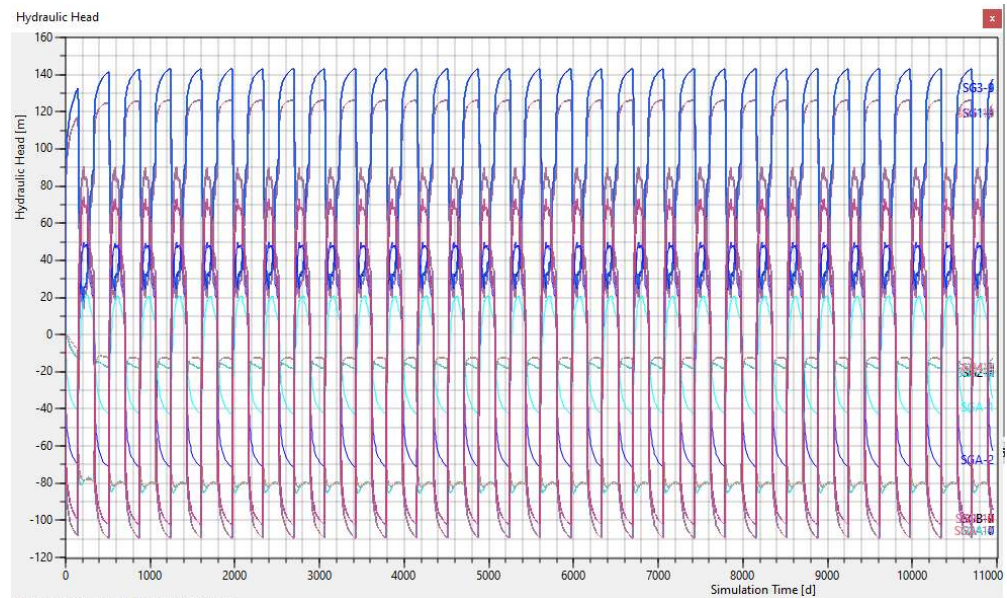


Figure 13 Scenario 1 - Hydraulic heads Vs. time (30 years of operation)

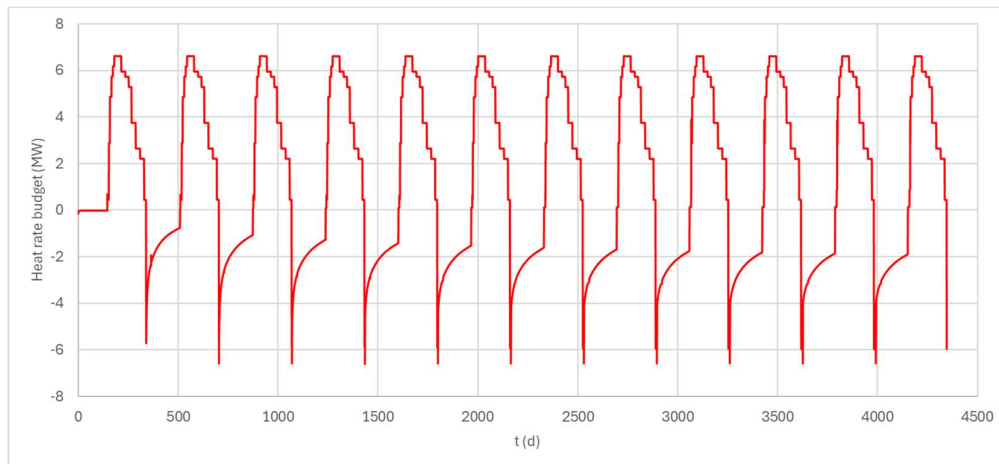


Figure 14 Scenario 1 - ATES Storage reservoir A3-a: Heat rate budget (MW) Vs. time – detail, to parameter stabilization.

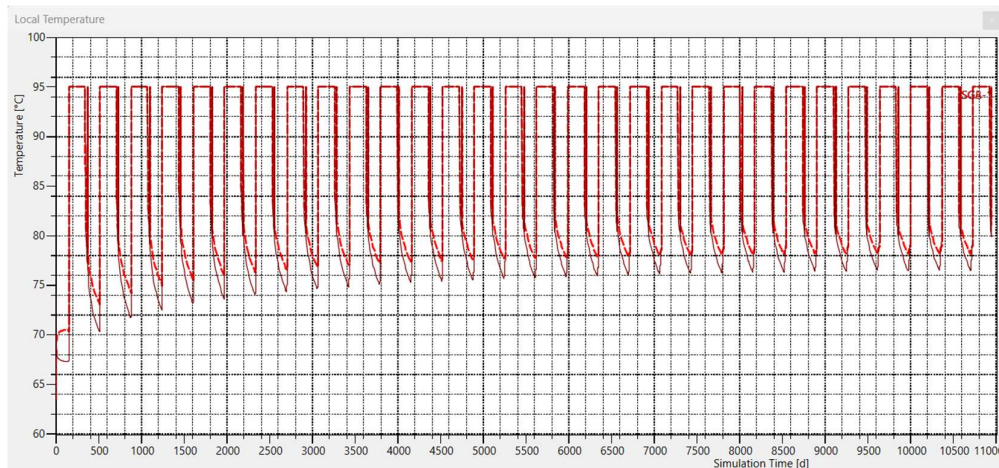


Figure 15 Scenario 1 - Temperature Vs. time, ATES wells: SG-A (red dash), SG-B (dark red, solid) - (30 years of operation)

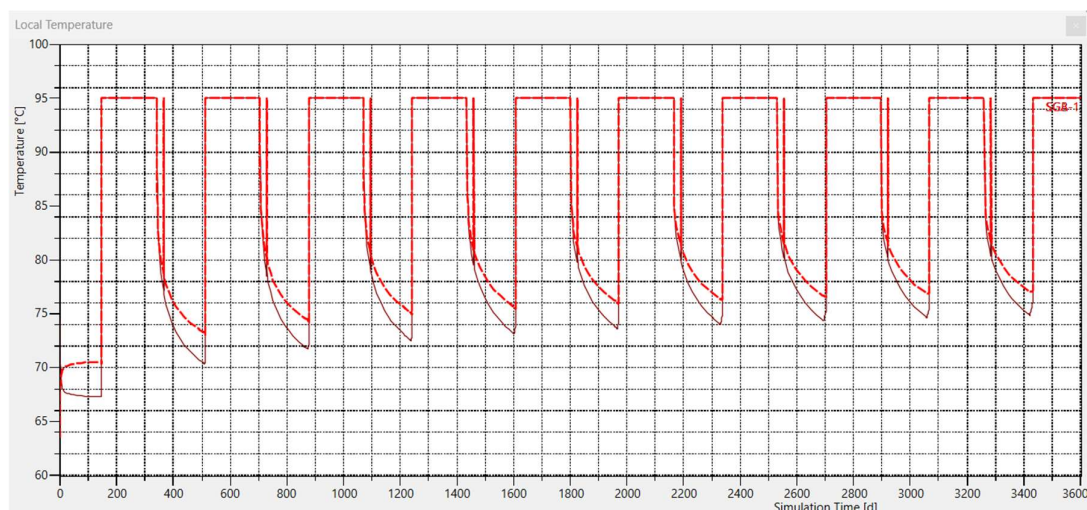


Figure 16 Scenario 1 - Temperature Vs. time, ATES wells: SG-A (red dash), SG-B (dark red, solid) – detail over 10 years of operation

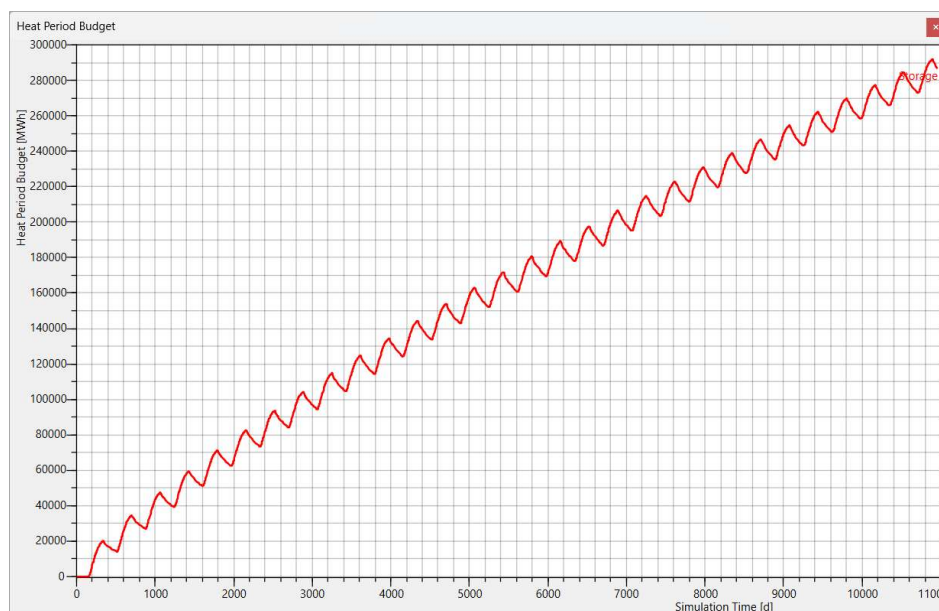


Figure 17 Scenario 1 - ATES Heat period budget (MWh) based on 30 years of operation.

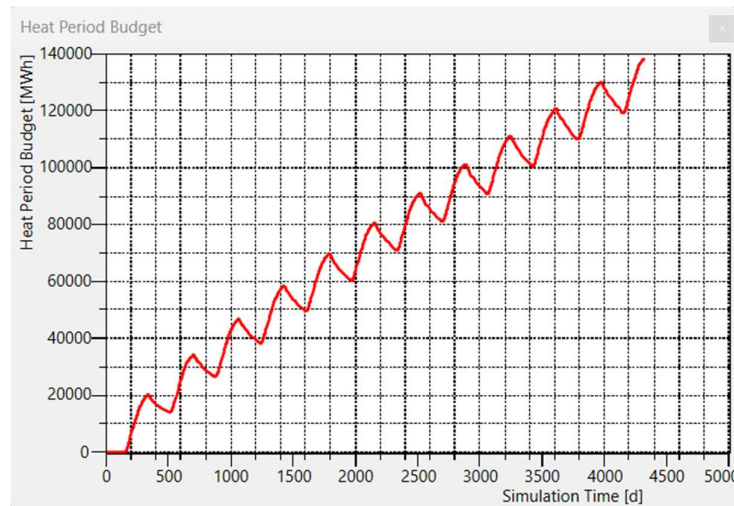


Figure 18 Scenario 1 - ATES Heat period budget (MWh) - detail, first decade of operation.

cycle	endtime (d)	stored (MWh)	discharged (MWh)	Eff%
1	510.9	20253.95	6327.9	31.24
2	875	20332.75	7713.72	37.94
3	1238.96	20321.09	8526.53	41.96
4	1603	20310.91	9091.28	44.76
5	1967	20301.86	9526.49	46.92
6	2331	20293.17	9827.21	48.43
7	2695	20285.1	10113.65	49.86
8	3059	20277.26	10426.9	51.42
9	3423	20249.8	10631.35	52.5
10	3787	20201.8	10805.99	53.49
11	4151	20155.17	10962.31	54.39
12	4515	20109.48	11088	55.14
13	4879	20064.76	11247.34	56.06
14	5243	20005.03	11354.69	56.76
15	5607	19930.96	11279.98	56.6
16	5971	19857.24	11521.86	58.02
17	6335	19784.7	11592.66	58.59
18	6699	19713.43	11657.85	59.14
19	7063	19642.78	11711.76	59.62
20	7427	19571.82	11763.94	60.11
21	7791	19501.95	11807.88	60.55
22	8155	19426.99	11848.55	60.99
23	8519	19344.13	11844.38	61.23
24	8883	19261.08	11907.29	61.82
25	9247	19170.82	11923.66	62.2
26	9611	19098.49	11946.16	62.55
27	9975	19017.1	11962.73	62.91
28	10339	18936.03	11975.91	63.24
29	10703	18850.51	11986.72	63.59
total		574270.16	314374.69	

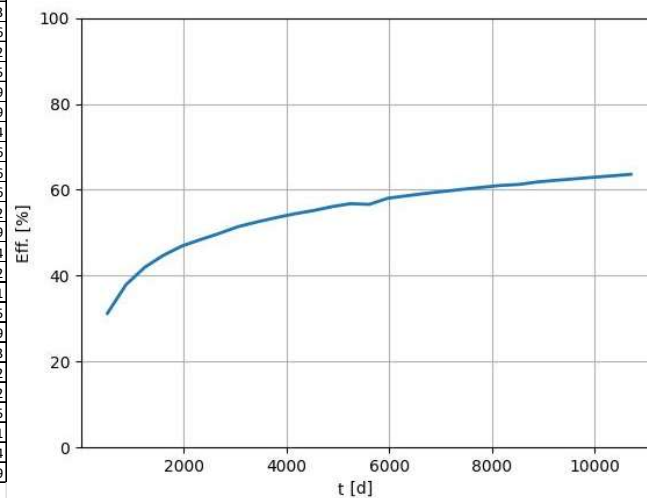


Figure 19 Scenario 1 - ATES efficiency (Heat stored / Heat recovered), annual storage cycles, based on 30 years of operation.

5.1.4 Preliminary estimation of exchanged power and process efficiency

The chart in Figure 20, presents the total pumping head (sum of extraction and injection heads) over a 30-year operational period for the ATES system and the overall production plant. The pumping head is a critical parameter as it directly affects operational efficiency, energy consumption, and long-term sustainability of the system.

The total pumping head fluctuates between ~350 m and ~550 m, with an average stable trend of ~450 m. This indicates that the system operates consistently without hydraulic resistance build-up or pressure losses over time.

The efficiency of the overall system (COP or EPEI - Energy Produced to Energy Invested) is determined by the ratio W_{th}/W_{el} , which represents the relationship between the exchanged

thermal power and the electrical energy required for reinjecting the fluids into the reservoir via a booster pump, considering the calculated flow rate and the necessary pressure integration.

The electrical consumption of a high-pressure pump can be estimated using the following formula:

$$W_{el} = \frac{\rho(\text{kg/m}^3) \cdot g(\text{m/s}^2) \cdot Q(\text{m}^3/\text{s}) \cdot H(\text{m})}{\mu} \quad (1)$$

Where:

W_{el} = power (J/s, W)

ρ = fluid density (kg/m^3),

g = gravitational acceleration (m/s^2)

Q = flow rate (m^3/s)

H = extraction + reinjection pressure (mH_2O)

μ = pump efficiency (dimensionless)

Considering an approximate pump efficiency of $\mu = 0.7$ (70%), based on the physical parameters, flow rate values, and related pumping injection pressure, the calculated values of W_{el} , efficiency, and net power are reported in the following Figure 21.

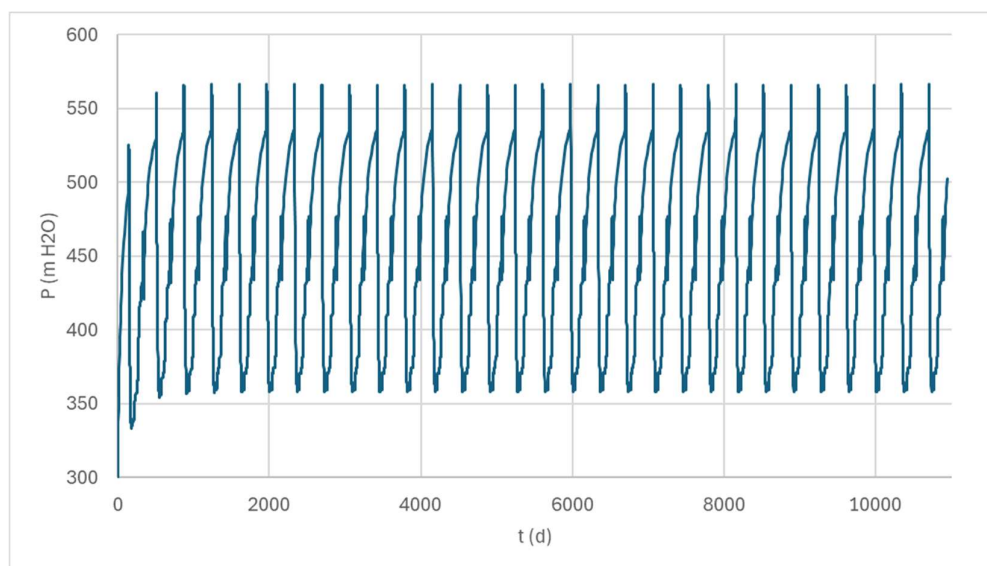


Figure 20 Scenario 1 - Total pumping head (extraction/injection) vs. time – Overall production plant + ATEs system (30 years of operation)

¹ Equivalente alla formulazione classica con pressione in mH₂O, $P(W) = \rho(\text{kg/m}^3) \cdot g(\text{m/s}^2) \cdot Q(\text{m}^3/\text{s}) \cdot H(\text{m}) / \mu$

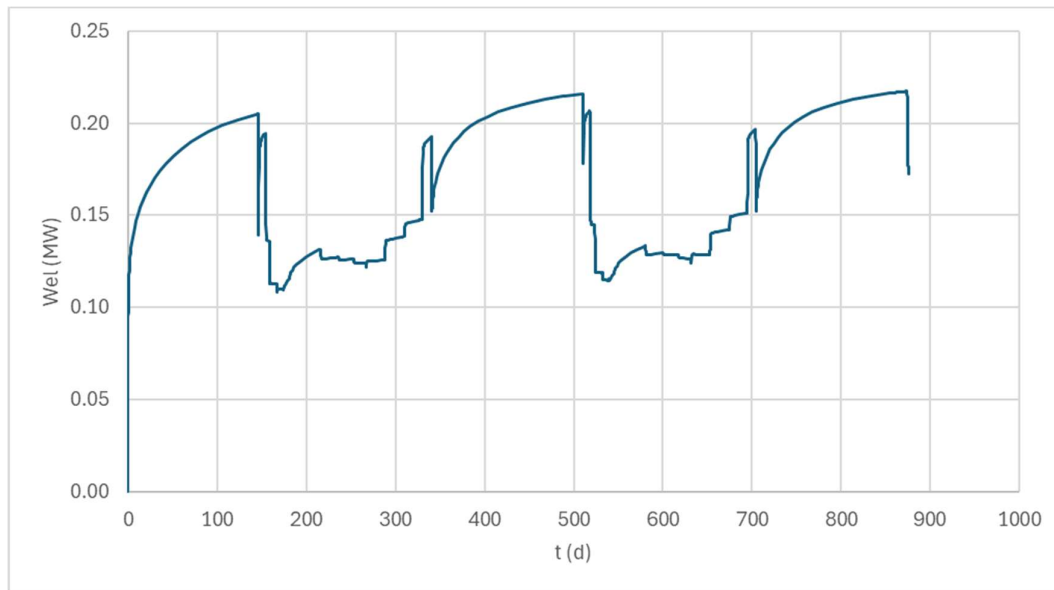


Figure 21 Scenario 1 - Energy invested for pumping and injection vs. time.

5.1.5 Sensitivity analysis and model uncertainty

Based on the thermal and hydrodynamic analysis, a sensitivity analysis assesses parameter variations related to the major identified inefficiencies in the ATEs system. The main objectives are to evaluate system response to extreme conditions and to identify potential solutions to improve performance.

The analysis focuses on two key uncertainties:

a) Minimum permeability values (10th percentile) to analyze the worst-case hydraulic response and pumping requirements.

The current hydraulic analysis shows that total pumping heads are high (Σ positive negatives: ~450 m H₂O average, with fluctuations between 350-550 m H₂O, rif. Figure 20), suggesting that hydraulic resistance is significant.

If permeability is lower than expected (10th percentile case), this causes increased pressure losses, leading to higher pumping energy demand and/or reduced well productivity/injectivity, requiring adjustments in operational flow rates.

b) Minimum longitudinal/transverse dispersivity values to evaluate their impact on thermal containment and efficiency.

Dispersivity parameters (longitudinal and transverse) control how heat is transported and mixed in the aquifer: Higher dispersivity = More heat mixing and lateral spreading, increasing losses, Lower dispersivity = More confined heat storage, but potentially higher localized temperature gradients.

As Analysis approach, the minimum values of longitudinal and transverse dispersivity case assesses:

- thermal containment effects (whether heat plumes become more compact);
- heat recovery efficiency trends (potential improvements if heat loss is reduced).

- potential risks of excessive temperature gradients (if too localized, heat transfer is impaired).

5.1.5.1 Permeability

The hydraulic heads were re-calculated using the minimum K value resulting from the hydrogeological and stratigraphic study, $K_h = 4.2E-7$ m/s). Ratio K_h/K_v is maintained on the original value ≈ 6 .

The chart in Figure 22 displays hydraulic head variations over time under the above conditions of reduced permeability.

Compared to the previous hydraulic head analysis with average permeability, the fluctuations in hydraulic head are significantly larger (higher pressure buildup during injection and greater drawdown during extraction). The maximum positive heads (injection phase) exceed 200-240 m, while the negative heads (extraction phase) reach -160 to -180 m.

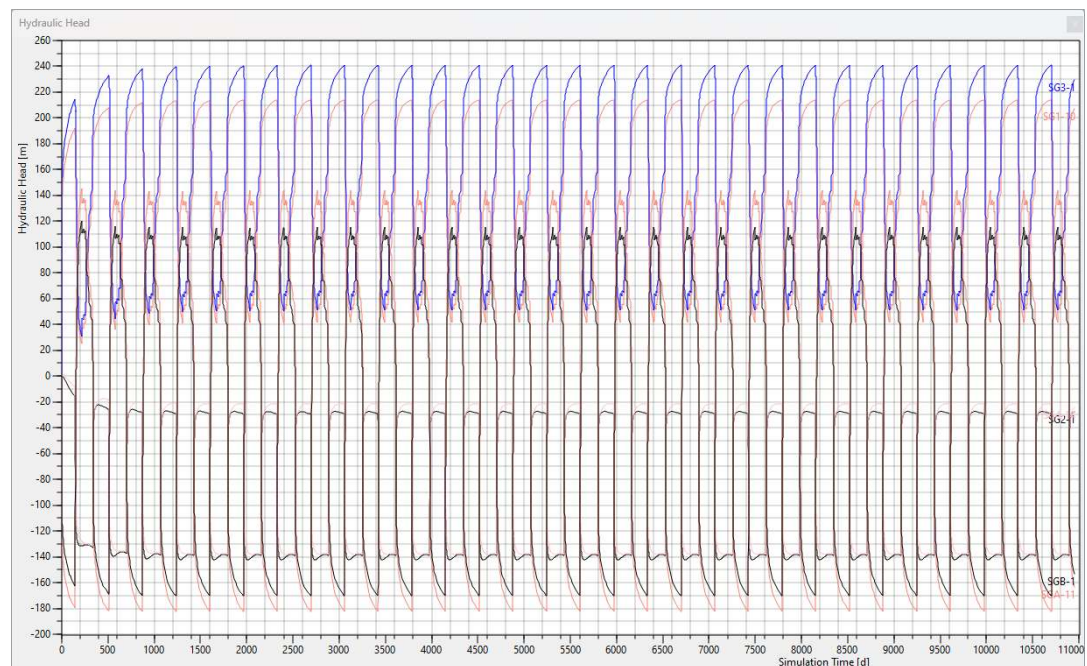


Figure 22 Scenario 1 (sensitivity analysis), $K_{min} (K_{x,y} = 4.2E-7$ m/s) - Hydraulic heads Vs. time (30 years of operation)

Note that:

- the calculated head losses and gains in the production / ATEs system refer to reservoir hydraulics, meaning they account for fluid flow through the aquifer, but do not directly represent the actual pressure conditions at the wellhead. The wellhead drawdown and pressure buildup depend on additional well-specific factors, such as well efficiency, skin effect, and local flow dynamics, which in turn are influenced by well design and its effective realization. Well efficiency in deep geothermal typically ranges from 60% to 85%.
- potential geotechnical issues due to increased pressure in the fine-sandy and silty-sandy reservoir deposits is outside the present Scope Of Work. Issues as formation damage due to sand mobilization reducing injectivity over time, reservoir compaction, dislodgement of fine particles clogging well screens and reducing efficiency, internal erosion or fines migration impacting reservoir stability should be carefully evaluated through geotechnical modelling.

5.1.5.2 Heat transport parameters

Scenario 1 plant is a bidirectional ATES System. Since this ATES system does not operate with separate injection and extraction wells, but instead both wells alternate between heat injection and recovery seasonally, the traditional method of estimating longitudinal dispersivity based on well spacing is not directly applicable. Instead, dispersivity should be assessed based on the characteristic scale of thermal transport within the reservoir, considering the flow dynamics created by seasonal operation.

Due to the well length, simulations showed the dimension of the plume radius not exceeding the hundred of meters.

According to empirical relationships for dispersivity in fine sands and silty sands (Gelhar et al., 1992; Schulze-Makuch, 2005):

$$\alpha L \approx 0.01-0.1 \times L$$

where L is the characteristic flow path length (here, the thermal plume radius of 100 m). Applying this rule:

- lower bound (conservative, minimal dispersion strong thermal containment):

$$\alpha L = 1 \text{ to } 5 \text{ m}$$

- mid-range (best estimate for fine sands, balancing recovery and controlled heat spread):

$$\alpha L = 5 \text{ to } 10 \text{ m}$$

- upper bound (Higher dispersion, moderate heat spreading but with increased losses):

$$\alpha L = 10 \text{ to } 15 \text{ m}$$

The chart displays the evolution of the heat period budget over time for the ATES system under two different dispersivity conditions:

- red line: standard Mid-range case with 50th percentile dispersivity values ($\alpha L = 10 \text{ m}$, $\alpha T = 1 \text{ m}$).
- dotted blue line: minimum dispersivity case ($\alpha L = 1 \text{ m}$, $\alpha T = 0.1 \text{ m}$), representing a scenario where thermal dispersion is significantly reduced.

This sensitivity analysis investigates how reduced dispersivity affects heat storage and recovery efficiency. The gap between the two curves grows with time, indicating that heat dispersion effects become more pronounced over multiple operational cycles.

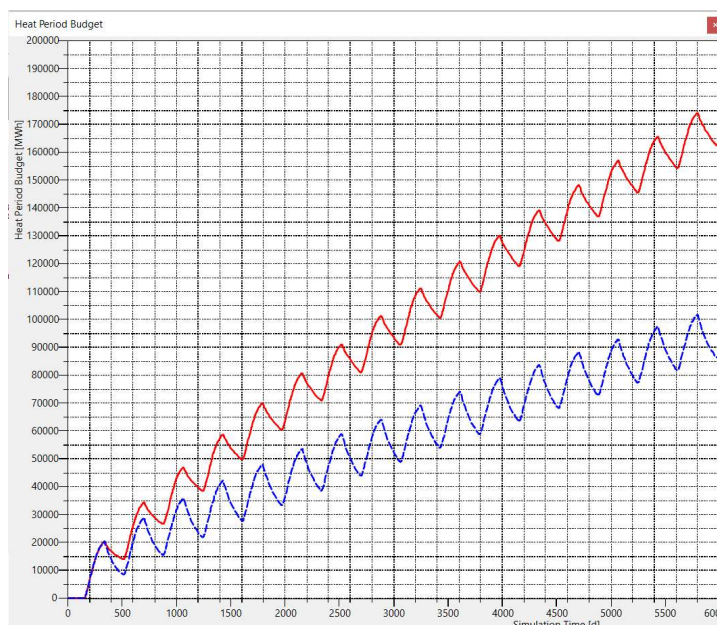


Figure 23 Scenario 1 (sensitivity analysis) - Heat reate budget of the ATEs storage over time resulting from the sensitivity analysis on the model input parameters (based on 30 years of operation): in red: standard 50th percentile dispersivity ($\alpha L=10$ m, $\alpha T=1$ m), dotted bue: minimum dispersivity values ($\alpha L=1$ m, $\alpha T=0.1$ m)

A simplified assumption can be made that ATEs efficiency varies linearly with dispersivity. This allows us to estimate efficiency values for different αL scenarios using a linear interpolation approach.

So, from the sensitivity analysis the calculated ATEs efficiency results:

$\eta \approx 62\%$ for $\alpha L = 10$ m (best estimate)

$\eta \approx 74\%$ For $\alpha L = 1$ m (lower bound, best scenario)

$\eta \approx 55\%$ For $\alpha L = 15$ m (upper bound, worst-case scenario, from linear interpolation)

5.2 Scenario 2

5.2.1 Model setup

Scenario 2 consists of two independent and autonomous systems.

The geothermal production section, as in the previous Scenario 1, utilizes the deep reservoir A3-a and includes two geothermal doublets, with production wells SG2 and SG4 and reinjection wells SG1 and SG3.

In addition, a bi-directional ATEs system is planned within the A1-a reservoir (wells P1, P2, “greenhouses” area), at depths of approximately 200 to 360 m below ground level, for the seasonal storage of heat. This stored heat is seasonally generated using heat pump, with its electricity demand supplied by solar power.

Same as for Scenario 1 the production wells are drilled from the same drilling station located in the "greenhouses" area, while the reinjection wells are drilled from the existing platform in the "San Giovanni" area.

All production / reinjection wells are inclined at 36°. The length of the wells in the model domain (well filter development in target reservoir A3-a) is:

- *production wells*: SG2 = 720 m, SG4 = 766 m

- *reinjection wells*: SG1 = 562 m, SG3 = 508 m

The ATES wells are vertical, fully completed in the reservoir A1-a, filter length approximately 160 m.

The wellhead locations, their projections, and their three-dimensional positions within the stratigraphic model are shown in the following Figure 24 and Figure 25.

For the production simulation, the same detailed model setup of the A3-1 reservoir was used (excluding SG-A, SG-B pumping locations). and considering new pumping-injection.

Same as in the previous case preliminary simulations indicated that the dynamic footprint of the system extends beyond the originally reconstructed volume of the geological-geothermal model.

For this reason, the model domain was expanded beyond its initial volume, with the sole purpose of applying boundary conditions outside the system's area of influence on the piezometric field. This adjustment was based on a wider buffer zone around the extraction and reinjection wells to ensure accurate hydraulic boundary representation.

The area and volume of validity for the model results are, in any case, referred to the geological-stratigraphic investigation volume and the refined computational grid (see previous Figure 9, yellow volume).

The ultimate reservoir A3-a model grid, deconstructed, consists of 13.7E+6 tetrahedral elements, with a minimum diameter of 1 m around the wells. The model was initially run in steady-state to redefine, on the new computational grid, the same thermal state already simulated under static conditions ($t=0$ condition for dynamic simulations). Subsequently, the model was run in transient state (flow/heat transport) under the conditions corresponding to the operational design rule.

The stand-alone model of the ATES system involves the extraction and detailed refinement of the specific shallow complex (depth 0–360 m), including A1-a aquifer. The structured/layered model consists of 202,450 elements (triangular prisms). The domain, covering the local "Greenhouses" area where the ATES system is planned, extends within a 600 m buffer around the wells.

The model features a refined grid resolution of 1 m around the wells and a vertical refinement (slice spacing) of 10 m.

In this phase 3 different "Operational Design Rule Scenarios" were tested (Scenarios 2-a, 2-b, 2-c), as illustrated in Figure 26, Figure 27 and Figure 28. The diagram specifically represents the flow rates of individual production, storage, and reinjection wells (note: positive values indicate extraction, while negative values indicate reinjection). Additionally, the reinjection temperature is specified: 95°C for storage wells and 35°C for reinjection wells (Scenarios 2-a, 2-b) and 60°C (Scenario 2-c).

The figure shows the typical annual trend. All simulations were conducted assuming a 30-year operational period, with the annual cycle repeated successively throughout the entire timeframe.



Figure 24 Wellheads and projection of oriented wells (ref. Figure 25). A3-2 reservoir: production (SG2, SG4), reinjection (SG-1, SG-3). Aquifer A1-a: ATES storage (vertical: SG-A, SG-B)

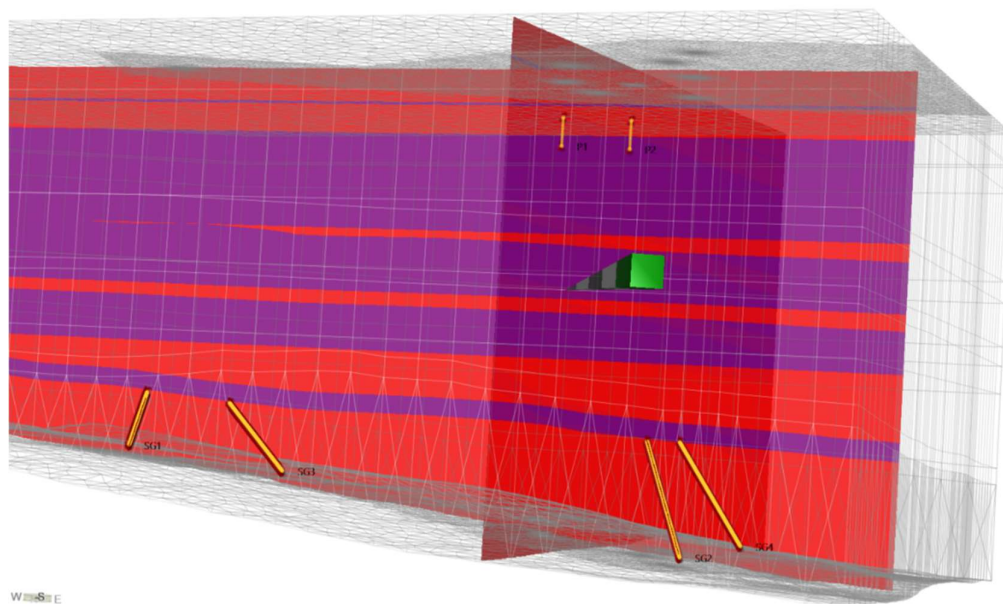


Figure 25 Stratigraphic model including production / reinjection wells (deep reservoir A3-a), and the independent heat storage doublet (shallow reservoir A1-a)

Table 3 “Operational Design Rule Scenarios” tested

Scenario	ATES Injection T°C	ATES injection Q l/s	Stored heat source
2-a	95	Constant, ± 30.0	Heat pump
2-b	95	Variable, max ± 60.0	Heat pump
2-c	60	Variable, max ± 56.2	Seasonal redundancy from deep production doublets

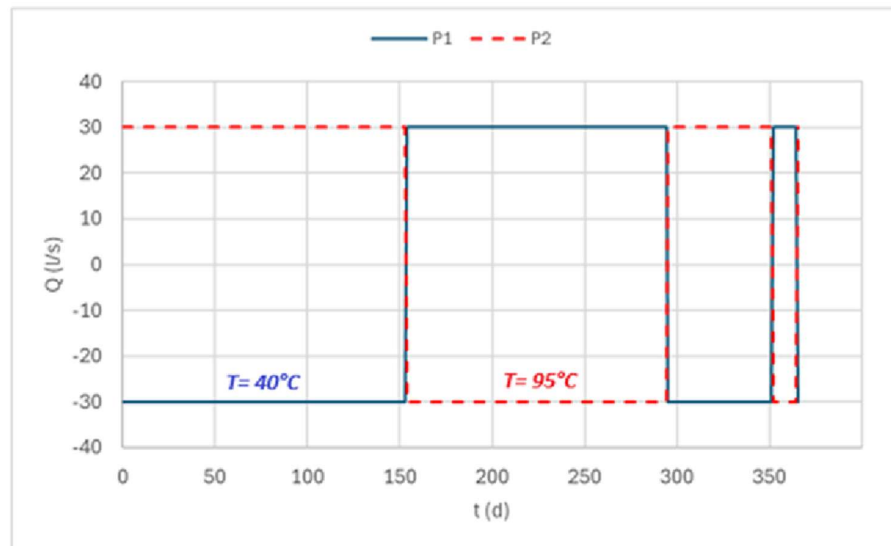


Figure 26 Scenario 2-a - Annual pumping schemes (discharge, injection temperature), cyclic. Note: positive Q values = extraction, negative Q values = reinjection

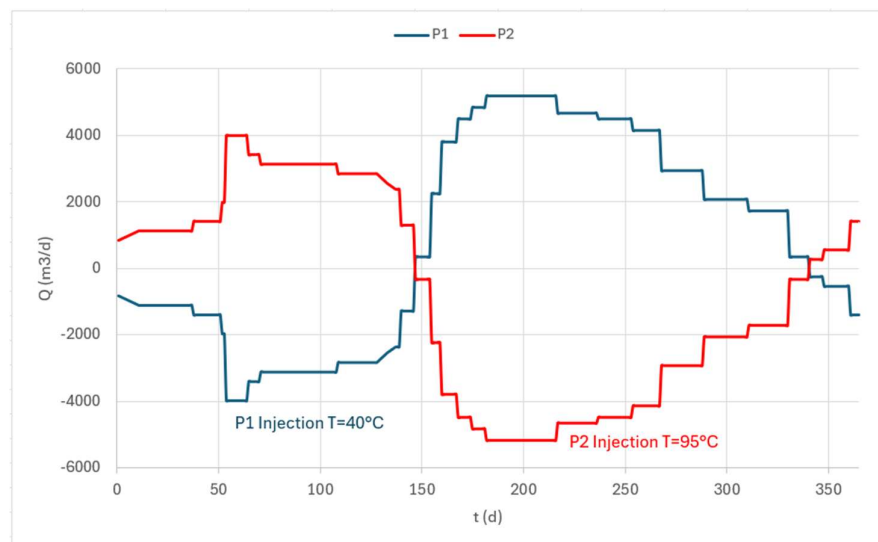


Figure 27 Scenario 2-b - Annual pumping schemes (discharge, injection temperature), cyclic. Note: positive Q values = extraction, negative Q values = reinjection

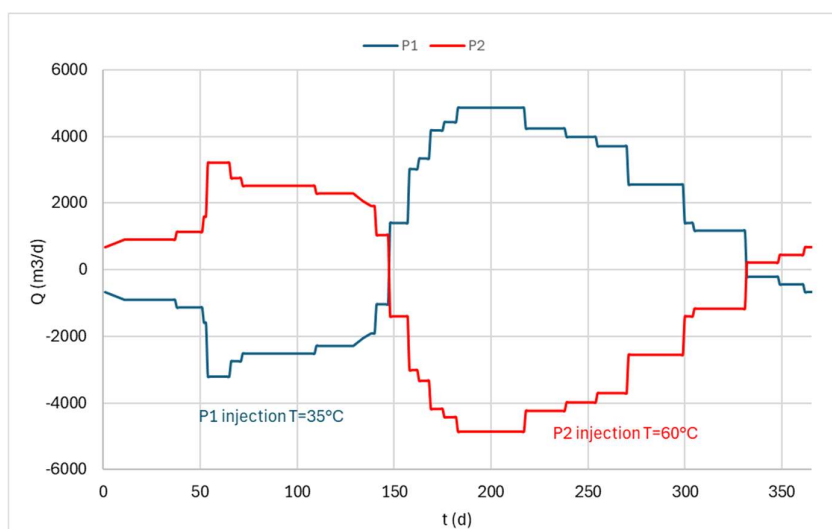


Figure 28 Scenario 2c (injection temperature optimization) - Annual pumping schemes (discharge, injection temperature), cyclic. Note: positive Q values = extraction, negative Q values = reinjection

5.2.2 Simulation results: heat storage section (reservoir A1-a)

5.2.2.1 Heat recharge pattern “a” (Scenario 2-a)

The simulation results are presented in the "time-dependent plots of key parameters" (Figure 31+Figure 36), as previously described and consistently generated for all analyzed scenarios.

- *Hydraulic heads* along the well axis (m) – ref. Figure 31, Figure 32.

The oscillations in hydraulic head are highly regular, showing a predictable seasonal pattern corresponding to annual heat injection and extraction cycles.

The consistent amplitude and frequency suggest that the ATEs system is operating under stable hydraulic conditions, with no long-term pressure drift.

The maximum and minimum hydraulic heads fluctuate in a limited range between +10 m and -10 m, which indicates balanced injection and extraction rates throughout each cycle.

Long-term hydraulic buildup is limited, meaning the system is well-sized for the reservoir, which leads to minimal risk of excessive overpressure or drawdown, reducing geotechnical risks such as formation compaction or leakage.

- *Heat rate budget* (MW) – ref. Figure 33.

The chart shows a periodic heat rate pattern over time (~365-day cycles), confirming the seasonal operation of the shallow ATEs system. Peaks (~ +9 MW) correspond to periods of heat injection (storage phase), while troughs (~ -9 MW) correspond to periods of heat extraction (recovery phase).

The first cycle exhibits a more pronounced transient response, likely due to initial thermal imbalance and adaptation of the aquifer to cyclic storage conditions. In subsequent cycles, the

heat rate budget stabilizes, indicating that the system reaches a predictable quasi-steady-state operation.

The stable pattern suggests no significant thermal breakthrough or short-circuiting occurring within the modeled time frame. No cumulative thermal drift (gradual loss of stored energy due to diffusion) or thermal degradation of the aquifer over cycles is observed, supporting the long-term thermal sustainability of the system.

- *Water temperature* at ATES storage wells – ref. Figure 34.

The early years show a steeper decline in post-extraction temperatures, indicating that the system was still stabilizing in its initial cycles. This suggests an initial phase where thermal equilibrium had not yet been established, and some heat may have been dissipated into the surrounding formation.

After a few cycles, the temperature decline during extraction becomes less severe, suggesting thermal equilibration of the storage volume. The system begins to stabilize, and seasonal heat recovery becomes more predictable.

Over time, the base temperature (post-extraction phase) remains stable, without a significant upward or downward trend. This suggests:

Limited long-term heat accumulation in the surrounding formations, indicating that the system is efficiently cycling thermal energy.

Consistent seasonal heat recovery, meaning that most of the injected energy is being successfully recovered.

The red curve (P2) shows a stable seasonal pattern of hot water injection ($\sim 90^{\circ}\text{C}$) and recovery, confirming that the system maintains a predictable thermal regime over time. The blue curve (P1) remains at lower temperatures ($\sim 35\text{--}40^{\circ}\text{C}$), suggesting a controlled separation between the warm and cool thermal zones within the storage system.

The long-term stability of the temperature cycles suggests that the ATES system is thermally sustainable and highly effective under current operational conditions.

- *Heat period budget* (MWh) - Figure 35, and *Thermal recovery efficiency charts* for the ATES system (Figure 36)

The heat period budget increases progressively over time, showing a clear seasonal cyclic pattern across the 30-year simulation period. Each cycle represents a full storage and extraction event.

A positive long-term trend suggests that heat is gradually accumulating in the system. However, the high thermal recovery efficiency ($\sim 90\text{--}95\%$) after 30 years indicates that most of the injected heat is retained within the active thermal storage zone and successfully recovered over subsequent cycles.

The 3D isosurface visualization of the temperature field (Figure 30) confirms that the thermal plumes remain compact and vertically stratified; the temperature gradients (ref. also Figure 29) are relatively steep, meaning that most of the stored heat remains localized around the wells, which aligns with the high observed recovery efficiency.

Unlike Scenario 1, where the elongated heat plume resulted in lower recovery efficiency ($\sim 60\text{--}65\%$) due to lateral heat losses, Scenario 2-a shows higher recovery efficiency ($\sim 90\text{--}95\%$) after 30 years, suggesting that injected heat remains within the active storage zone. These factors suggest that this configuration is better suited for long-term seasonal thermal storage, as thermal retention is significantly higher, and the system stabilizes with minimal energy losses (see par. 7.1 for details).

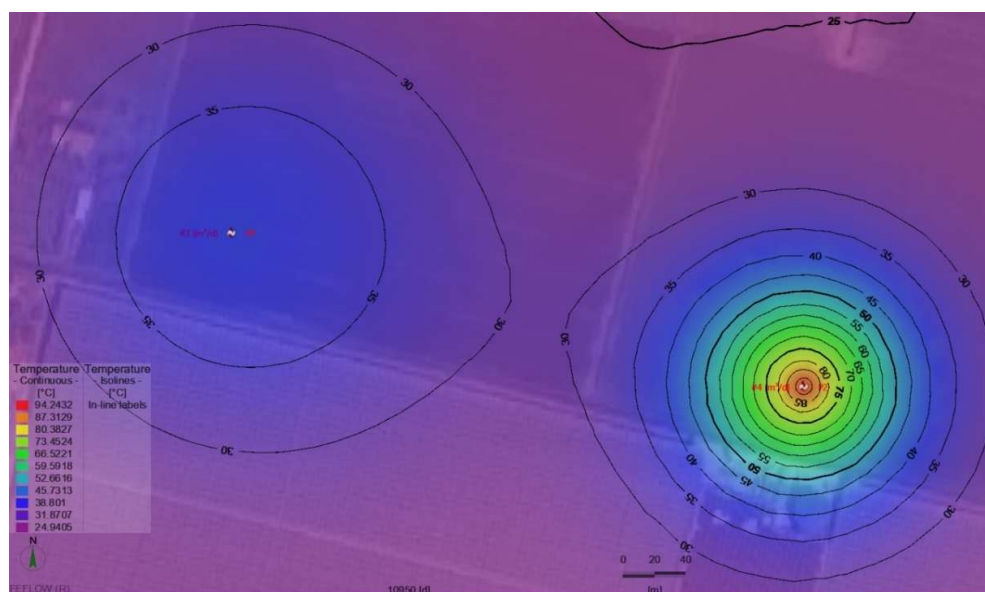


Figure 29 Temperature contours at the base of reservoir A1-a (heat storage wells), at year 30 of operation

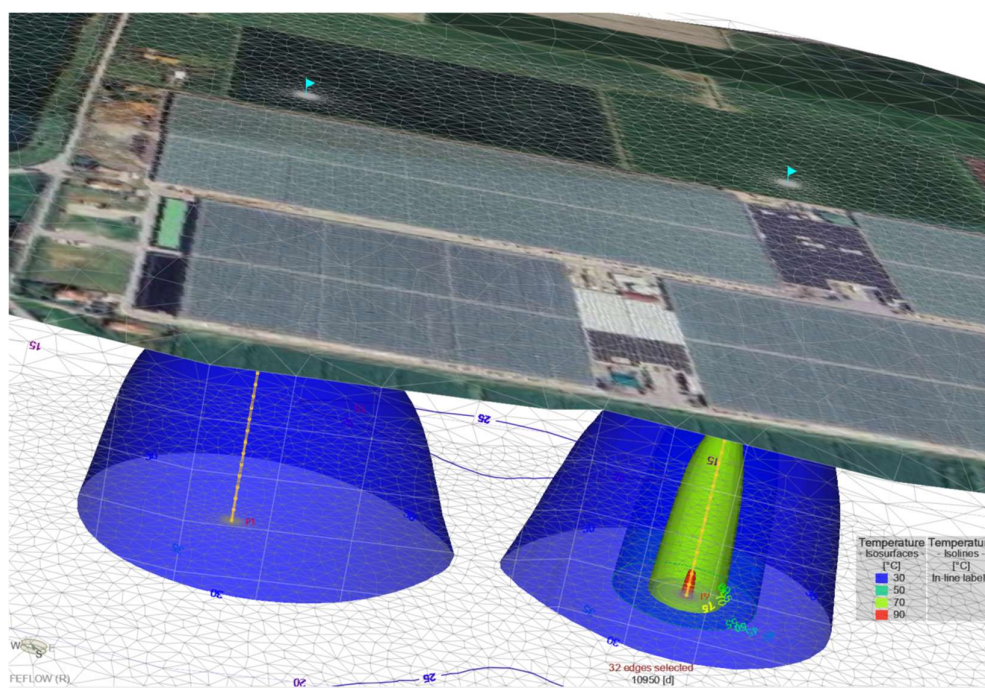


Figure 30 Temperature isosurfaces, reservoir A1-a (heat storage wells), at year 30 of operation

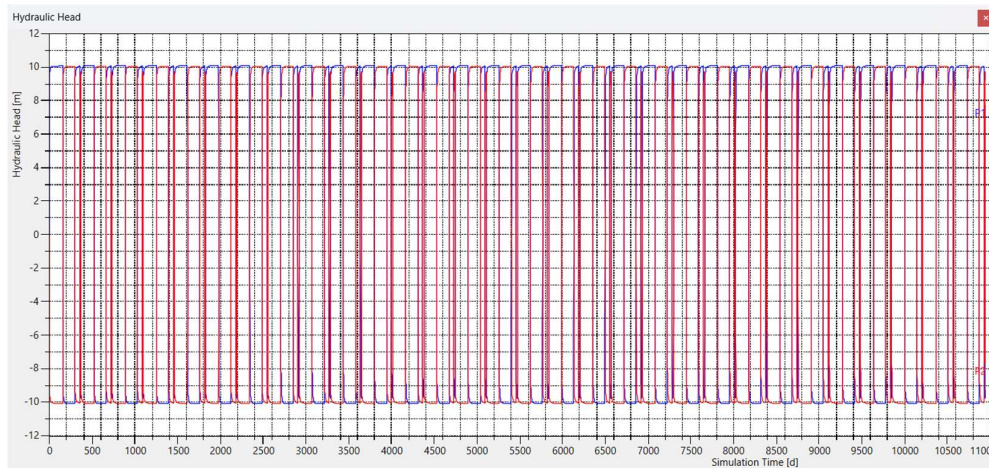


Figure 31 Scenario 2-a: hydraulic heads Vs. time (30 years of operation)

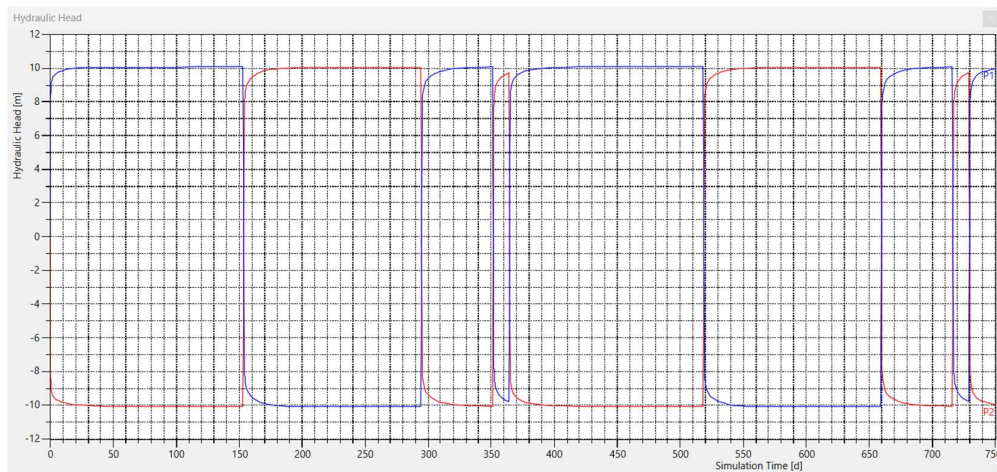


Figure 32 Scenario 2-a: hydraulic heads Vs. time (detail)

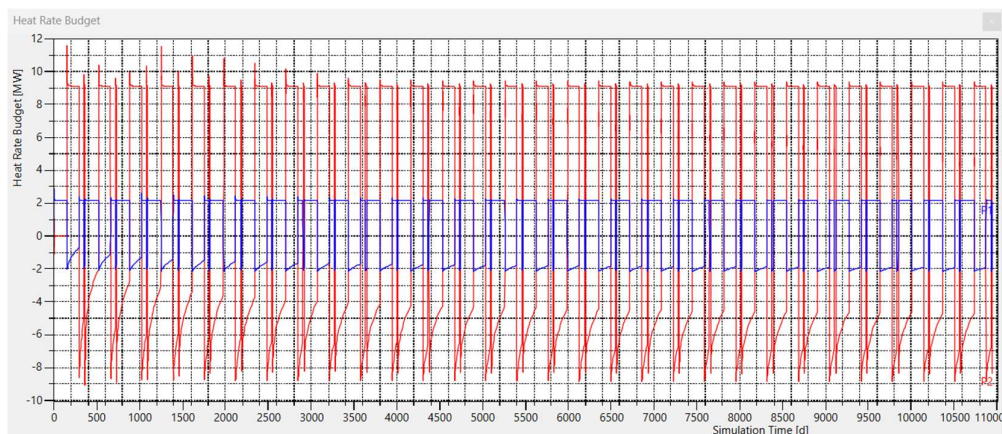


Figure 33 ATEs Storage reservoir A1-a: Heat rate budget (MW) Vs. time (P1 blue, P2 red) - (30 years of operation)

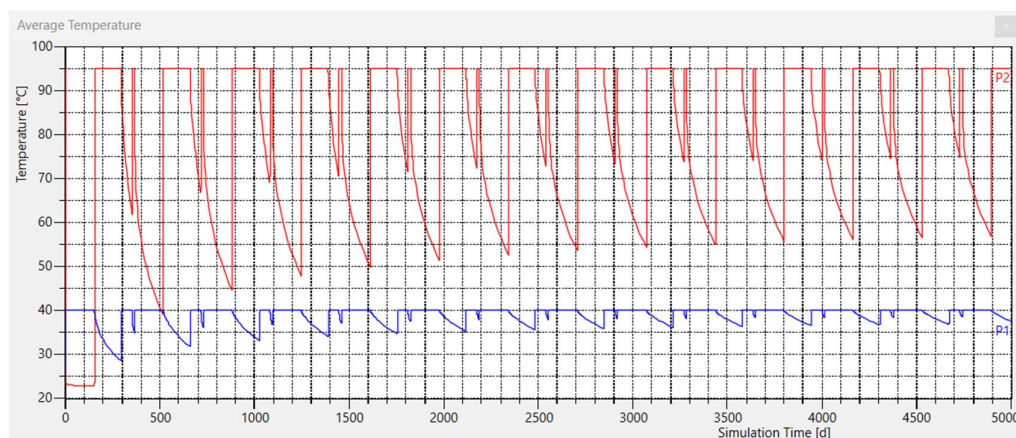


Figure 34 Scenario 2-a: temperature Vs. time, ATEs wells (P1 blue, P2 red) – detail.

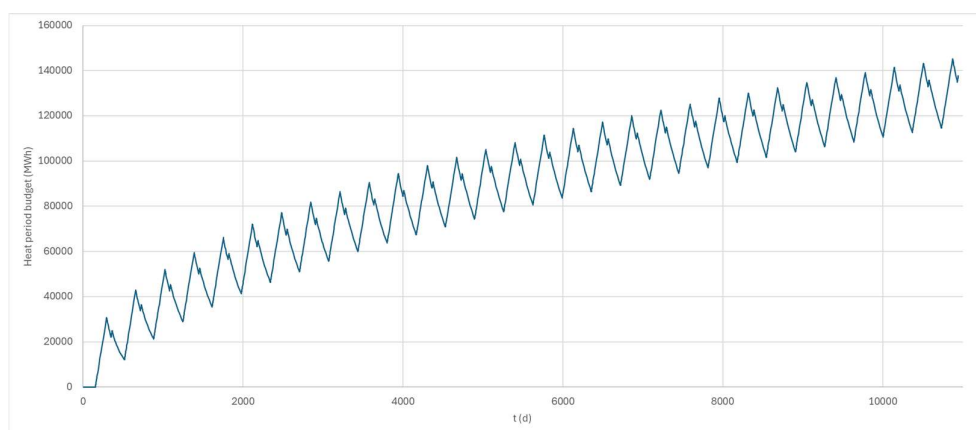


Figure 35 Scenario 2-a: ATEs Heat period budget (MWh) based on 30 years of operation

cycle	endtime (d)	stored (MWh)	discharged (MWh)	Eff%
1	517	29319	12229	41.71
2	883	30694	21358	69.58
3	1248	30665	23137	75.45
4	1613	30673	24123	78.65
5	1977	30669	24800	80.86
6	2342	30646	25530	83.31
7	2707	30662	25961	84.67
8	3072	30661	26125	85.21
9	3436	30658	26396	86.10
10	3801	30624	26818	87.57
11	4166	30655	27015	88.13
12	4531	30708	27128	88.34
13	4895	30723	27297	88.85
14	5260	30646	27512	89.77
15	5625	30677	27554	89.82
16	5990	30644	27643	90.21
17	6354	30618	27730	90.57
18	6720	30615	27832	90.91
19	7084	30613	28036	91.58
20	7449	30697	28095	91.52
21	7814	30698	28178	91.79
22	8178	30607	28257	92.32
23	8543	30605	28232	92.25
24	8908	30603	28296	92.46
25	9273	30699	28456	92.69
26	9638	30654	28267	92.21
27	10004	30653	28539	93.10
28	10369	30677	28641	93.36
29	10733	30619	28702	93.74
total		887682	767887	

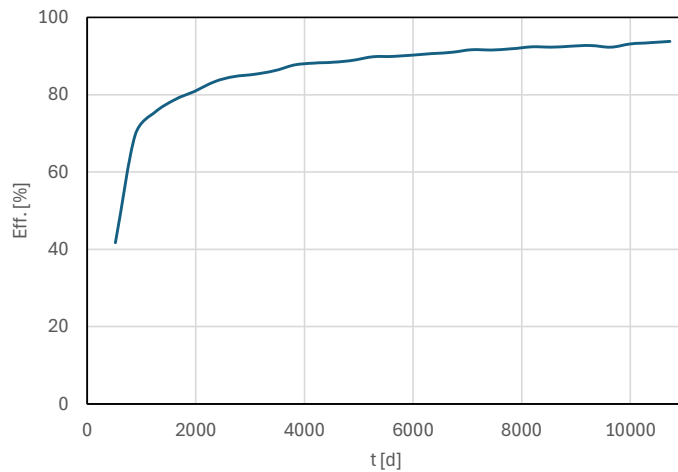


Figure 36 Scenario 2-a: ATES efficiency (Heat stored / Heat recovered), annual storage cycles, based on 30 years of operation

5.2.3 Key insights on Scenario 2-a ATES performance

Overall, Scenario 2-a shows a well-contained and high-efficiency ATES operation, with strong long-term thermal stability and limited energy losses.

✓ Positive Aspects

Stable Seasonal Operation – The system maintains consistent heat injection and extraction cycles (~365-day periodicity), confirming a predictable long-term behaviour

High Thermal Recovery Efficiency (~90-95%) – The system stabilizes with minimal heat losses, ensuring efficient seasonal heat cycling.

Stable Long-Term Performance – The heat period budget follows a predictable seasonal pattern, with no signs of progressive thermal drift or efficiency loss.

⚠ Key Issues & Limitations

Flow Rate and Injection Strategy Optimization – Further adjustments could fine-tune the heat transfer process to maximize efficiency while minimizing operational costs.

5.2.3.1 Heat recharge pattern “b” (Scenario 2-b)

The simulation results are presented in the "time-dependent plots of key parameters" (Figure 37÷Figure 45), as previously described and consistently generated for all analyzed scenarios.

- *Hydraulic heads* along the well axis (m) – ref. Figure 37.

The hydraulic head variations follow a periodic pattern (~365-day cycles), confirming the seasonal operation of the ATES system. Peaks (~ +20 m) correspond to injection phases (storage period), while troughs (~ -20 m) correspond to extraction phases (recovery period).

The first few cycles show a more pronounced transient response, likely due to reservoir adaptation to the new operational scheme. As the cycles progress, the head fluctuations stabilize, indicating that the system reaches a predictable quasi-steady-state operation.

The absence of a long-term pressure drift suggests that the system remains hydraulically balanced, with no progressive pressure buildup or depletion over time.

the predictability and stability of the head cycles confirm that the system is operating within a sustainable hydraulic range.

The long-term impact on well performance due to repeated cycles of pressure buildup and drawdown, with higher peak values compared to Scenario 2-a, remains outside the scope of this SOW.

As pointed out before, in bidirectional ATES systems, where the maximum head difference is inherently amplified, this effect could be particularly significant. Given the fine-sandy to silty-sandy nature of the reservoir, a detailed assessment should be conducted during the design phase to evaluate potential implications on well integrity and operational efficiency.

- *Heat rate budget* (MW) – ref. Figure 42.

The heat period budget follows a progressive upward trend, confirming that a portion of the injected heat remains unrecovered after each cycle. This suggests gradual heat accumulation in the reservoir, supporting the interpretation that thermal energy is not being fully extracted during the recovery phase (low recovery efficiency, see below).

- *Water temperature* at ATES storage wells – ref. Figure 40, Figure 41.

In the early years, post-extraction temperatures exhibit a steeper decline, indicating that the system was still adjusting to thermal cycling and that heat retention had not yet stabilized. As the simulation progresses, the extraction-phase temperature drops become less pronounced, suggesting that the thermal storage volume is gradually stabilizing and that thermal equilibrium is being established.

Compared to Scenario 2-a, the temperature recovery at P2 remains more consistent, with reduced long-term drift. Over time, the baseline temperature for each cycle remains stable, with no significant accumulation or loss trends.

For this specific ATES operation scheme, the high temperature retention at P2 (~90°C) is not to be considered an indicator of efficient heat storage, but rather a sign that a significant portion of the stored heat is not effectively recovered during extraction cycles (low recovery efficiency, see below).

- *Heat period budget* (MWh) - Figure 43, Figure 44, and *Thermal recovery efficiency charts* for the ATES system (Figure 45).

The heat period budget follows a continuous upward trend, confirming that not all injected heat is being recovered during each extraction phase. This suggests that heat is gradually accumulating in the system, likely due to inefficient thermal recovery.

The thermal recovery efficiency stabilizes at approximately 55-60%, significantly lower than in Scenario 2-a.

The thermal plume extends vertically and laterally (Figure 39), but maintains a relatively confined shape, suggesting that heat retention is occurring within the primary storage zone. The high-temperature core (~90°C) remains well-defined, reinforcing that significant residual heat is retained rather than recovered. Temperature gradients (Figure 38) are more gradual compared to Scenario 2-a, indicating that heat is spreading over a larger area, which can contribute to losses.

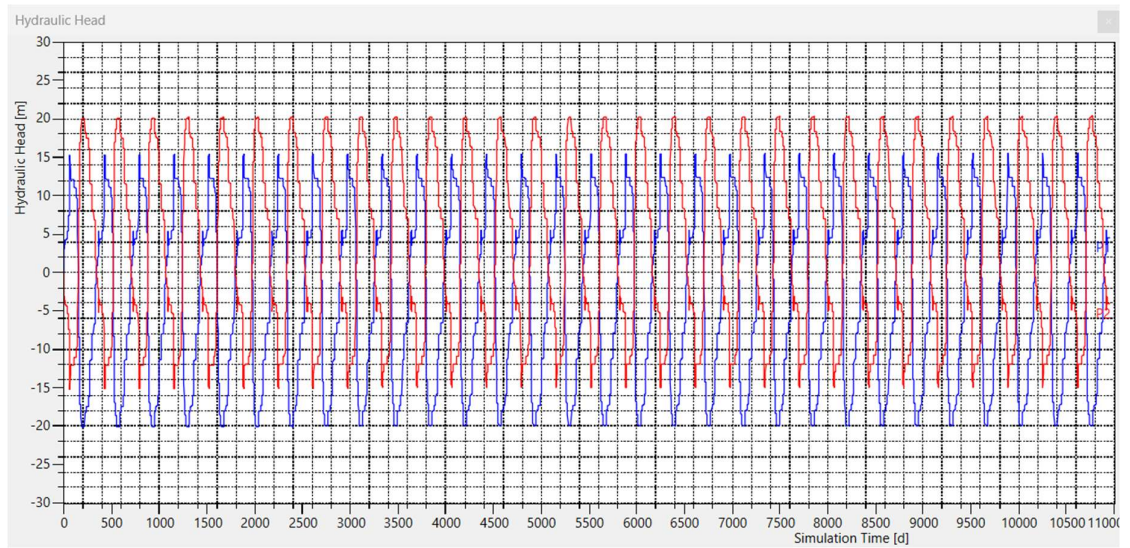


Figure 37 Scenario 2-b: hydraulic heads Vs. time (30 years of operation)

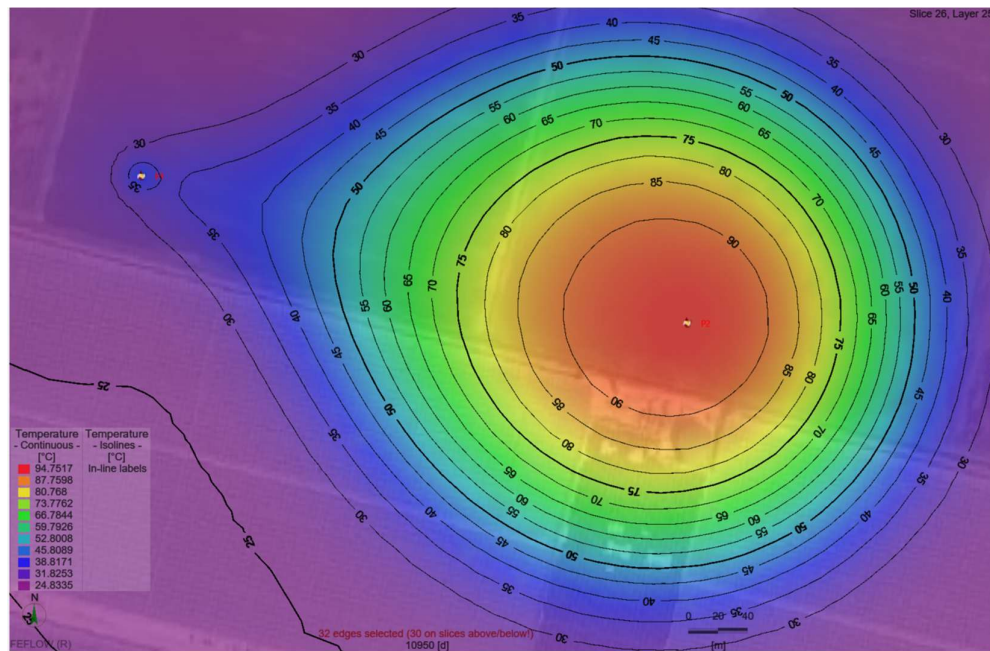


Figure 38 Scenario 2-b: temperature contours at the base of reservoir A1-a (heat storage wells), at year 30 of operation. Note: Due to the specific operational pattern of the ATEs system, an insufficient recovery of the injected heat is observed, leading to the formation of a large temperature bubble

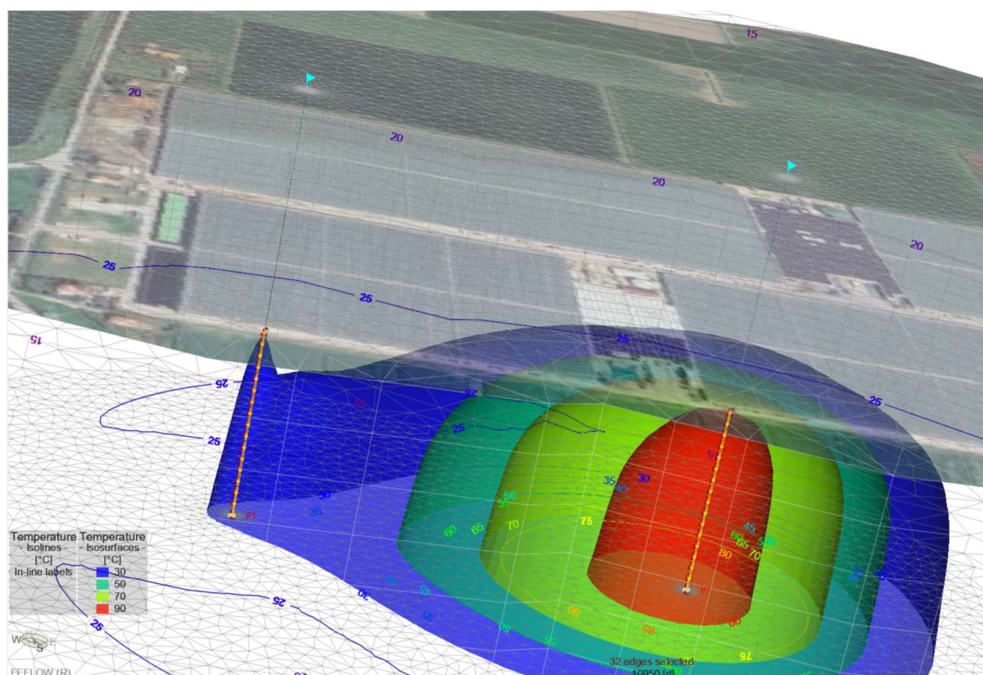


Figure 39 Scenario 2-b: temperature isosurfaces, reservoir A1-a (heat storage wells), at year 30 of operation. Note: Due to the specific operational pattern of the ATEs system, an insufficient recovery of the injected heat is observed, leading to the formation of a large temperature bubble

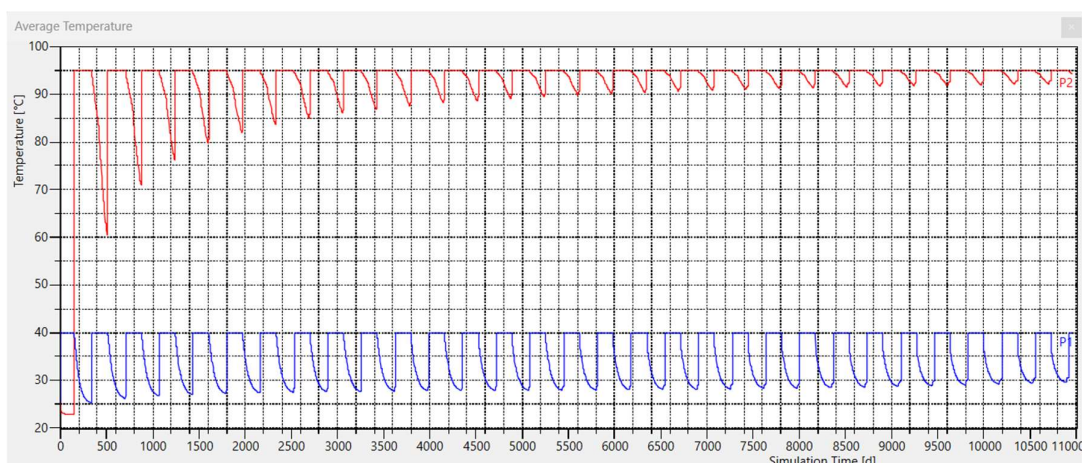


Figure 40 Scenario 2-b: temperature Vs. time, ATEs wells (P1 blue, P2 red) - (30 years of operation)

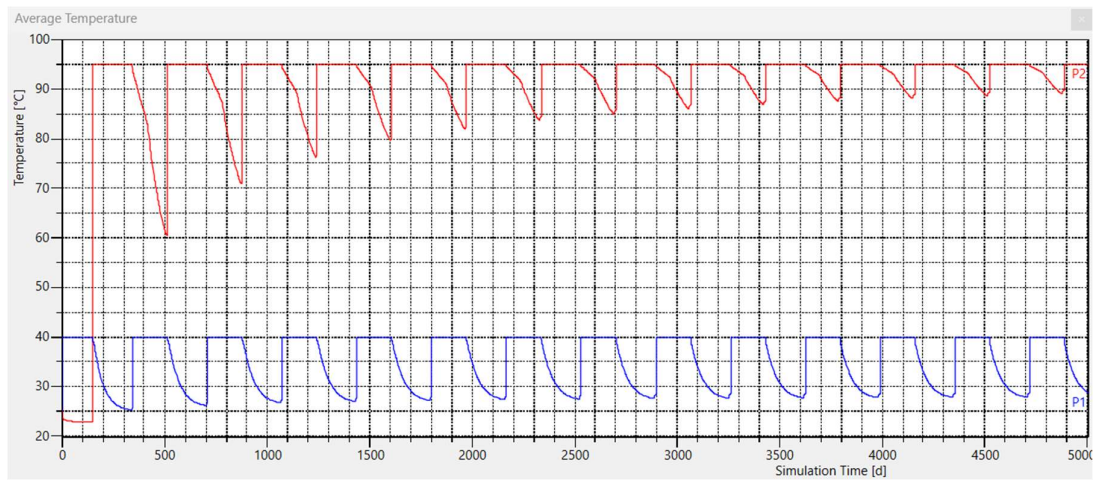


Figure 41 Scenario 2-b: temperature Vs. time, ATES wells (P1 blue, P2 red) – detail

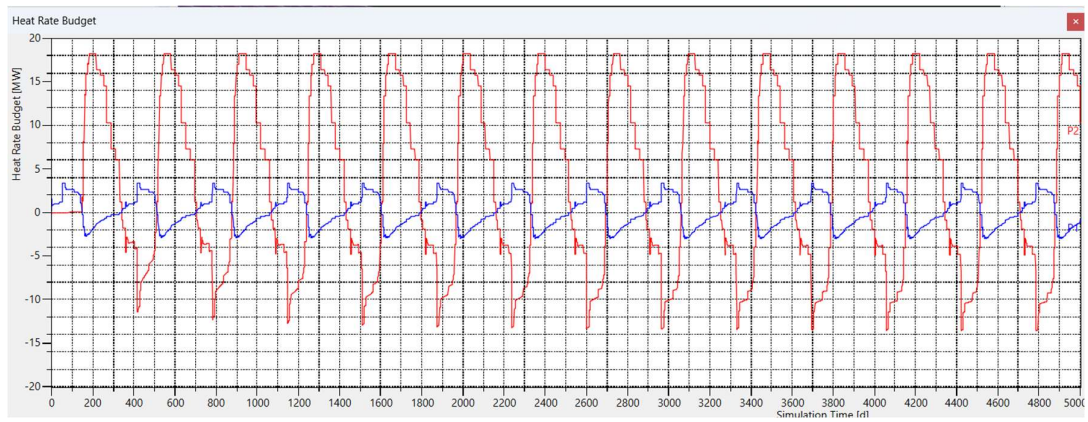


Figure 42 Scenario 2-b: heat rate budget (MW) Vs. time, ATES wells (P1 blue, P2 red) – detail

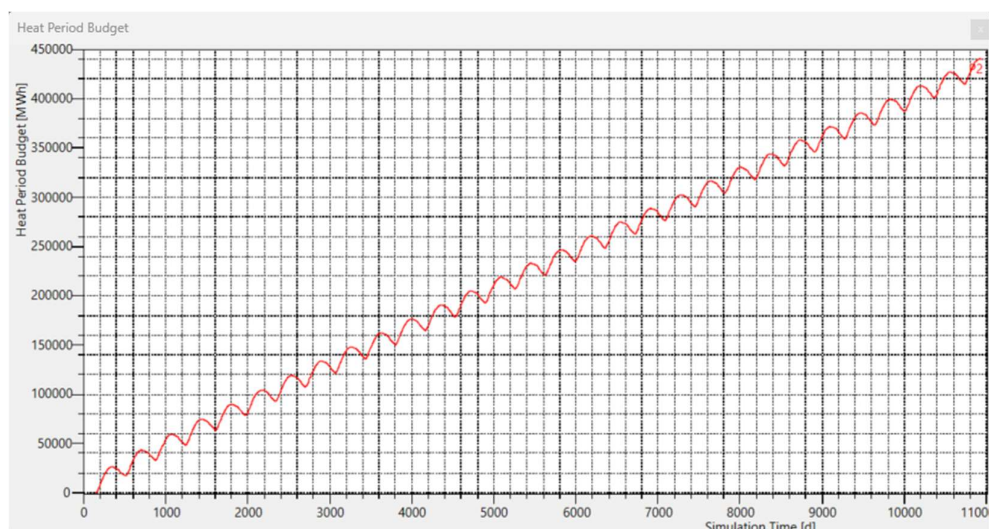
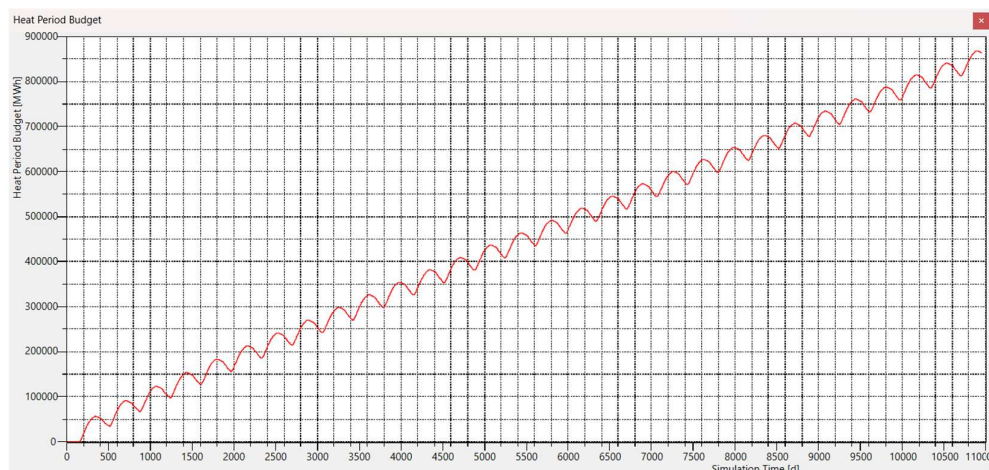


Figure 43 Scenario 2-b: ATEs Heat period budget (MWh) based on 30 years of operation

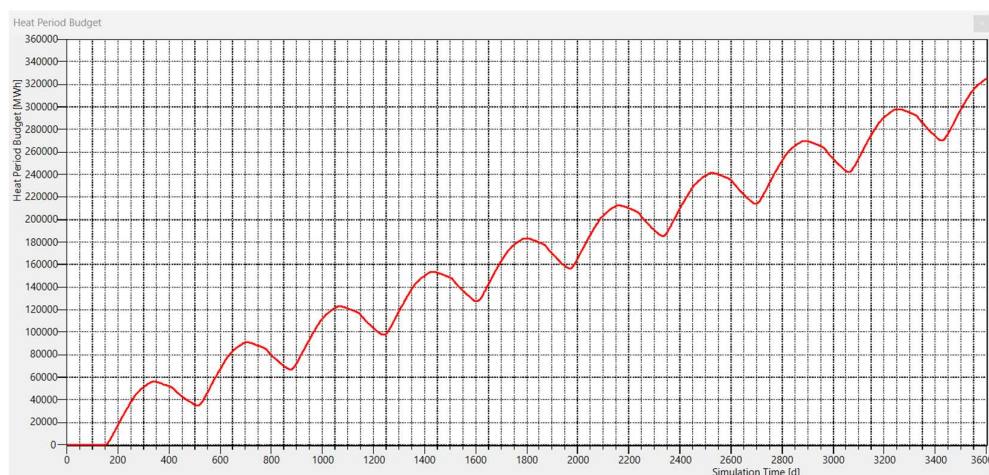


Figure 44 Scenario 2-b: ATEs Heat period budget (MWh) - detail, first decade of operation

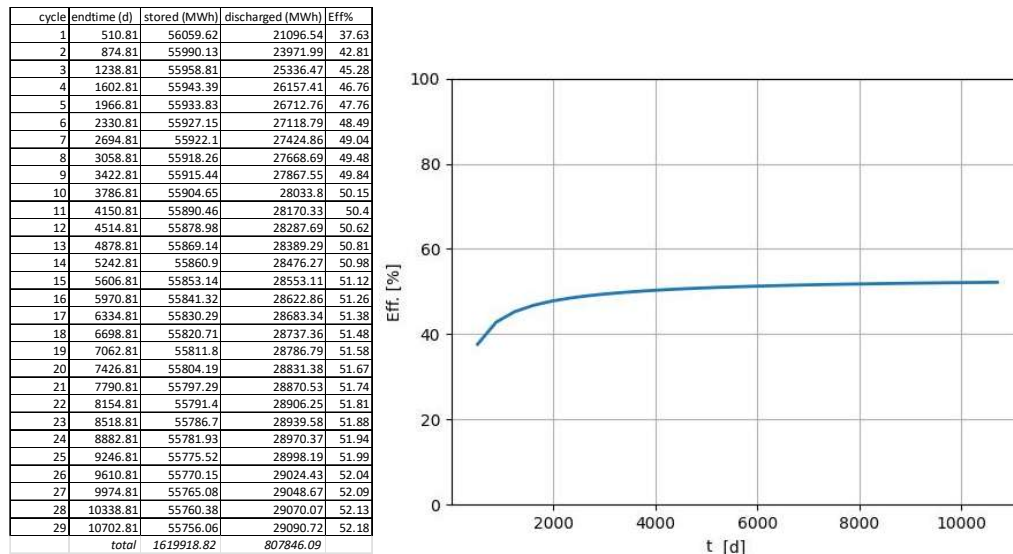


Figure 45 Scenario 2-b: ATES efficiency (Heat stored / Heat recovered), annual storage cycles, based on 30 years of operation

5.2.4 Key insights on Scenario 2-b ATES performance

Scenario 2-b demonstrates stable hydraulic operation and provides a reliable high-temperature thermal supply. However, lower efficiency, progressive heat accumulation, and long-term well integrity concerns require further investigation. Flow optimization could mitigate these inefficiencies and improve system performance.

✓ Positive Aspects

Stable seasonal operation – The system maintains consistent heat injection and extraction cycles (~365-day periodicity), confirming a predictable long-term behavior.

Well-Defined Thermal Plume – The heat plume remains structurally contained, with a strong thermal gradient around the storage zone, preventing excessive short-circuiting.

High-Temperature Water Availability – Despite lower recovery efficiency, the system provides relatively stable high-temperature water (~90°C) during recovery cycles, ensuring consistent thermal supply.

No Significant Hydraulic Instabilities – The pressure cycles stabilize over time, with no progressive overpressure buildup or long-term depletion trends.

⚠ Key Issues & Limitations

Lower Thermal Recovery Efficiency (~55-60%) – Compared to Scenario 2-a (~90-95%), the system exhibits persistent inefficiencies, with a significant fraction of injected heat remaining unrecovered.

Progressive Heat Accumulation – The heat period budget follows a continuous upward trend, suggesting that stored energy is not fully balanced by extraction, leading to massive long-term thermal buildup in the aquifer.

Excessive Lateral and Vertical Heat Dispersion – The thermal plume extends beyond the effective recovery zone, increasing conductive and convective heat losses.

Potential Geotechnical and Well Integrity Concerns – The repeated cycles of alternating injection and extraction induce large variations in pressure (drawdown and buildup cycles), which could impact long-term well performance and formation stability, particularly given the fine-sandy to silty-sandy nature of the reservoir.

5.2.4.1 Heat recharge pattern “c” (*Optimization, Scenario 2-c, 2-c1*)

The Scenario **2-c** represents an optimized version of the previous Scenario 2-b. It is based on storing excess heat produced by deep geothermal doublets during summer and recovering it during peak demand periods for greenhouse district heating, complementing geothermal production. The solution does not involve the operation of heat pumps. ATES is based on a storage temperature of 60°C (injection temperature at P2).

At the current stage of project development, an additional calculation scenario (**2-c1**) has been introduced, featuring an increased ATES storage temperature of 70°C. This adjustment aims to meet the energy demand during the initial years of storage operation, which are characterized by lower efficiency and reduced end-of-cycle discharge temperatures compared to the stabilized condition.

The simulation results are presented in the same "time-dependent plots of key parameters" (Figure 46÷Figure 55) previously described and consistently generated for all analyzed scenarios.

The results confirm that ATES exhibits performance similar to that of the previous Scenario 2-b, offering a lower-temperature alternative for exclusive use with energy exchange from a purely geothermal source. It also presents a viable option for intermediate solutions (e.g., storage temperatures of 70°C, varian 2-c1) that involve partial integration with heat pumps.

- *Hydraulic heads* along the well axis (m) – ref. Figure 46.

Scenario 2-c does not lead to a significant change in flow rates compared to the previous Scenario 2-b but only results in a reduction in injection temperatures and, consequently, the stored energy. As a result, no substantial variations are observed in hydraulic loads under dynamic conditions, particularly regarding peak values during extraction and reinjection. For further details, reference should be made to the observations already provided for Scenario 2-b (see graph in previous Figure 37 and corresponding description). Scenarios 2c and 2c-1 are effectively equivalent in terms of hydraulic loads, differing only in reinjection temperature.

- *Heat rate budget* (MW) – ref. Figure 52.

The heat period budget follows a progressive upward trend, confirming that a portion of the injected heat remains unrecovered after each cycle, as typical of the same pattern observed for the previous Scenario b-2. This suggests gradual heat accumulation in the reservoir, supporting the interpretation that thermal energy is not being fully extracted during the recovery phase (low recovery efficiency, see below).

- *Water temperature* at ATES storage wells – ref. Figure 50, Figure 52

In the early years, post-extraction temperatures exhibit a steeper decline, indicating that the system was still adjusting to thermal cycling and that heat retention had not yet stabilized. As the simulation progresses, the extraction-phase temperature drops become less pronounced, suggesting that the thermal storage volume is gradually stabilizing, and that thermal equilibrium is being established.

Compared to Scenario 2-a, in Scenario 2-c (same as the previous 2-b) recovery at P2 remains more consistent, with reduced long-term drift. Over time, the baseline temperature for each cycle remains stable, with no significant accumulation or loss trends.

For this specific 2c ATES operation scheme, the high temperature retention at P2 (~57-58°C) is not to be considered an indicator of efficient heat storage, but rather a sign that a significant portion of the stored heat is not effectively recovered during extraction cycles (low recovery efficiency, see below). The same considerations apply to variant 2c-1 (Figure 51).

- *Heat period budget* (MWh) - Figure 53, Figure 54, and *Thermal recovery efficiency charts* for the ATES system (Figure 55).

The heat period budget follows a continuous upward trend, confirming that not all injected heat is being recovered during each extraction phase. This suggests that heat is gradually accumulating in the system, likely due to inefficient thermal recovery.

Same as the Scenario 2-b, the thermal plume for the “*lower T variant*” 2-c extends vertically and laterally (Figure 48), but maintains a relatively confined shape, suggesting that heat retention is occurring within the primary storage zone. The high-temperature core (~50°C) remains well-defined, reinforcing that significant residual heat is retained rather than recovered. Temperature gradients (Figure 47) are more gradual compared to Scenario 2-a, indicating that heat is spreading over a larger area, which can contribute to losses.

The thermal recovery efficiency stabilizes at approximately 60%, significantly lower than in Scenario 2-a, and slightly lower than the same Scenario 2-b. In Solution 2-c, the recovery rate reaches its lowest value among the tested scenarios, even lower than in Scenario 2-b, due to the reduced temperature gradient with the ATES reservoir. Note that the recovery efficiency for the Scenario 2-c (ATES 60°C) and 2-c1 (variant, ATES 70°C) variants are nearly overlapping.

This condition highlights the potential for improving ATES system management, which should be assessed in future project phases and corresponding modeling, with the possibility of reducing the energy input while maintaining the same amount of recovery.

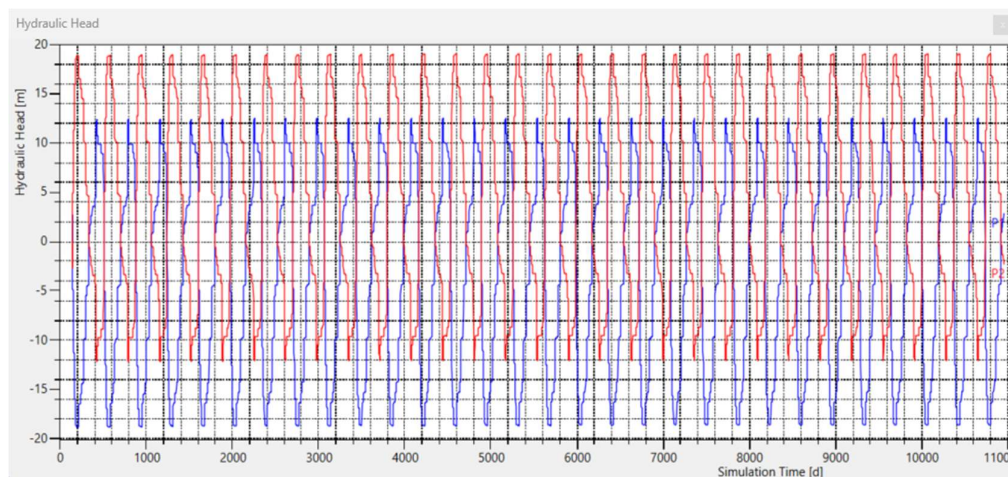


Figure 46 Scenario 2-c: hydraulic heads Vs. time (30 years of operation)

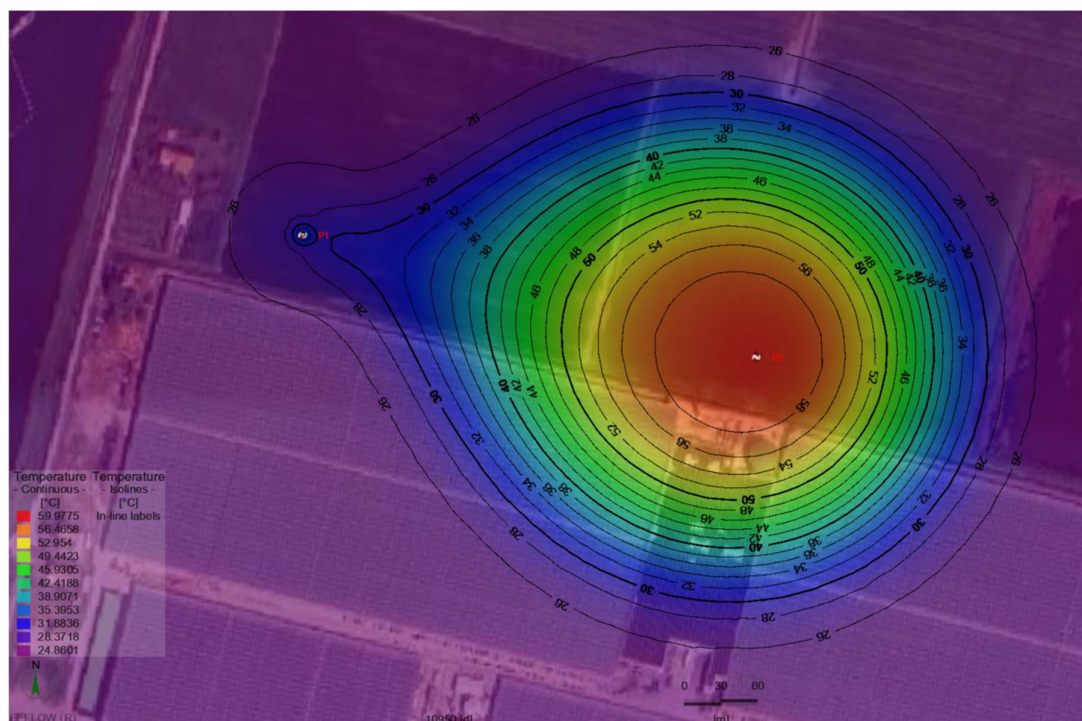


Figure 47 Scenario 2-c: temperature contours at the base of reservoir A1-a (heat storage wells), at year 30 of operation. Note: Due to the specific operational pattern of the ATEs system, an insufficient recovery of the injected heat is observed, leading to the formation of a large temperature bubble

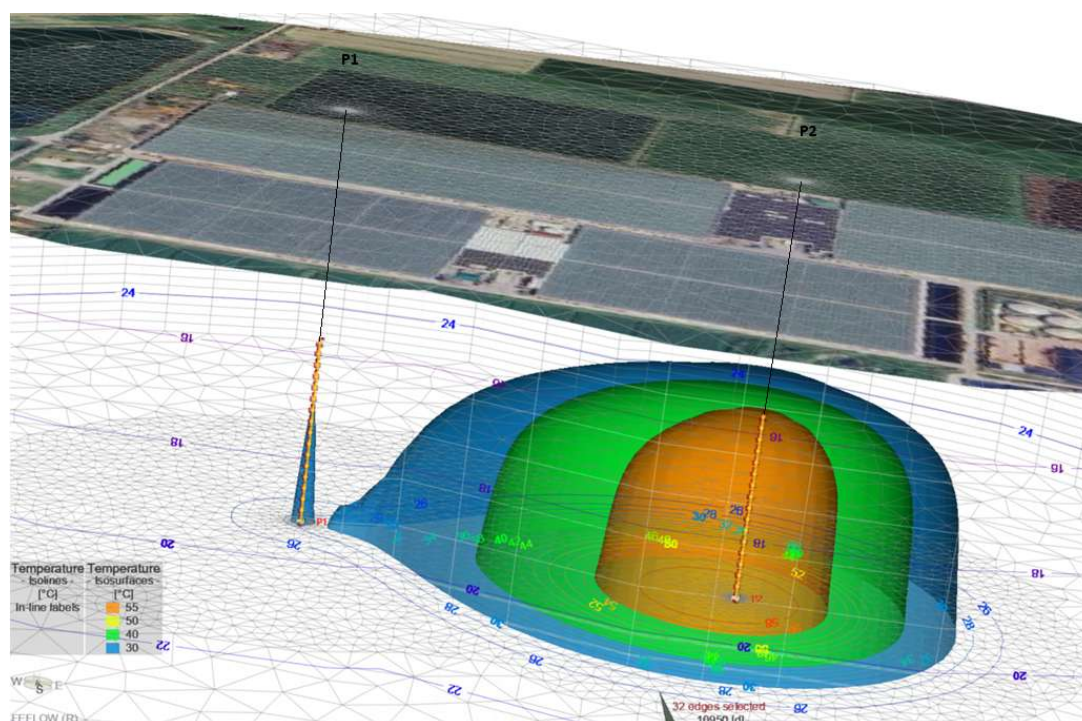


Figure 48 Scenario 2-c: temperature isosurfaces, reservoir A1-a (heat storage wells), at year 30 of operation. Note: Due to the specific operational pattern of the ATEs system, an insufficient recovery of the injected heat is observed, leading to the formation of a large temperature bubble

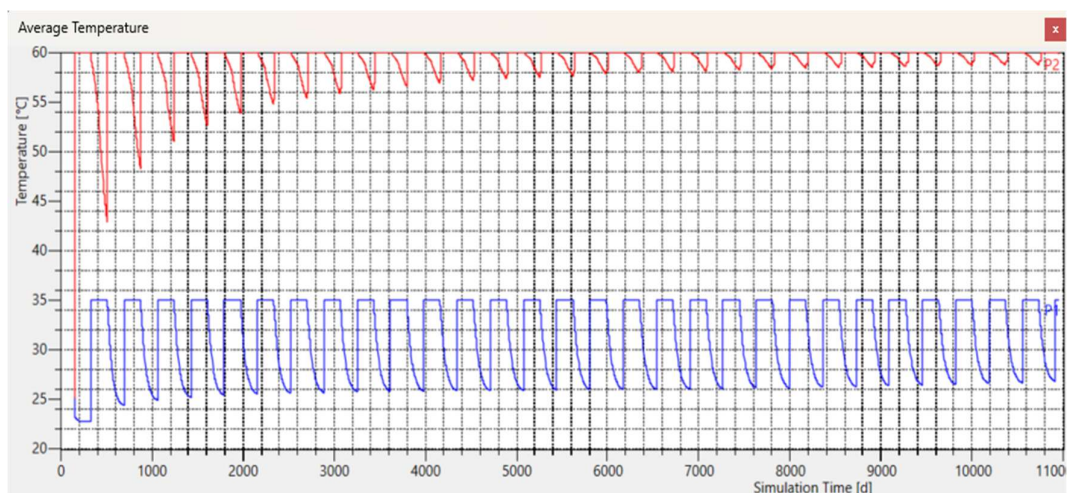


Figure 49 Scenario 2-c: temperature Vs. time, ATEs wells (P1 blue, P2 red) - (30 years of operation)

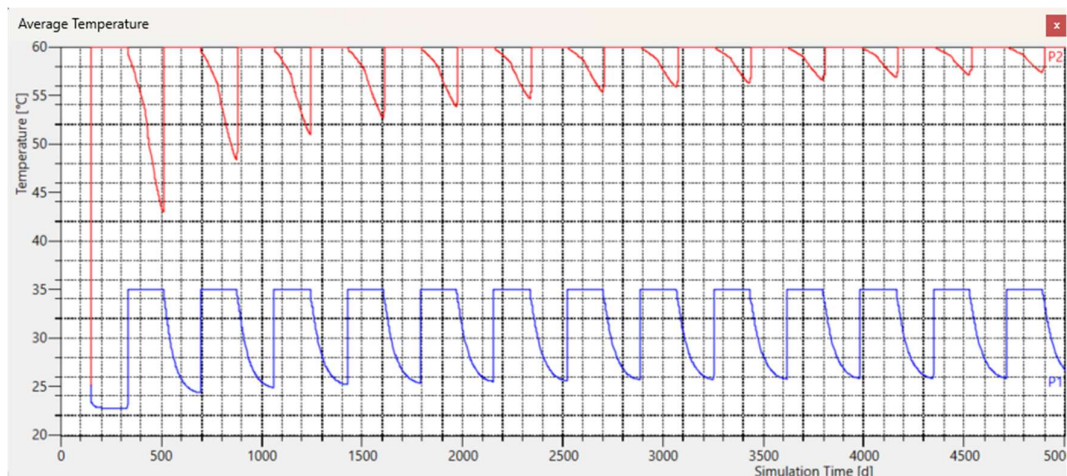


Figure 50 Scenario 2-c: temperature Vs. time, ATEs wells (P1 blue, P2 red) – detail.

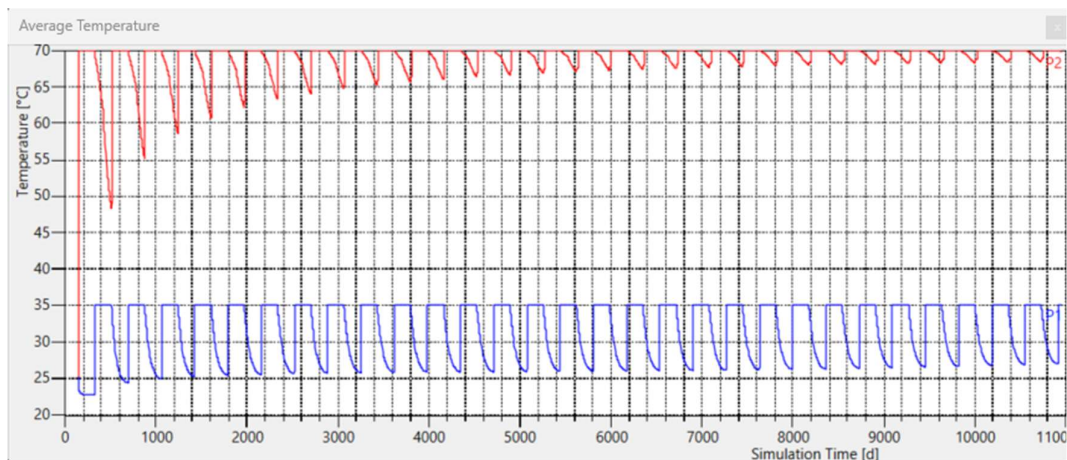


Figure 51 Scenario 2-c1 (variant, ATEs at $T=70^{\circ}\text{C}$): temperature Vs. time, ATEs wells (P1 blue, P2 red) - (30 years of operation)

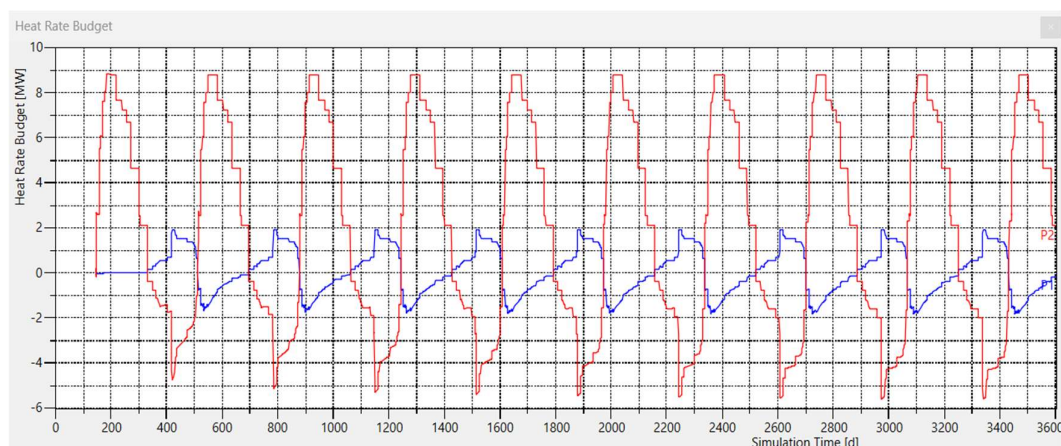


Figure 52 Scenario 2-c: heat rate budget (MW) Vs. time, ATES wells (P1 blue, P2 red) – detail

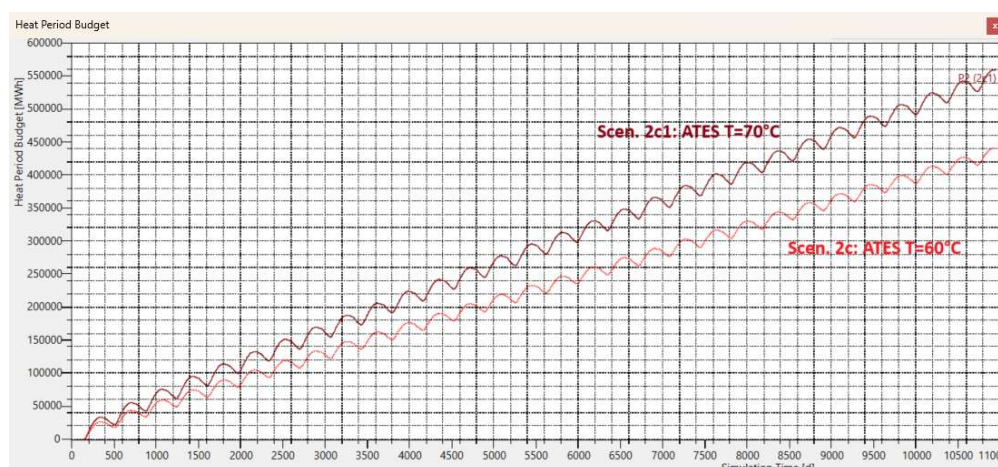


Figure 53 Scenario 2-c (e variante 2c1): ATES Heat period budget (MWh) based on 30 years of operation.



Figure 54 Scenario 2-c (e variante 2c1): ATES Heat period budget (MWh) - detail, first decade of operation.

cycle	endtime (d)	stored (MWh)	discharged (MWh)	Eff%
1	512.55	26246.2	9017.95	34.36
2	877.55	26197.26	10233.91	39.06
3	1242.55	26169.46	10802.23	41.28
4	1607.55	26155.09	11140.91	42.6
5	1972.55	26146.25	11372.27	43.49
6	2337.55	26140.54	11538.56	44.14
7	2702.55	26136.42	11662.82	44.62
8	3067.55	26133.4	11761.36	45.01
9	3432.55	26131.02	11841.09	45.31
10	3797.55	26129.27	11906.73	45.57
11	4162.55	26128.02	11961.84	45.78
12	4527.55	26125.16	12008.57	45.97
13	4892.55	26120.48	12048.61	46.13
14	5257.55	26116.55	12083.40	46.27
15	5622.55	26113.42	12113.34	46.39
16	5987.55	26110.7	12140.18	46.5
17	6352.55	26108.26	12163.87	46.59
18	6717.55	26105.83	12184.99	46.68
19	7082.55	26103.78	12204.29	46.75
20	7447.55	26101.99	12222.15	46.82
21	7812.55	26100.84	12237.82	46.89
22	8177.55	26099.87	12251.88	46.94
23	8542.55	26098.49	12264.41	46.99
24	8907.55	26096.59	12276.04	47.04
25	9272.55	26094.91	12286.55	47.08
26	9637.55	26093.42	12296.21	47.12
27	10002.55	26092.22	12304.82	47.16
28	10367.55	26091.07	12313.10	47.19
29	10732.55	26089.91	12321.00	47.23
total		757576.42	342960.9	

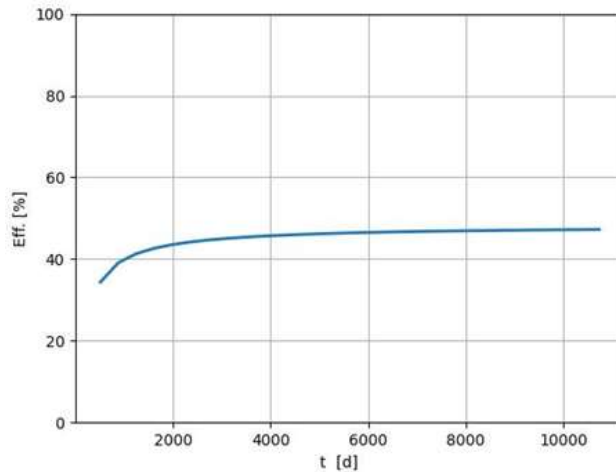


Figure 55 Scenario 2-c: ATEs efficiency (Heat stored / Heat recovered), annual storage cycles, based on 30 years of operation.

cycle	endtime (d)	stored (MWh)	discharged (MWh)	Eff%
1	512.55	33305.60	11443.05	34.36
2	877.55	33242.55	12987.21	39.07
3	1242.55	33207.04	13708.40	41.28
4	1607.55	33188.69	14138.48	42.60
5	1972.55	33177.43	14431.81	43.50
6	2337.55	33169.91	14642.66	44.14
7	2702.55	33164.55	14800.37	44.63
8	3067.55	33160.66	14925.31	45.01
9	3432.55	33157.86	15026.07	45.32
10	3797.55	33155.73	15109.49	45.57
11	4162.55	33154.18	15179.32	45.78
12	4527.55	33150.53	15238.71	45.97
13	4892.55	33144.42	15289.51	46.13
14	5257.55	33139.25	15333.70	46.27
15	5622.55	33135.04	15371.68	46.39
16	5987.55	33131.76	15405.53	46.50
17	6352.55	33128.53	15435.71	46.59
18	6717.55	33125.42	15462.59	46.68
19	7082.55	33122.55	15486.90	46.76
20	7447.55	33120.61	15509.53	46.83
21	7812.55	33118.71	15529.33	46.89
22	8177.55	33117.03	15547.37	46.95
23	8542.55	33115.43	15563.10	47.00
24	8907.55	33113.00	15577.91	47.04
25	9272.55	33110.77	15590.99	47.09
26	9637.55	33108.75	15603.15	47.13
27	10002.55	33107.04	15614.18	47.16
28	10367.55	33104.88	15624.14	47.20
29	10732.55	33103.42	15634.09	47.23
total		961281.34	435210.26	

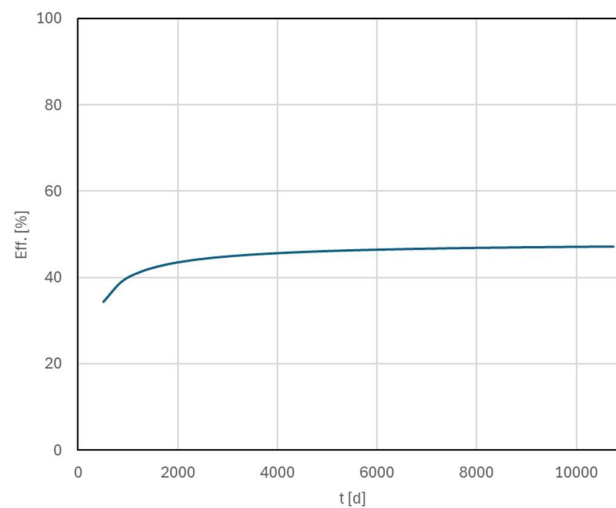


Figure 56 Scenario 2-c1: ATEs efficiency (Heat stored / Heat recovered), annual storage cycles, based on 30 years of operation.

5.2.5 Key insights on Scenario 2-c ATEs performance

The scenarios 2-c and 2-c1 represent an optimization of scenario 2-b, based on a variable thermal power input regime in the ATEs system, tested across different temperature values. As a result, the key insights are largely comparable. A common aspect among these scenarios is the surplus of stored energy compared to the recovered energy in each annual cycle, leading to progressive heat accumulation, which in turn limits system efficiency. Flow optimization could mitigate these inefficiencies during the detailed design and sizing phase to ensure optimal performance.

✓ Positive Aspects

Stable seasonal operation – The system maintains consistent heat injection and extraction cycles (~365-day periodicity), confirming a predictable long-term behavior.

Well-Defined Thermal Plume – The heat plume remains structurally contained, with a strong thermal gradient around the storage zone, preventing excessive short-circuiting.

Water Availability at *close-to-stored* temperature for each ATEs cycle – Despite lower recovery efficiency, the system provides relatively stable temperature water during recovery cycles, ensuring consistent thermal supply.

No Significant Hydraulic Instabilities – The pressure cycles stabilize over time, with no progressive overpressure buildup or long-term depletion trends.

⚠ Key Issues & Limitations

Lower Thermal Recovery Efficiency (~55-60%) – Compared to Scenario 2-a (~90-95%), the system exhibits persistent inefficiencies, with a significant fraction of injected heat remaining unrecovered.

Progressive Heat Accumulation – The heat period budget follows a continuous upward trend, suggesting that stored energy is not fully balanced by extraction, leading to massive long-term thermal buildup in the aquifer.

Excessive Lateral and Vertical Heat Dispersion – The thermal plume extends beyond the effective recovery zone, increasing conductive and convective heat losses.

Potential Geotechnical and Well Integrity Concerns – The repeated cycles of alternating injection and extraction induce large variations in pressure (drawdown and buildup cycles), which could impact long-term well performance and formation stability, particularly given the fine-sandy to silty-sandy nature of the reservoir.















5.2.6 Simulation results: heat production section (reservoir A3-a)

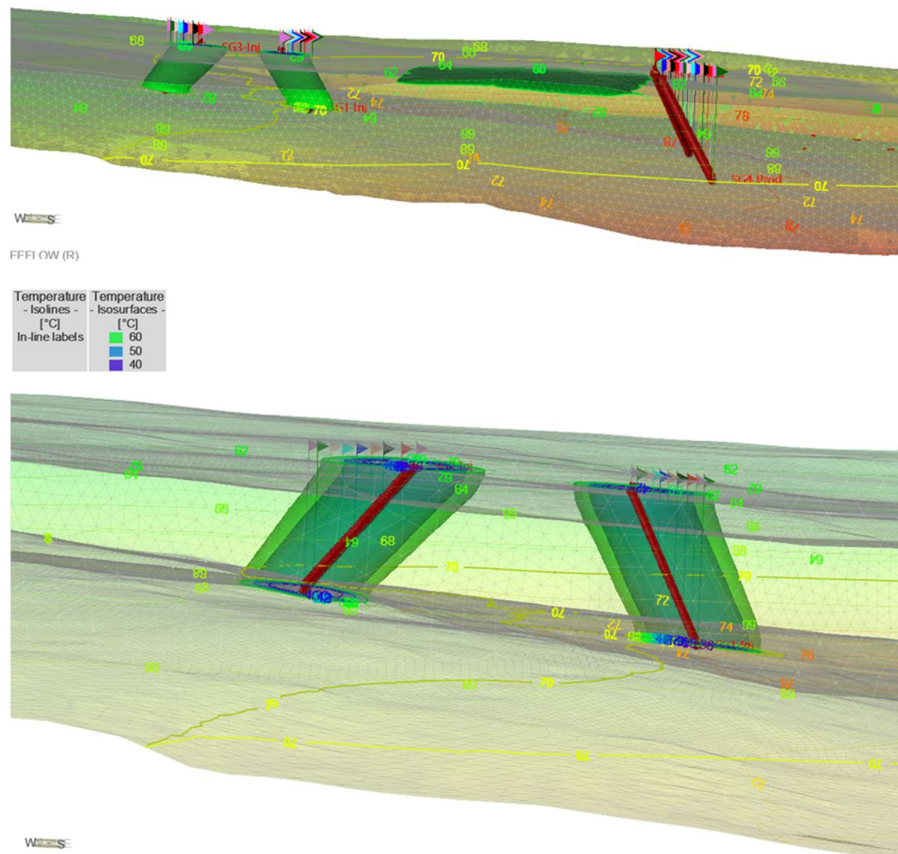
The hydraulic head distribution shows a stable pressure regime, with injection wells maintaining consistent overpressure (~+140 m) and production wells stabilizing at ~ -100 m. This suggests steady-state operation with no long-term depletion trends, confirming that the system is hydraulically balanced under the given operational parameters.

The temperature at production wells (SG2, SG4) remains stable (~70°C), while reinjection wells (SG1, SG3) operate at lower, controlled temperatures (~35°C), preventing thermal breakthrough and ensuring sustainable long-term operation.

The heat rate budget and period budget confirm a continuous net energy extraction over time, with stable production at ~8.5 MW. The cumulative heat period budget shows a steady decrease, reflecting continuous energy withdrawal without significant residual heat accumulation in the reservoir. This indicates that the geothermal doublets effectively sustain production while avoiding excessive heat losses to the surrounding formations.

Overall, the system demonstrates stable hydraulic and thermal performance, with no significant pressure imbalances, thermal degradation, or operational inefficiencies. The well configuration and flow rates appear well-optimized for long-term sustainable energy extraction.

Temperature - Isolines - [°C] In-line labels	Temperature - Isosurfaces - [°C]	Temperature - Continuous - [°C]
 60	 80.0428	
 50	 75.5316	
 40	 71.0204	
	 66.5092	
	 61.998	
	 57.4868	
	 52.9756	
	 48.4644	
	 43.9532	
	 39.442	
	 34.9308	



22805154-01-00102.docx

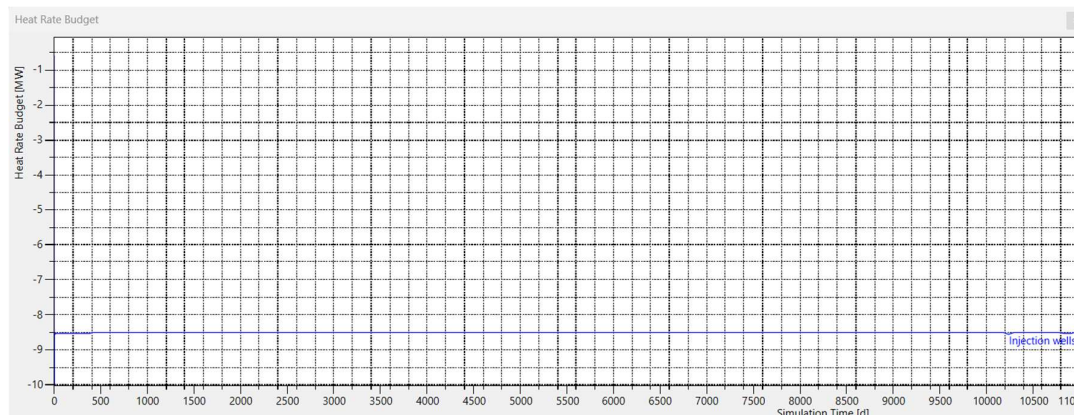


Figure 59 Production - Heat period budget (MWh) based on 30 years of operation.

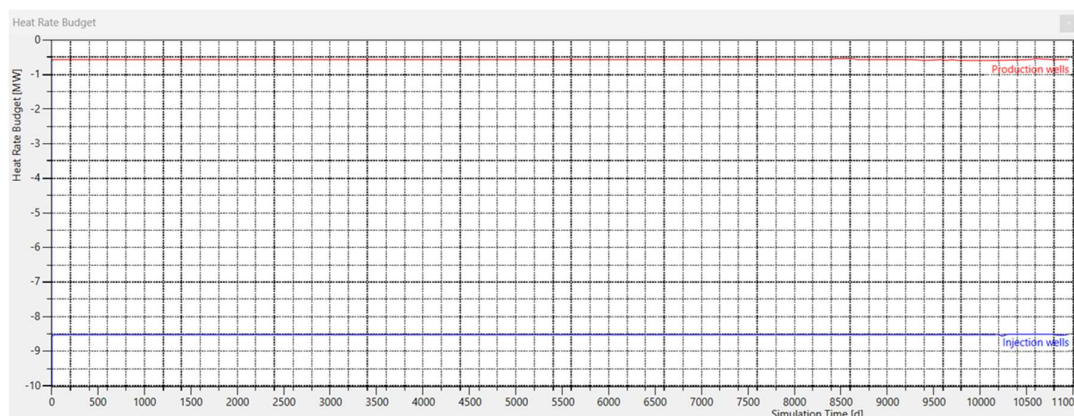


Figure 60 Heat rate budget (MWh) for the section of heat production (reservoir A3-a) based on 30 years of operation.

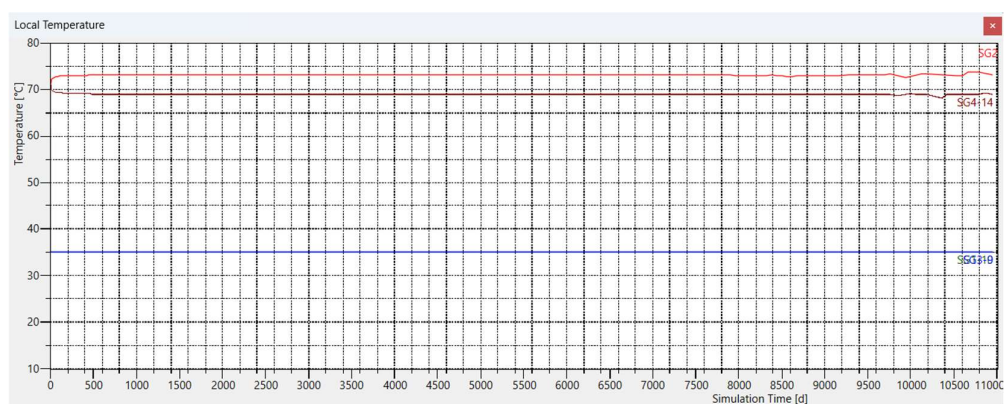


Figure 61 Temperatures Vs. time (°C) for the section of heat production (reservoir A3-a) based on 30 years of operation.

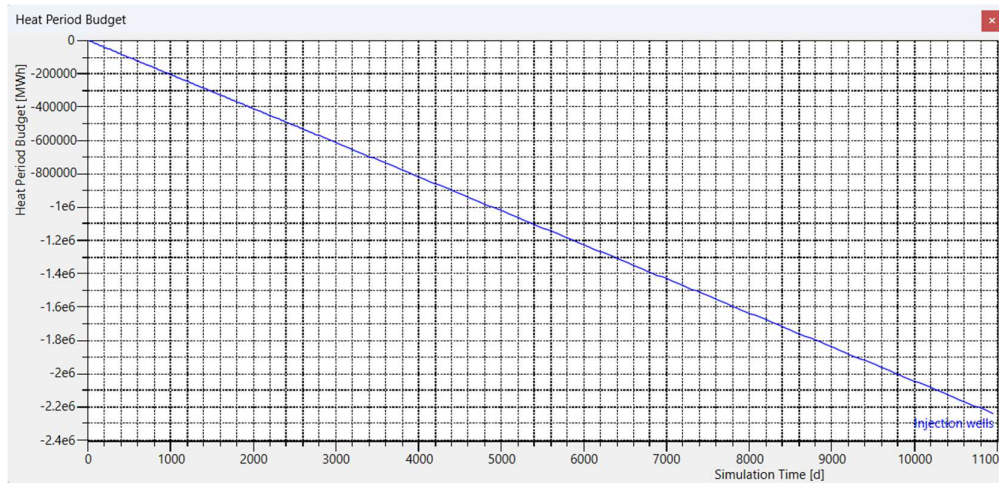


Figure 62 Heat period budget (MWh) for the section of heat production (reservoir A3-a) based on 30 years of operation.

5.2.7 Sensitivity analysis and model uncertainty

Based on the evaluations already reported regarding the uncertainty analysis for Scenario 1 (ref. par. 5.1.5), a sensitivity analysis assesses parameter variations related to the major identified inefficiencies in the ATES system. The main objectives are to evaluate system response to extreme conditions and to identify potential solutions to improve performance.

The analysis focuses on two key uncertainties:

- a) permeability values to analyze the effect on thermal storage and the worst-case hydraulic response and pumping requirements.
- b) transverse dispersivity values to evaluate their impact on thermal containment and efficiency.

Dispersivity parameters (longitudinal and transverse) control how heat is transported and mixed in the aquifer: Higher dispersivity = More heat mixing and lateral spreading, increasing losses, Lower dispersivity = More confined heat storage, but potentially higher localized temperature gradients.

The temperature curves, in Figure 63 (detailed view) and Figure 64 (30 years of operation), illustrate the impact of different model input parameters on thermal performance. The analysis evaluates the effects of permeability (K), dispersivity (α_L), and thermal conductivity modifications.

Key observations, Scenario 2a:

- 1) Increasing Permeability ($K = 1E-4$ m/s) has no significant effect.

The green curve ($K = 1E-4$ m/s) closely follows the standard case (purple), indicating negligible impact on temperature dynamics and overall system efficiency. The explanation is that in an ATES system, pumping and reinjection rates are regulated, meaning that even if permeability increases, the same amount of water is being injected and extracted. In a confined aquifer, increasing permeability results in a lower hydraulic gradient to sustain the same flow rate. However, this does not change the physical heat transport properties of the system—the temperature distribution and recovery efficiency remain identical.

Reducing dispersivity (light blue curve, $\alpha_L = 1$ m) significantly enhances thermal recovery, reducing temperature drop rate, as it prevents heat from spreading too far, keeping it available for extraction. Increasing thermal conductivity (orange curve) has only a minor effect, as conduction

is a much slower mechanism compared to advection and dispersion. Since ATES operates in cyclic thermal balance, heat transfer from the rock matrix is relatively slow, meaning conductivity changes have minimal short-term impact.

This heat period budget analysis highlights the impact of different longitudinal dispersivity values on thermal storage and recovery efficiency over time. The three curves in Figure 65 represent:

$\alpha_L = 1\text{m}$ (red): lowest dispersivity;

$\alpha_L = 10\text{m}$ (black): reference case;

$\alpha_L = 25\text{m}$ (blue): highest dispersivity.

Lower Dispersivity ($\alpha_L = 1\text{m}$) Improves Thermal Retention (Red Curve) leading to a theoretical efficiency close 100% (energy stored \approx energy recovered);

The blue curve, higher dispersivity ($\alpha_L = 25\text{m}$) exhibits the highest stored heat values, with a steeper increase in cumulative heat over time, meaning Heat spreads over a larger volume, reducing recoverable energy per cycle. The stabilized efficiency of recovery drops $\approx 70\%$.

So, from the sensitivity analysis the calculated ATES efficiency results:

$\eta \approx 93\%$ (theoretical value) for $\alpha_L = 10\text{ m}$ (best estimate)

$\eta \approx 100\%$ (theoretical value) for $\alpha_L = 1\text{ m}$ (lower bound, best scenario)

$\eta \approx 79\%$ For $\alpha_L = 25\text{ m}$ (upper bound, worst-case scenario)

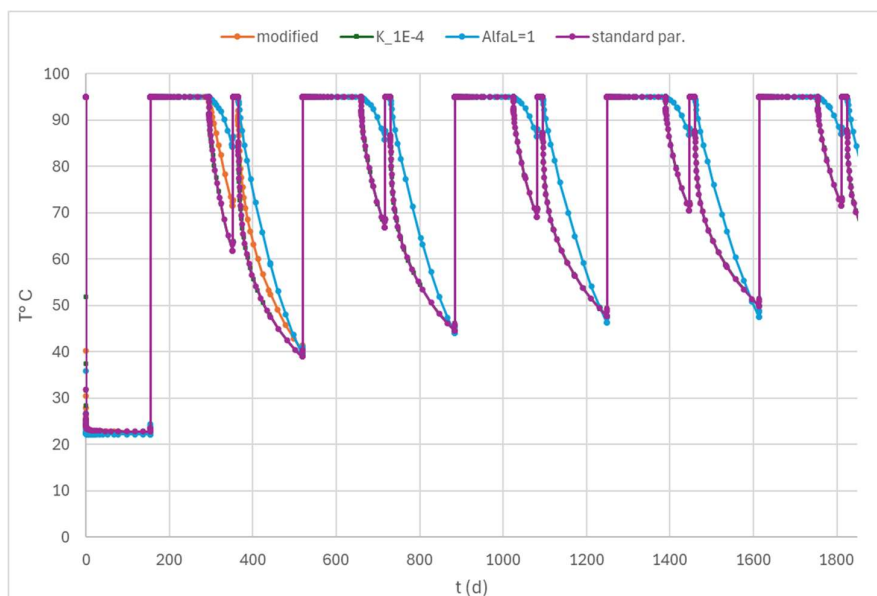


Figure 63 Scenario 2-a - Temperature curves of the ATES storage over time resulting from the sensitivity analysis on the model input parameters (5 years operation)

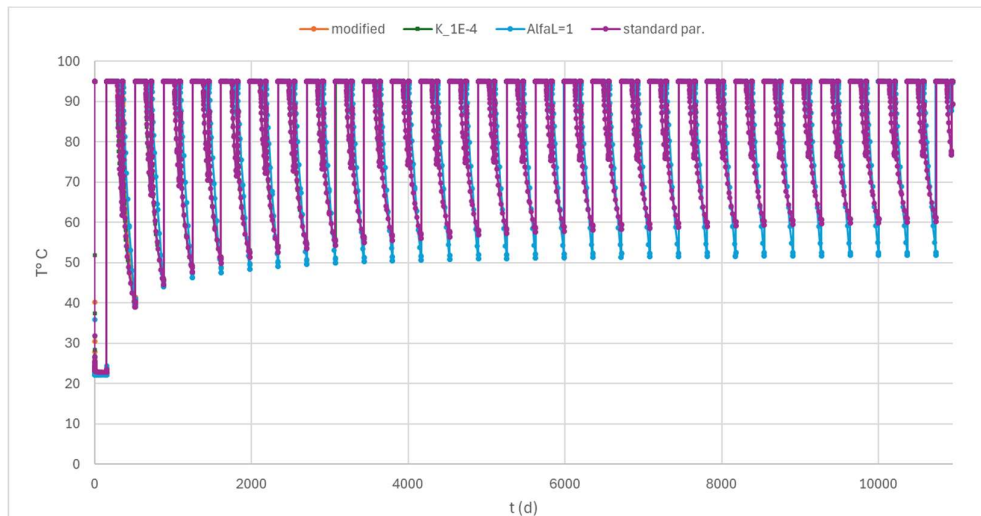


Figure 64 Scenario 2-a - Temperature curves of the ATES storage over time resulting from the sensitivity analysis on the model input parameters (based on 30 years of operation)

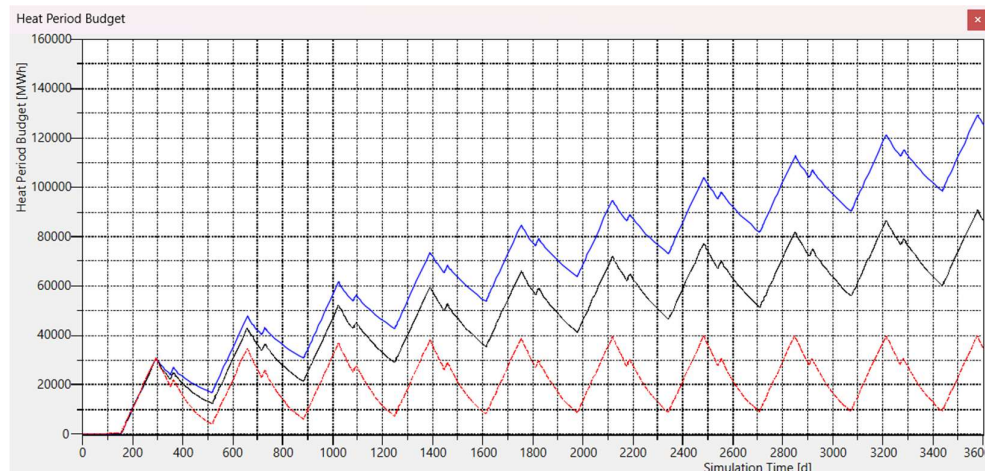


Figure 65 Scenario 2-a – Heat rate budget (detail) – Heat period budget (detail) for dispersivity values $\alpha_L=1$ m (red), $\alpha_L=10$ m (reference value, black), $\alpha_L=25$ m (blue)

The analysis of the sensitive parameter, longitudinal and transverse dispersivity (α_L , α_T), was repeated for scenario 2-C, which serves as the reference for the set of simulations involving seasonally modulated energy injection and extraction (Scenarios 2-B, 2-C, 2-C1).

It can be observed, Figure 66, Heat Period Budget, that the blue curve, representing higher dispersivity (worst-case, $\alpha_L = 25$ m), shows the highest stored heat values, with a steeper increase in cumulative heat over time. This indicates that heat spreads over a larger volume, ultimately reducing the recoverable energy per cycle. As a result, the stabilized recovery efficiency drops to approximately 41,03%.

The Figure 67 chart illustrates the evolution of average temperature in the ATES system over time for different longitudinal dispersivity values.

It is evident that the higher dispersivity (black curve $\alpha_L = 25$ m, worst-case) leads to a faster and more significant temperature drop at the end of each cycle. This confirms increased thermal spreading, reducing the system's ability to recover stored heat efficiently. In contrast, the lower dispersivity (blue curve) maintains higher temperatures over time, indicating better heat retention and recovery efficiency.

This confirms that higher dispersivity negatively impacts ATEs performance by spreading heat over a larger volume, decreasing the system's long-term thermal efficiency.

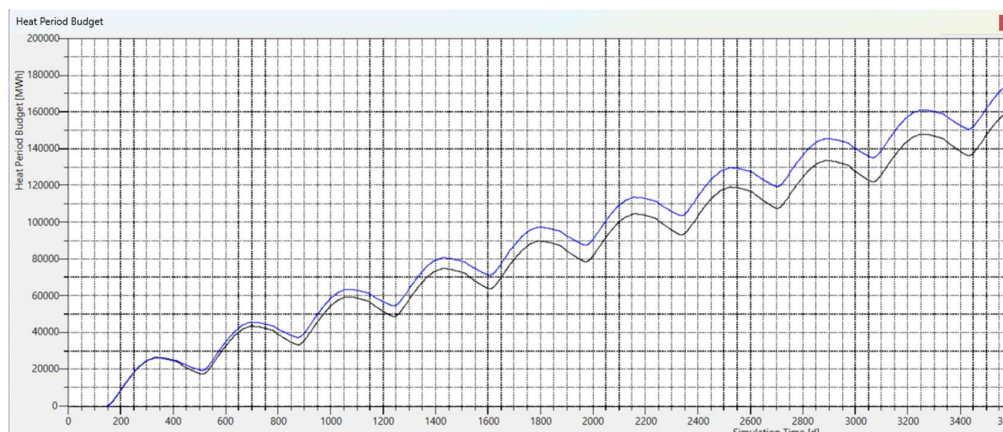


Figure 66 Scenario 2-c – Heat rate budget (detail) – Heat period budget (detail) for dispersivity values $\alpha L=10$ m (reference value, black), $\alpha L=25$ m (blue)

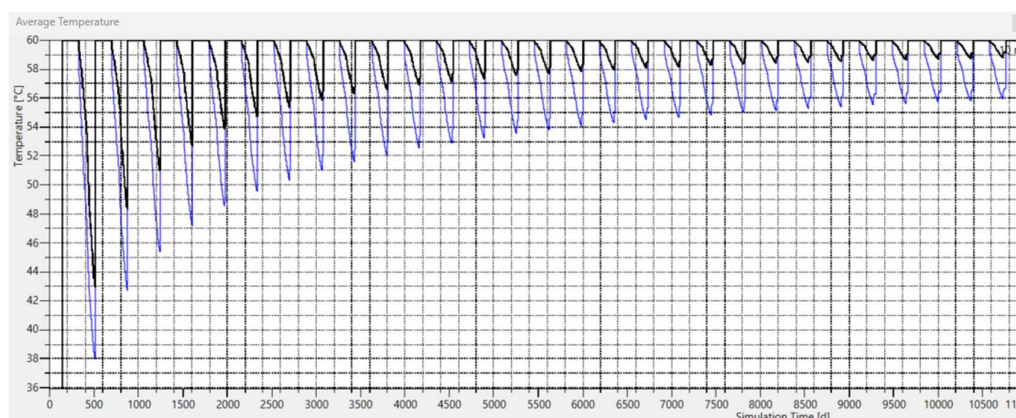


Figure 67 Scenario 2-c – Temperature chart – Heat period budget (detail) for dispersivity values $\alpha L=10$ m (reference value, black), $\alpha L=25$ m (worst-case, blue) - Note the reduction in the minimum temperature at the end of each recovery cycle in the 'conservative' scenario ($\alpha L=25$ m) compared to the standard ($\alpha L=10$ m)

6 Thermal interference evaluation: assessing and minimizing ATEs heat transfer to shallow aquifers

To complement the reservoir models designed for the three-dimensional simulation of the aquifer complexes involved in the ATEs system, detailed models have been developed, extending to the upper aquifer complexes (the shallow aquifer system).

In a predominantly static context (i.e., without gradient-driven flow), this specific modeling aims to assess heat transfer by conduction through the confining aquitards and the potential interference of the ATEs heat plume with the upper aquifers, for both energy and environmental evaluations.

To achieve this, two-dimensional vertical section models have been implemented, allowing for a highly refined computational grid discretization at the aquitards. This level of detail is essential for accurately simulating conductive heat transfer.

The reference stratigraphic framework is presented in Table 4 and Figure 68, providing a more detailed representation of the multi-aquifer system previously identified as a single unit, "Aquifer Unit A0-a" (see Table 1 for reference). This framework is based on the stratigraphic and geothermal characterization report, which should be consulted for further details.

The "main aquitard," within the alternating delta-front sedimentary sequences, separates the shallow aquifer system— which is, in fact, brackish— from the deeper multi-aquifer system. Within this deeper system, specifically in Aquifer Unit A1-a, the ATES system is located.

6.1 Model setup

The hydrogeological and thermophysical parameters used for the modeling are the same as those applied in the 3D models for Aquifer A1-a (ref. Table 2). However, the following additions have been made, based on the stratigraphic and geothermal characterization report, which should be consulted for further details:

- for aquitards, mainly silty clays, hydraulic conductivity $K_{x,y}=1\text{E-}8$ m/s, maintaining $K_{x,y}/K_z=6$; porosity $\phi = 0.3$ (adim.).
- for shallow aquifer complex, +A2 aquifer, conductivity $K_{x,y}=1\text{E-}4$ m/s, maintaining $K_{x,y}/K_z=6$.

The thermal model has been recalibrated under static conditions (Figure 69) to replicate the pre-operational temperature field. This was achieved by assigning a geothermal heat flux boundary condition of 62 mW/m^2 at the base of the model and a temperature boundary condition of 15.5°C at ground level.

The model has been implemented with variable fluid density as a function of temperature. This condition is irrelevant for the ATES study, where forced convection due to pumping and reinjection eliminates the influence of density-dependent flow. However, for assessing flow dynamics in the upper aquifers (particularly A2), buoyancy-driven flow may become significant in the absence of gradient-driven flow, as a result of heating at the base aquitard. By incorporating the expansion coefficient in this way, the model is allowed to better capture how ATES operations indirectly affect the upper aquifer.

In this regard, a linear dependence of density on temperature has been assumed by assigning a thermal expansion coefficient of 0.00025 1/K .

In the 2D model, dynamic conditions cannot be introduced by directly assigning pumping and injection wells, as this approach is only suitable for fully 3D configurations. Instead, dynamic conditions have been implemented by exporting time-varying hydraulic heads from the full 3D model and reimporting them as Head (Dirichlet) boundary conditions.

Since the ATES system involves both pumping and reinjection, but does not represent a perfectly symmetrical process, a modulation function has been applied to adjust the assigned heads. This adjustment is based on the calibration of the thermal plume to better reflect the actual heat distribution preventing the typical over-advection of the 2D approach.

It is important to note that the 2D approach is a simplification and does not precisely replicate the full 3D geometry of the problem (i.e. loss of radial flow effects in 2D, no transverse dispersive effects). However, it is a valuable tool for isolating and accurately computing conductive heat transfer through the aquitards and assessing the resulting thermal interference with the shallow aquifer system.

6.2 Simulation results

6.2.1 Scenario 2-b

The simulation results under dynamic conditions are presented in Figure 70+Figure 75. Based on the project's priority considerations, the simulations were conducted using the seasonally modulated variable flow rate scheme, aligned with greenhouse heating demand. In particular, the analysis focuses on scenario variants 2-c (injection at 60°C) and 2-c1 (injection at 70°C).

The modeling results illustrate the thermal and flow dynamics within the ATEs system, with a particular focus on heat conduction through the upper confining aquitard and its influence on density-driven flow in the overlying aquifer.

The aquitard, acting as an impermeable barrier, primarily facilitates pure conductive heat transfer from the thermal plume in the ATEs reservoir below to the upper aquifer system. The temperature gradient induced by this process triggers density-driven convection in the overlying aquifer, as observed in the formation of localized convective cells (Figure 71, upper image). These convective patterns result from the buoyancy-driven movement of heated, lower-density water rising and cooler, higher-density water sinking. The same Figure 71, lower image, presents the flowlines at 30 years (10,950 days), marking the end of the ATEs operational period.

Figure 72 provides additional insights by illustrating the maximum temperature evolution over time at different monitoring points above the confining aquitard. The following key observations emerge: Curve 1 (top of the ATEs confining layer) shows the most significant temperature increase, confirming that heat transfer is primarily occurring via conduction across the aquitard. Curves 2, 3, and 4, representing progressively shallower observation points, show a progressively smaller temperature increase, indicating a dampening effect of conductive dissipation and vertical dispersion within the upper aquifer.

The simulation confirms that density-driven flow remains confined within this timescale, with no significant expansion beyond the main aquitard into the shallow multi-aquifer complex.

6.2.2 Scenario 2-c, 2c-1

This Scenario 2-c as previously detailed maintains the same pumping scheme as the previous case but with a reduced ATEs storage temperature of 60°C, or 70°C for the variant 2-c1.

The vertical model was applied for the 2-c1 simulation, the potentially more impactful of the two "low temperature" option.

A key observation from the thermal distribution, confirming previous scenario results, is that the temperature influence remains effectively contained within the aquitard. The 10°C isotherm, which marks the limit of thermal disturbance, remains within the aquitard layer and does not extend into the shallow multi-aquifer complex. This confirms that thermal leakage beyond the main aquitard is negligible, preserving the thermal stability of the overlying groundwater system.

Comparing with the 2-b 95°C storage scenario, the overall thermal footprint in the upper aquifer is further reduced, demonstrating that lower storage temperatures enhance thermal containment while still allowing for efficient energy storage and recovery.

These results reinforce the effectiveness of the aquitard as a thermal barrier, ensuring controlled heat containment and negligible thermal influence on the overlying aquifer system in this configuration.

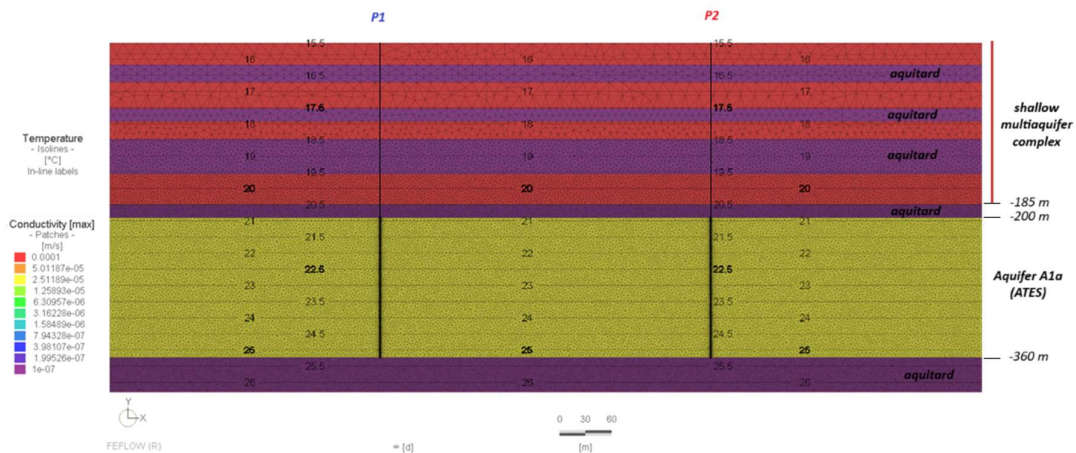
6.3 Key insight

A crucial outcome of the analysis is that thermal influence does not extend beyond the main aquitard. This ensures that the ATES system does not significantly alter temperatures in the shallow multiaquifer complex as stratigraphically defined, preventing potential environmental impacts on groundwater resources.

These findings support the hydrothermal sustainability of the ATES operation by demonstrating that heat transfer is effectively contained within the targeted reservoir system, with negligible thermal interference in the overlying aquifer layers.

Table 4 Reference hydro stratigraphic table for the vertical section model

Aquifer/aquitard	depth	aquifer code	
Aquifer	0-25	A0	Shallow multiaquifer complex
Aquitard	25-45		
Aquifer	45-75	A1-sup	
Aquitard	75-90		
Aquifer	90-110	A1-inf	
Aquitard	110-150		Main aquitard
Aquifer	150-185	A2	
Aquitard	185-200		
Aquifer	200-360	A1-a	ATES reservoir
Aquitard	360-895	(only top layer represented)	



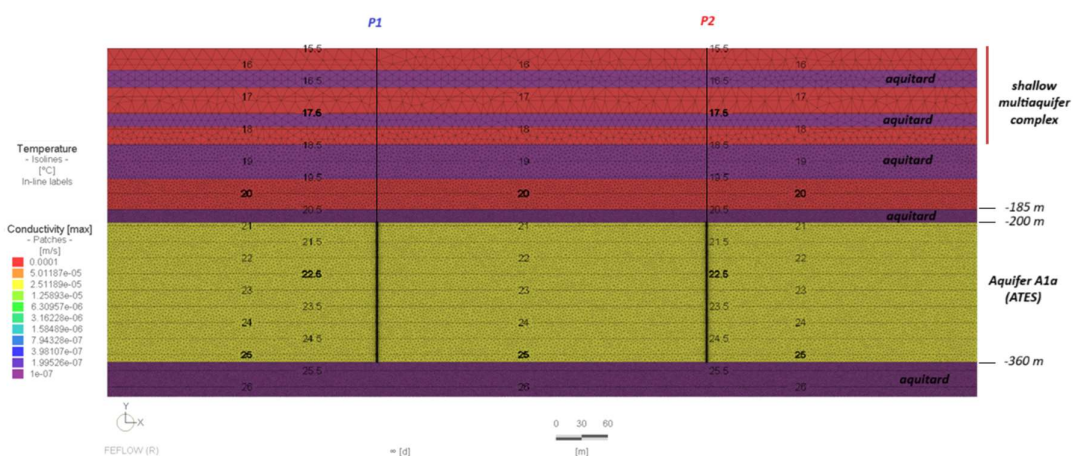


Figure 68 Grid of the model in vertical section, based on the stratigraphic schematization, from aquifer A1a (ATES wells) to the surface.

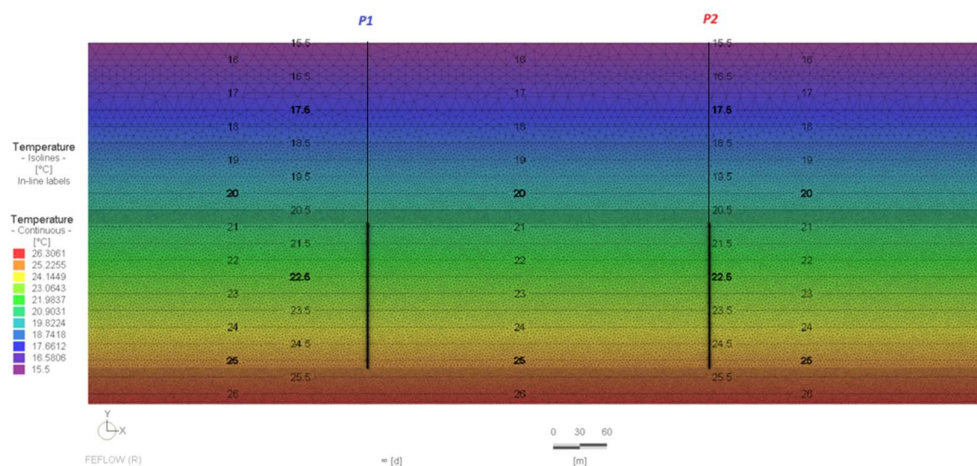


Figure 69 Static thermal model in vertical section.

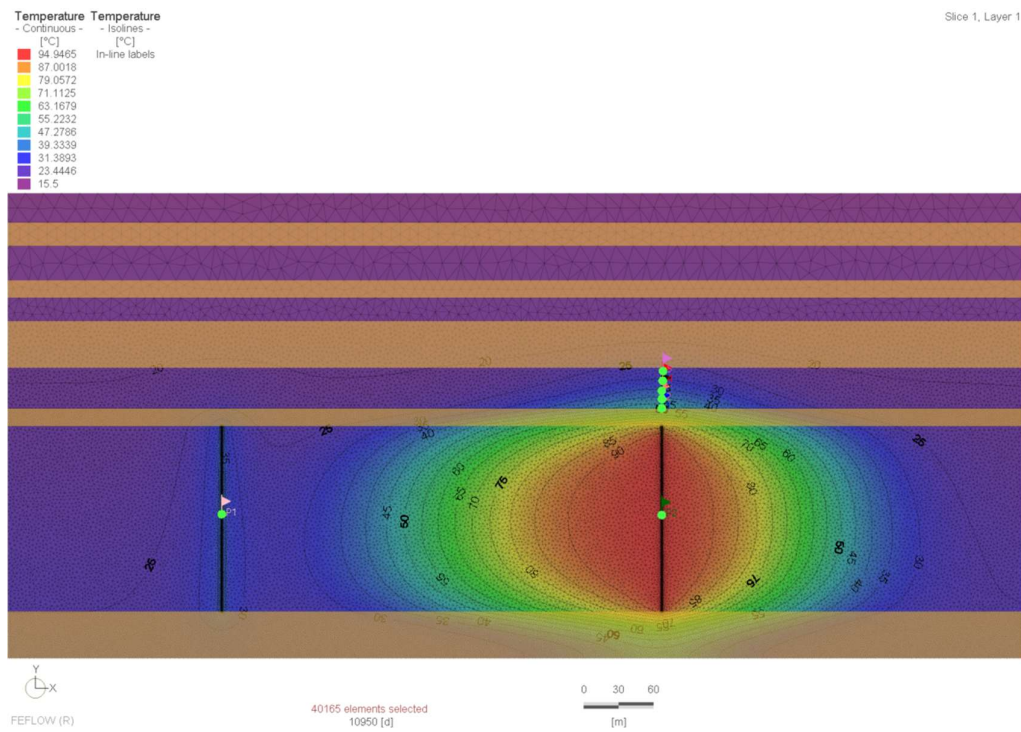


Figure 70 Scenario with ATES storage at $T=95^{\circ}\text{C}$ (comparable to Scenario 2-b). Temperature contours, vertical section, at year 30 of operation.

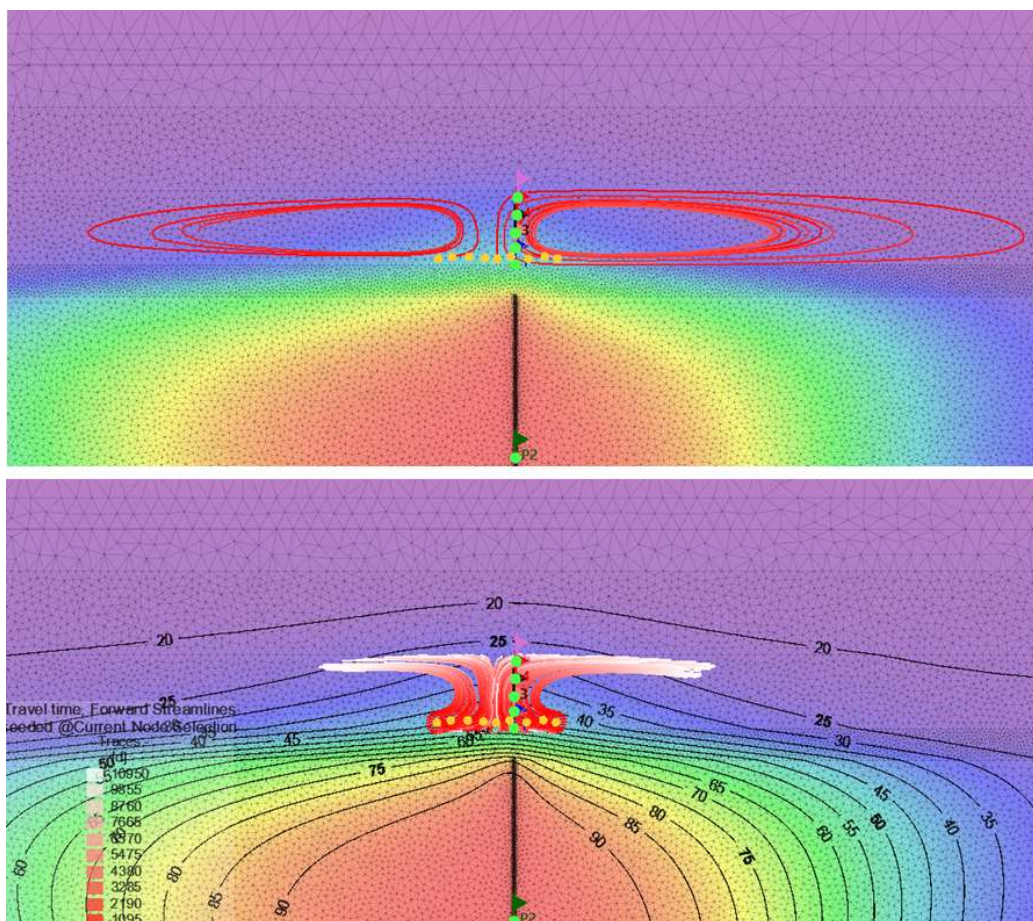


Figure 71 Flow through convective cells above the confining aquitard and the heat plume. The density driven movement over the 30 years of ATEs operation is very limited, and no additional gradient-driven flow is expected (hydraulic gradient close to 0)

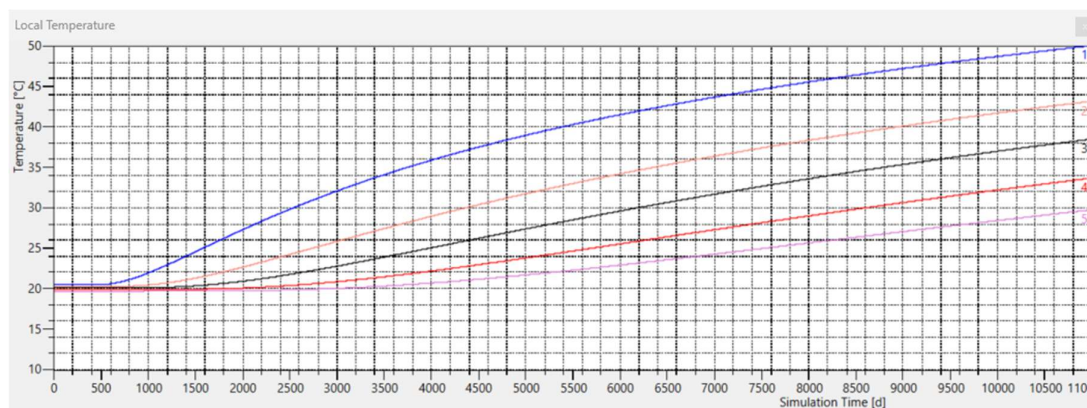


Figure 72 Max temperature chart at observation points above the confining aquitard of reservoir A1-a (ATES, storage at T=95°C) – from bottom to top: curve 1 (top of the aquitard), followed by curves 2, 3, and 4.

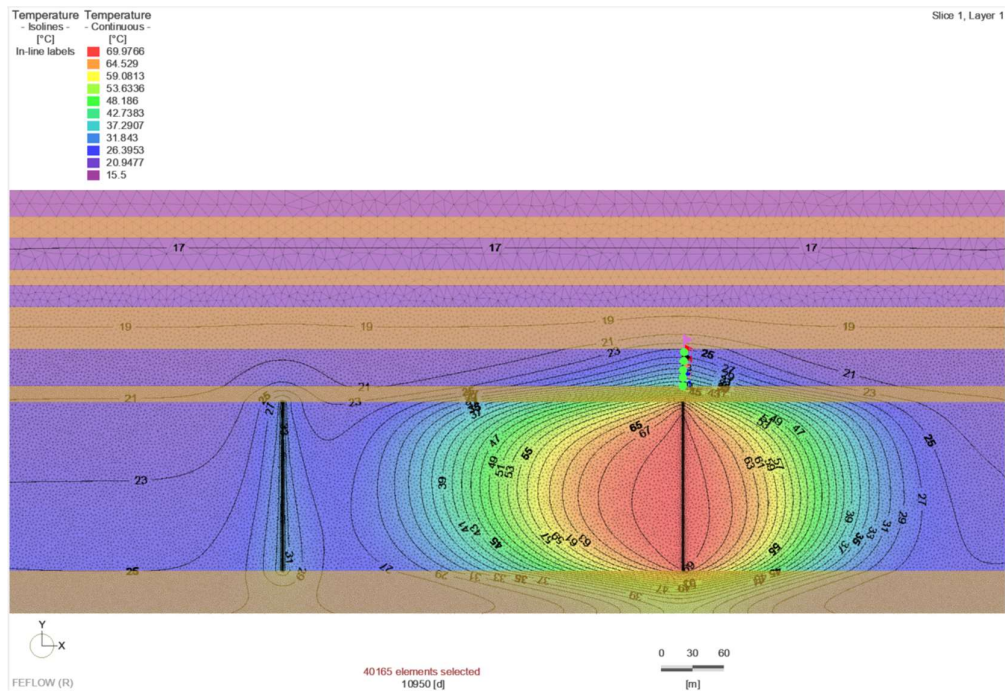


Figure 73 Scenario 2c-1 with ATES storage at $T=70^{\circ}\text{C}$ (optimization of Scenario 2-c). Temperature contours, vertical section, at year 30 of operation.

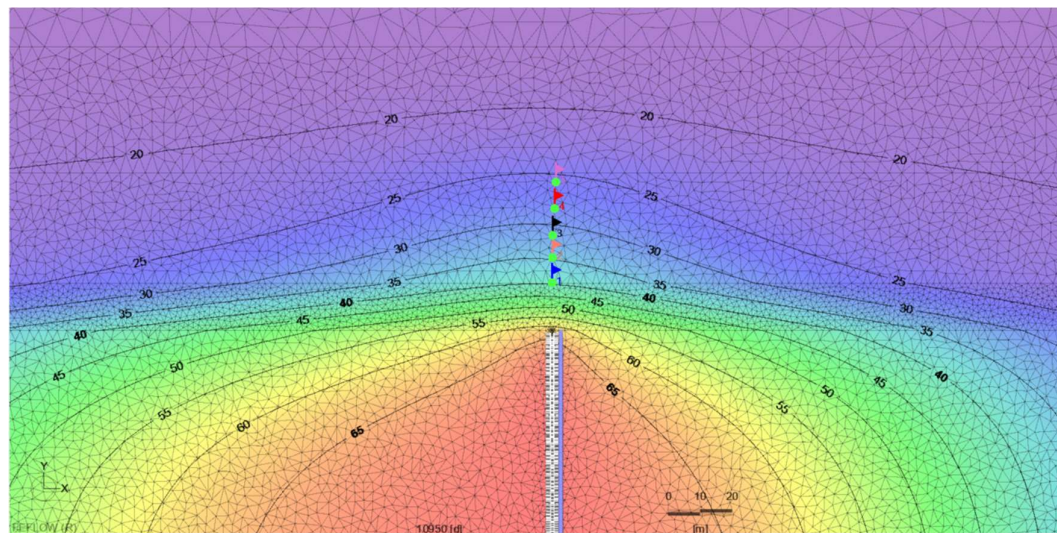


Figure 74 Detail of the previous figure (ATES storage at $T=70^{\circ}\text{C}$), heat plume diffusion by conduction through the aquitard.

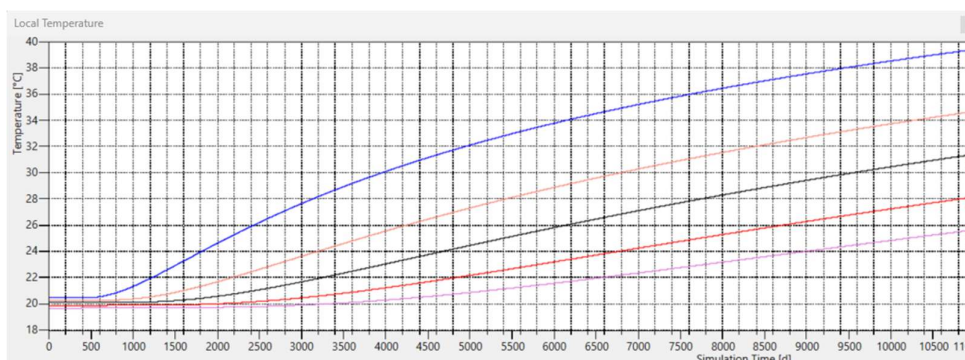


Figure 75 Max temperature chart at observation points above the confining aquitard of reservoir A1-a (ATES, storage at $T=70^{\circ}\text{C}$) – from bottom to top: curve 1 (top of the aquitard), followed by curves 2, 3, and 4.

7 Summary of simulation results

7.1 ATES Sections (storage wells)

The simulation results compare three different ATES (Aquifer Thermal Energy Storage) system configurations:

Scenario 1: Deep reservoir (aquifer A3-a, max depth ≈ 2400 m);

Scenarios 2-a and 2-b: Shallow reservoir (≈ 200 – 360 m).

The following Table 5 provides key metrics, including total thermal energy stored and recovered (GWh), efficiency (%), and minimum recovered water temperature (T_{\min} , $^{\circ}\text{C}$) over 30 years of operation. The parameters are derived from the modeling analysis using the 50th percentile values of the reservoir's hydrodynamic and thermophysical parameters. The bar chart in Figure 76 visually compares these parameters, highlighting differences in stored and recovered energy, efficiency, and T_{\min} across the three scenarios.

A key aspect to highlight is that the three scenarios exhibit significantly different amounts of stored energy (GWh in), which makes a direct comparison of efficiency and recovery performance less straightforward.

Scenario 1 stores 574 GWh, significantly lower than Scenarios 2-a (887.68 GWh) and 2-b (1619.18 GWh). The lower amount of energy stored in Scenario 1, compared to Scenarios 2-a and 2-b, is also influenced by the higher initial temperature of the deep reservoir, which reduces the thermal gradient and, consequently, the amount of heat that can be effectively injected and stored.

The larger input energy in Scenario 2-b naturally results in higher recovered energy, but efficiency comparisons must take into account this discrepancy in initial storage.

A breakdown of key performance metrics shows:

Energy recovery performance: Scenario 2-b has the highest total recovered energy (807.85 GWh), followed by 2-a (767.76 GWh) and finally Scenario 1 (314 GWh). However, this does not translate to higher efficiency.

Note that for Scenarios 2-a, 2-b, the stored energy balance refers only to the ATES well, with seasonal injection ranges from 95°C (Scenario 1, 2-a) to 60°C – 70°C (2-c, 2-c1). It does not

account for the injection into the "cold" well downstream of utilization, where discharge occurs at 40°C, leading to a further increase in the reservoir enthalpy.

Efficiency (%): Scenario 2-a achieves the highest ATES efficiency (up to 92%) while increasing the amount of stored energy does not necessarily lead to proportional gains in efficiency, likely due to higher thermal losses in Scenario 2-b, 2-c (and variant 2-c1).

As for the relatively low efficiency for Scenario 1 (54.7%), several factors related to ATES wells geometry and depth likely contribute to the higher heat losses and lower recovery:

- increased heat dissipation over longer well lengths (extended contact with surrounding formations); An active well length / filter development of 630 m significantly increases the surface area exposed to the surrounding rock formations. Over time, more heat is lost through conduction;
- larger thermal diffusion footprint: the longer well path means heat spreads over a wider zone, reducing the temperature contrast necessary for efficient heat recovery;
- the inclined orientation may result in non-optimal interaction with the thermal plume; the combination of inclined wells and a horizontal permeability contrast likely contributes to dispersivity, increasing lateral heat dispersion, making effective recovery more difficult.

Unlike vertical wells, where heat may stay more confined within the target reservoir, inclined wells increase the interaction with heterogeneous thermal and hydraulic conditions. In general, vertical well configurations, yet less effective on the hydraulic point of view (increased dynamic heads) may provide better thermal control in layered systems with lower vertical permeability, ensuring that heat remains in a more recoverable zone.

Minimum recovered water temperature (Tmin): despite the shallow aquifer's low initial temperature (25°C), Scenario 2-b maintains the highest Tmin (86.9°C), reflecting in maximum ΔT with the reservoir temperature (Tmin-Tref. $\approx 62^\circ\text{C}$); the higher heat input, (1619.18 GWh), leading to a larger thermal mass, helps maintain higher temperatures over time, reducing overall cooling effects; on the other side Scenario 1 exhibit the minimum (worse) ΔT value (Tmin-Tref. $\approx 7^\circ\text{C}$) as an additional indicator of reduced ATES performance.

Table 5 ATES options: total thermal energy stored / recovered, efficiency %, minimum temperatures (first year cycle, average minimum, stabilized) after 30 years of operations (29 complete storage-recovery cycles).

(*) Note: WCS for 2-C, Efficiency 41,02% (total recovered 310 GWh over 30 years of operation)

Scenario	ATES Inj. T	Thermal energy in/out (GWh)			Minimum temp. recovered water (°C)		
		stored (in)	recovered (out)	Efficiency (%)	min (year 1)	med-min	final (30 y)
1	95°C	574	314	54.7	70.5	75.2	76.5
2-a	95°C	887.68	767.76	86.5	40.0	55.7	60.2
2-b	95°C	1619.18	807.85	49.9	60.4	86.9	92.1
2-c (*)	60°C	757.58	342.96	45.27	42.9	57.7	58.8
2-c1	70°C	961.28	435.21	45.27	48.3	67.1	69.2

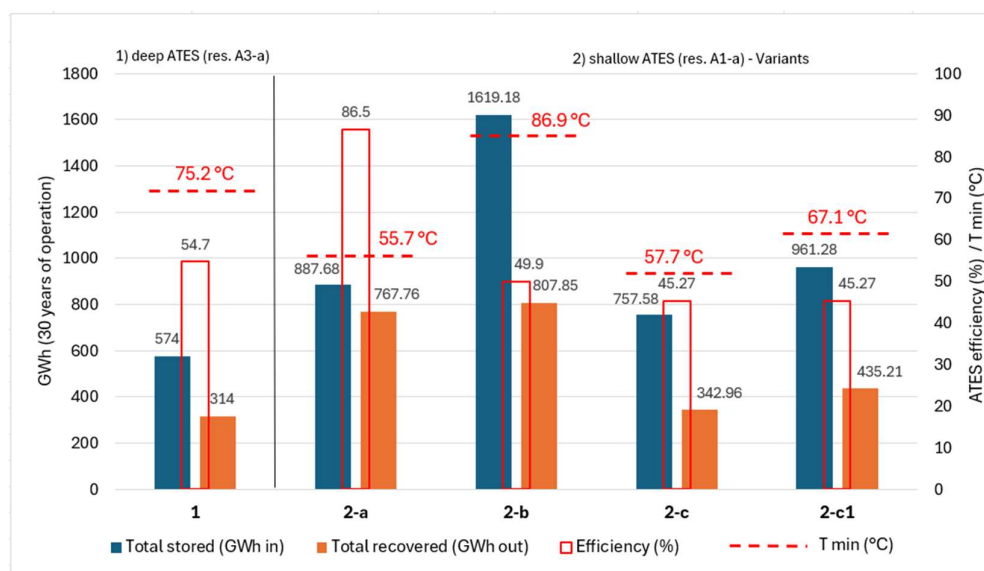


Figure 76 ATEs system performance - 30 years of operation: total heat stored and recovered (GWh), efficiency (%), minimum fluid temperature (average value), ref. Table 5

7.2 Production (geothermal well doublets)

The production system, consisting of two oriented doublets in the deep reservoir, achieves a total thermal energy production of 2239 GWh over 30 years of operation in the simulated scenario.

From a thermal management perspective:

- no thermal drift is observed in the pumping wells, indicating that production temperatures remain stable throughout the operational period.
- thermal short-circuiting is effectively excluded, as the temperature front does not cause premature thermal breakthrough between injection and production wells. This holds true for all scenarios, including Scenario 1, where the ATEs wells are located in the same "greenhouses" area, confirming that there is no thermal interference between the hot water bubble and the production wells.
- the cold bubble from the discharge wells remains confined within the "San Giovanni" area, preventing thermal interference with the pumping sections.

Sensitivity analysis confirms that thermal yield and total energy production remain unaffected by variations in the main reservoir parameters. However, the head difference between production and injection wells is significant, simulated under average (50th percentile) permeability conditions and becomes notably higher under the tested lower-permeability (10th percentile) scenario, where dynamic head reaches approximately -180 m for extraction and +240 m for injection. This condition should be carefully evaluated from both a technical and operational standpoint.

8 Conclusions

The choice of the most suitable ATES configuration depends on the specific application requirements, whether the system is designed to maximize efficiency, ensure high-temperature heat recovery, or optimize energy storage capacity. The simulation results suggest different trade-offs between these factors, highlighting the strengths and limitations of each scenario.

- For applications prioritizing energy efficiency: Scenario 2-a is the best option due to its high efficiency (up to $\approx 92\%$) and moderate storage requirements.
- For applications requiring high temperature output: Scenario 2-b is preferred due to its high T_{min} (86.9°C), making it ideal for process heat applications or district heating systems.
- For applications at lower temperatures (stabilized T_{min} of $\approx 57^{\circ}\text{C}$), it is possible to consider solutions that exclude the use of a heat pump (scenario 2-c), relying solely on storing the excess heat from geothermal production doublets. Alternatively, intermediate variants (scenario 2-c1, stabilized T_{min} $\approx 67^{\circ}\text{C}$) can be adopted as a more cautious approach to ensure sufficient heat supply, particularly in the initial years before the ATES system reaches thermal stabilization.

Regarding the possible adoption of scenario 2-c, the assumption of a conservative scenario 2-c1 can currently be considered appropriate, given the lower temperature values and reduced energy recovery observed in the worst-case 2-c scenario, as evaluated through the uncertainty analysis.

Within the options of Scenario 2, the lower-temperature variants (2-c and 2-c1) offer the additional advantage of reduced heat dispersion through conductive transfer across the confining aquitards, enhancing thermal containment. In any case, the detailed modeling analysis has shown that, for all Scenario 2 options, the heat plume does not interfere with the temperature of the shallow multi-aquifer system.

Scenario 1 is not recommended for ATES implementation due to low efficiency, higher losses, and suboptimal thermal recovery.

Furthermore, the configuration with an additional doublet of inclined wells, if implemented, could support energy harvesting from natural heat rather than ATES operations. This setup would allow for a higher energy production compared to the estimates of Scenario 1 as a pure storage system. Consequently, managing this configuration as an ATES system would be disadvantageous, as direct exploitation of the natural heat resource could yield better overall energy output.

It is also important to note that, unlike conventional unidirectional extraction and reinjection wells, which operate with a fixed flow direction, bidirectional ATES systems feature storage wells that alternate between injection and extraction on a seasonal basis. Under all conditions—and particularly in the tested low-permeability scenarios—this operational mode results in Scenario 1 experiencing alternating cycles of wellhead drawdown and pressure buildup. These cycles involve sudden reversals in flow direction, with maximum overall pressure variations reaching several hundred meters.

Potential geotechnical issues due to these pressure buildup/fall in the fine-sandy and silty-sandy reservoir deposits is out of the present modelling Scope Of Work. Particularly for the Scenario 1, possible issues as formation damage, reservoir compaction, dislodgement of fine particles, internal erosion or fines migration impacting reservoir stability should be carefully evaluated through geotechnical and well performance modelling.

The production system, consisting of two oriented doublets in the deep reservoir, achieves a total thermal energy production of 2239 GWh over 30 years of operation. The thermal energy yield per geothermal doublet significantly exceeds that of the ATES storage-based approach (Scenario 1),

confirming that direct energy harvesting from the deep reservoir is a more effective and efficient use of the resource in this configuration.

The simulation results indicate that no thermal drift or thermal short-circuiting occurs, ensuring stable production temperatures and effective thermal separation between injection and production wells. This suggests that the geothermal doublet system could likely be scalable within the technical limits of resource exploitation, allowing for potential expansion while maintaining thermal efficiency and reservoir sustainability.

In conclusion, it is important to emphasize that all evaluations conducted for the technical screening of the best solution are based on the currently available hydraulic and thermal parameters, as provided by FRI-EL consultants. As the project progresses, the availability of experimental data—starting from the well-testing phase—will be essential for reassessing and refining the simulation results